EES Batteries

REVIEW

View Article Online
View Journal | View Issue

Check for updates

Cite this: *EES Batteries*, 2025, **1**, 1444

Low-temperature sodium-ion batteries: challenges, engineering strategies, safety considerations, and future directions

M. Sai Bhargava Reddy, *[a,b] Daecheol Jeong, [a] Shampa Aich[b] and Vilas G. Pol *[a]

Sodium-ion batteries (SIBs) present a sustainable and cost-effective alternative to lithium-ion batteries (LIBs) for low-temperature (LT) applications, leveraging sodium abundance and reduced geopolitical risks. While SIBs exhibit superior capacity retention in cold environments compared with LIBs, their adoption faces challenges including sluggish Na^+ diffusion, increased electrolyte viscosity, unstable electrode–electrolyte interfaces, and electrode structural degradation. This review analyzes the mechanisms of LT performance limitations and evaluates strategies to overcome them. Electrolyte engineering, using optimized sodium salts, multi-solvent formulations, and functional additives, enhances ionic conductivity and stabilizes interfaces. Electrode modifications, such as defect engineering, nanostructuring, elemental doping for cathodes, and morphology tuning with porous architectures for anodes, mitigate kinetic barriers and volume expansion. Integrating advanced electrolytes with tailored electrodes improves charge storage efficiency and cycling stability at sub-zero temperatures, enabling applications in Arctic infrastructure, aerospace, and renewable energy storage. However, gaps persist in understanding solid–electrolyte interphase (SEI) formation, material scalability, thermal safety studies, and energy density optimization. Future research priorities include computational modeling of ion-transport mechanisms, sustainable recycling protocols, and hybrid systems with thermal management. Bridging fundamental insights with practical engineering charts a path towards high-performance LT-SIBs, crucial for decarbonizing energy systems in extreme environments and advancing global energy resilience.

Received 2nd July 2025,
Accepted 19th August 2025

DOI: 10.1039/d5eb00121h

rsc.li/EESBatteries

Open Access Article. Published on 20 August 2025. Downloaded on 18.02.26 05:05:09.
This article is licensed under a Creative Commons Attribution 3.0 Unported Licence.

Broader context

As the world accelerates its transition to renewable energy and electrified transportation, the demand for reliable energy storage solutions that perform in harsh and low-temperature (LT) environments is becoming increasingly urgent. Traditional lithium-ion batteries (LIBs), while widely used, face significant limitations in cold climates and extreme conditions, posing challenges for applications ranging from grid storage in northern regions to polar exploration and aerospace missions. This review addresses the critical problem of improving sodium-ion battery (SIB) performance at low temperatures by systematically analyzing the optimization of electrode materials, electrolyte compositions, and interfacial stability. Key findings include the development of advanced composite electrodes and tailored electrolyte systems that enhance ionic conductivity and maintain battery stability at sub-zero temperatures. These innovations not only help close the performance gap with LIBs but also leverage the abundance and low cost of sodium resources, offering a more sustainable and scalable alternative. By enabling energy storage in environments previously inaccessible to conventional batteries, LT SIBs have far-reaching implications for global energy security, climate resilience, and the advancement of clean technologies. The insights gained here will be helpful for future research, guide industrial development, and support policy initiatives aimed at a more robust and sustainable energy infrastructure.

1. Introduction

Sodium-ion batteries (SIBs) have emerged as a compelling alternative to lithium-ion technology, addressing urgent needs for sustainable and cost-effective energy storage solutions. The foundational advantage of SIBs lies in resource abundance, with sodium constituting approximately 2.3% of Earth's crust compared with lithium's mere 0.002%, ensuring material availability and reducing geopolitical risks associated with resource scarcity.[1] Na-containing metal oxide and polyanion cathode materials can be fabricated from naturally abundant transition metals such as iron, manganese, vanadium, and titanium, without using cobalt.[2] This abundance translates to

[a]*Davidson School of Chemical Engineering, Purdue University, West Lafayette, 47907 IN, USA. E-mail: msbhagi96@gmail.com, vpol@purdue.edu*
[b]*Department of Metallurgical and Materials Engineering, Indian Institute of Technology, Kharagpur, 721302 West Bengal, India*

© 2025 The Author(s). Published by the Royal Society of Chemistry

Open Access Article. Published on 20 August 2025. Downloaded on 18.02.26 05:05:09.
This article is licensed under a Creative Commons Attribution 3.0 Unported Licence.

economic benefits, as sodium precursors are significantly less expensive than their lithium counterparts. Additionally, cost savings are enhanced by using aluminum instead of copper for anode current collectors, leveraging sodium's electrochemical compatibility with aluminum substrates.[3] This positions SIBs with hard-carbon anodes and cobalt-free cathodes as sustainable, lower-cost alternatives to LIBs for applications like short-range electric vehicles and large-scale energy storage in a world increasingly reliant on wind, solar, and hydroelectric power, which require reliable battery performance.[4–6]

Building on their material advantages, the development of sodium-ion full cells (SIFCs) traces back to the 1960s, as detailed in ref. 7. Despite several accomplishments, commercialization and scaled-up production of SIFCs remain in early stages. By 2027, sodium-ion solutions are predicted to produce 3.8 terawatt hours of energy but will fall short of demand. By 2030, production capacity is forecast to reach 6.4 terawatt hours, yet demand is expected to be 7.6 terawatt hours.[8] From a mechanistic perspective, SIBs operate *via* a "rocking-chair" mechanism, where sodium ions shuttle between cathode and anode during charge/discharge cycles, mirroring LIBs.[7] This similarity facilitates manufacturing synergies, enabling producers to repurpose existing LIB production lines with minimal modification.

Turning to electrochemical properties, sodium ions present both challenges and opportunities for battery performance due to their larger ionic radius (1.02 Å *vs.* lithium's 0.76 Å). This size difference results in slower solid-state diffusion but can benefit electrolyte interactions through lower desolvation energy barriers, critical for low-temperature operations. Sodium (23 g mol^{-1}) is heavier than lithium (6.9 g mol^{-1}), and its electrochemical potential (−2.71 V *vs.* standard hydrogen electrode) offers a reasonable voltage window, though slightly lower than lithium's (−3.04 V), leading to marginally reduced energy density.[7] However, the weight of cyclable Na or Li is a small fraction of the electrode mass, and capacity is primarily determined by the host structures.[9]

1.1. Importance of low-temperature performance

Energy storage systems operating in sub-zero conditions face universal challenges, including sluggish ion diffusion, increased electrolyte viscosity, and elevated interfacial charge-transfer resistance, all contributing to capacity fade and power loss. While LIBs suffer severe capacity losses below −20 °C, SIBs demonstrate greater resilience due to their distinct physicochemical properties.[10] This advantage stems from sodium's lower Lewis acidity, which weakens ion–solvent interactions and potentially reduces interfacial resistance at low temperatures.[11] Moreover, sodium's lower first ionization energy (495.8 *vs.* 520.2 kJ mol^{-1} for lithium) enhances its chemical and electrochemical reactivity, promoting more efficient processes at low temperatures.[10,12]

This resilience is evident in capacity retention metrics. At temperatures below −20 °C, conventional LIBs typically retain only 30–50% of their room-temperature capacity, whereas properly engineered SIBs can maintain 50–70% under identical conditions.[13] At extreme temperatures approaching −40 °C, many LIBs cease functioning, while certain SIB configurations continue operating, albeit with performance penalties.[14,15] Such performance advantages have significant practical implications for applications like Arctic infrastructure, remote monitoring stations, and cold-climate renewable energy installations, which require reliable operation across seasonal temperature variations. Aerospace applications encountering extreme temperature fluctuations also benefit from broader operational temperature windows.[16] Improved low-temperature performance reduces the need for costly thermal management systems, simplifying energy storage deployments. Despite limited prior research, significant progress in understanding SIBs' temperature-dependent performance over the last 15 years inspires this comprehensive summary (Fig. 1).

M. Sai Bhargava Reddy

M. Sai Bhargava Reddy is currently a doctoral researcher in the Department of Metallurgical and Materials Engineering at the Indian Institute of Technology (IIT) Kharagpur, working jointly with Purdue University, USA, as a SERB-OVDF fellow. His research focuses on the development and fundamental understanding of advanced materials for energy storage, with a particular emphasis on low-temperature Li/Na-ion batteries, 2D materials (MXenes), and nanomaterials for sensing applications.

Daecheol Jeong

Daecheol Jeong received his BSc degree in Chemical Engineering in 2023 from the Illinois Institute of Technology, USA. He is currently pursuing his PhD in Chemical Engineering at Purdue University, USA, under the supervision of Dr Vilas G. Pol and Brian M. Tackett. His research is dedicated to the design of advanced electrolytes and the engineering of electrode materials to enable reliable lithium-ion battery performance under ultra-low-temperature conditions.

Open Access Article. Published on 20 August 2025. Downloaded on 18.02.26 05:05:09.
This article is licensed under a Creative Commons Attribution 3.0 Unported Licence.

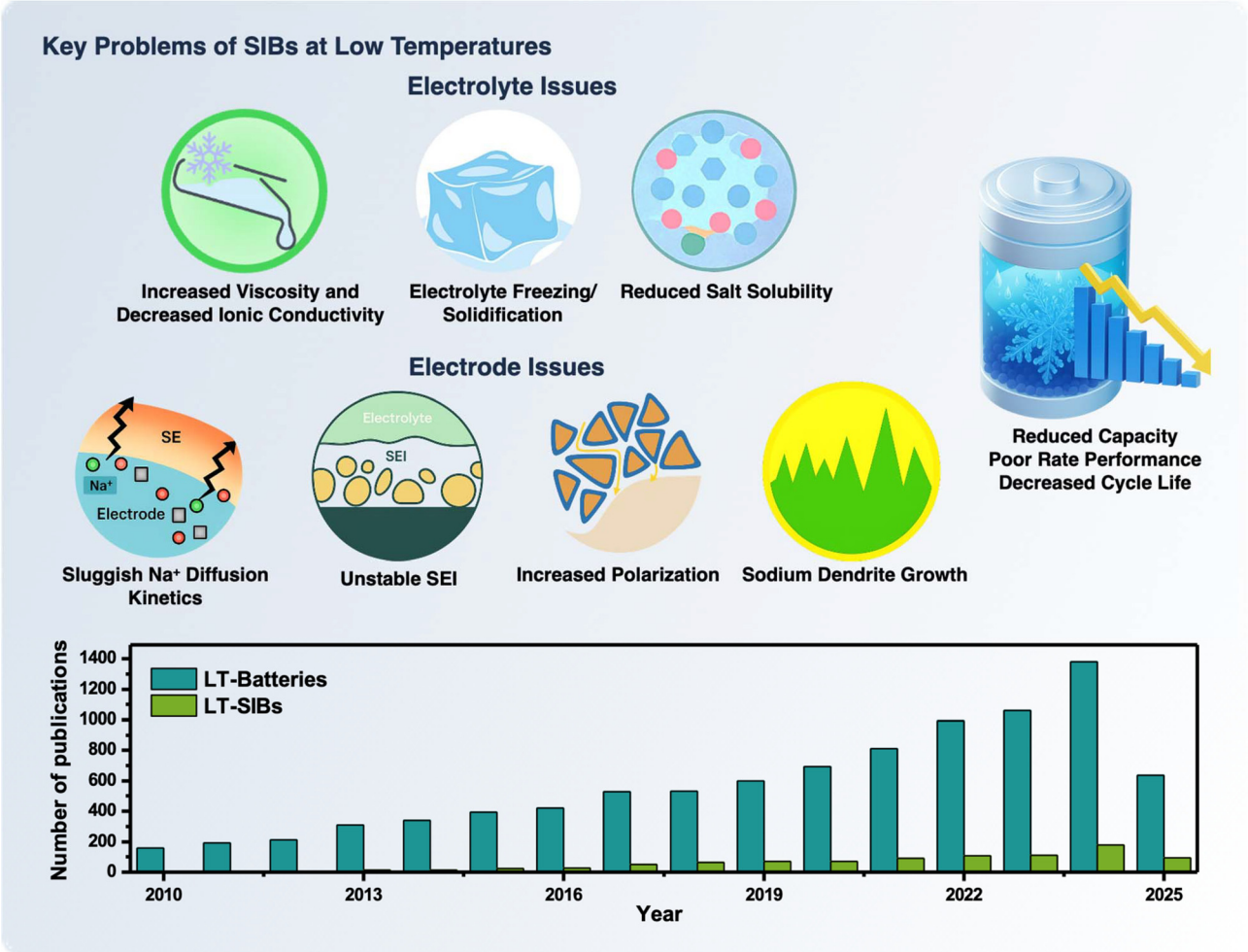

Fig. 1 Main challenges and the increasing trend of publications for low-temperature SIBs. Data from Web of Science as of June 8, 2025.

Shampa Aich

Shampa Aich is a Professor in the Department of Metallurgical and Materials Engineering at the Indian Institute of Technology (IIT) Kharagpur. Her research interests are focused on the field of metallurgical & materials science and engineering especially on smart materials (SMA/FMSMA), 2D materials, magnetic materials, biomaterials, and surface modifications.

Vilas G. Pol

Vilas G. Pol is a Professor of Chemical Engineering at Purdue University, IN, USA. He has authored/co-authored over 285 research publications (h-index 62) and is an inventor on 27 issued US patents with 10+ additional applications. He has delivered hundreds of invited, keynote, and plenary talks, including a TEDx presentation. Purdue University has honored him with Outstanding Engineering Teacher, Most Impactful Inventor, Seed for Success, Bravo, and Purdue Faculty Scholar awards. He has received more than 40 prestigious awards from professional societies including AIChE, ACS, MRS, ACerS, TMS, and Carbon. His accolades include a 2015 R&D 100 award, Intel Prize, two Guinness World Records™, Fellow of the Royal Society of Chemistry (FRSC), and a Fulbright Specialist.

© 2025 The Author(s). Published by the Royal Society of Chemistry

Open Access Article. Published on 20 August 2025. Downloaded on 18.02.26 05:05:09.
This article is licensed under a Creative Commons Attribution 3.0 Unported Licence.

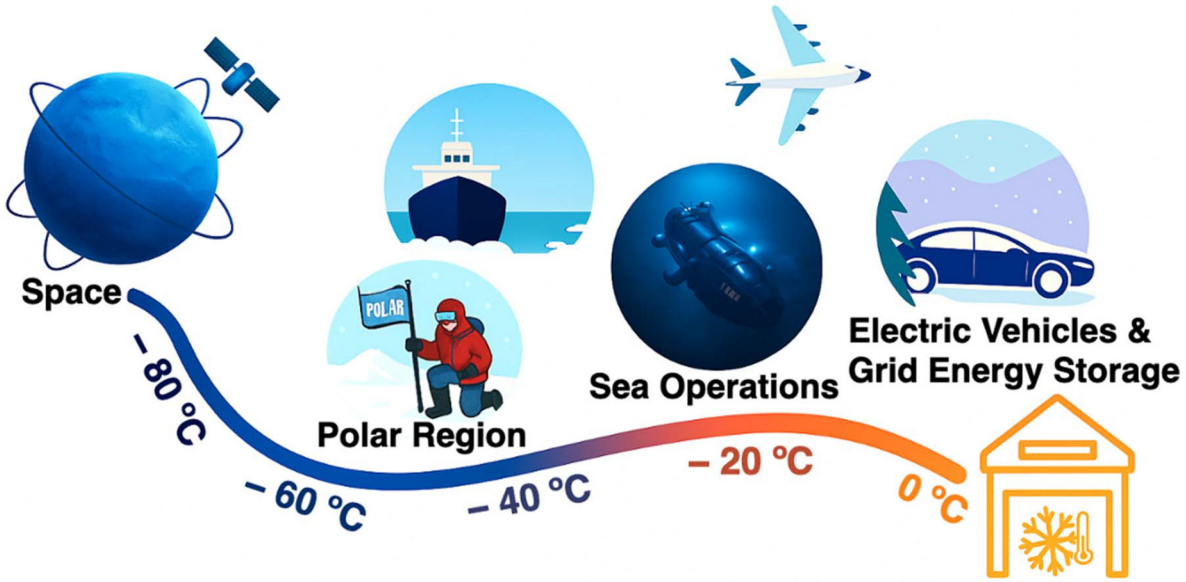

Fig. 2 Low-temperature SIB applications.

1.2. Emerging applications

Beyond material and performance advantages, SIBs are gaining traction due to their compatibility with lithium-ion manufacturing infrastructure and resilience in supply-disrupted scenarios where lithium or graphite availability is constrained.[17] Faradion's sodium-ion cells, for example, perform effectively across −20 to 60 °C and achieve cycle lifespans beyond 4000 cycles, making them suitable for stationary storage in cold climates and defense or aerospace applications.[18–20] Fig. 2 illustrates environmental conditions relevant to such use cases.

This extreme-temperature tolerance drives interest in Arctic military systems, Antarctic field operations (−50 °C), deep-sea electronics (near-freezing at 3000 m), and space exploration, including missions to Mars (<−125 °C), the Moon (−183 °C to 127 °C), and asteroids (−180 °C to 100 °C). These require power systems that operate autonomously without excessive heating, as batteries contribute 20–30% of a spacecraft's mass.[21] Such environments also demand high-current discharge capabilities for engine starting or powering space probes, autonomous underwater vehicles, remotely operated vehicles, and sensors, enabling critical operations in aerospace, deep space, and oceanographic data collection. Defense applications, like Arctic Patrol's UAVs and portable energy systems, leverage SIBs' stability under rapid discharge and resistance to thermal runaway.[22] Additionally, outdoor recreational products, such as heated ski gear and emergency communication devices, benefit from SIBs' extended temperature tolerance and fast-charging capabilities.[23]

While SIBs currently trail LIBs in energy density (120–160 Wh kg^{-1} *vs.* >250 Wh kg^{-1}), their cost, safety, and thermal robustness advantages position them for high-impact applications. Continued innovation in electrolytes, electrodes, and manufacturing is narrowing the performance gap, making SIBs a scalable solution for next-generation energy storage.

2. Challenges in low-temperature operation

2.1. Thermodynamic and kinetic limitations

SIBs face significant thermodynamic and kinetic challenges at low temperatures that degrade performance. Thermodynamically, conventional carbonate-based electrolytes freeze below −20 °C,[24,25] while sodium salts like $NaPF_6$ precipitate in single-solvent systems, disrupting ionic pathways.[10,13,26] Electrode materials such as $Na_3V_2(PO_4)_3$ undergo irreversible phase transitions at subzero temperatures, causing lattice strain and capacity loss.[24,27] Fig. 3(a) summarizes some of the challenges of LT SIB operation. Kinetically, sodium-ion diffusion coefficients drop exponentially below 0 °C, while charge-transfer resistance spikes by 3–5 times at −40 °C due to brittle SEIs with reduced NaF content.[10,28,29] High electrolyte viscosity and desolvation energy barriers (>0.85 eV in carbonates) further slow down the ion transport.[13,30] These challenges intersect critically during electrodeposition: while solvated Na^+ transport remains viable, the interfacial charge-transfer process, desolvation and SEI migration emerge as rate-limiting bottleneck due to temperature-sensitive energy barriers, with desolvation kinetics dominating resistance at high rates as shown in Fig. 3(b). Concurrently, fragile SEIs under low-temperature conditions exacerbate inhomogeneous Na^+ flux, accelerating dendrite growth and capacity decay.[31] Real-world testing reveals inconsistencies, with some SIBs retaining 90–95% capacity at −20 °C in controlled conditions as presented in Fig. 3(c),[32] but suffering 20% losses under thermal shock, alongside safety

Open Access Article. Published on 20 August 2025. Downloaded on 18.02.26 05:05:09.
This article is licensed under a Creative Commons Attribution 3.0 Unported Licence.

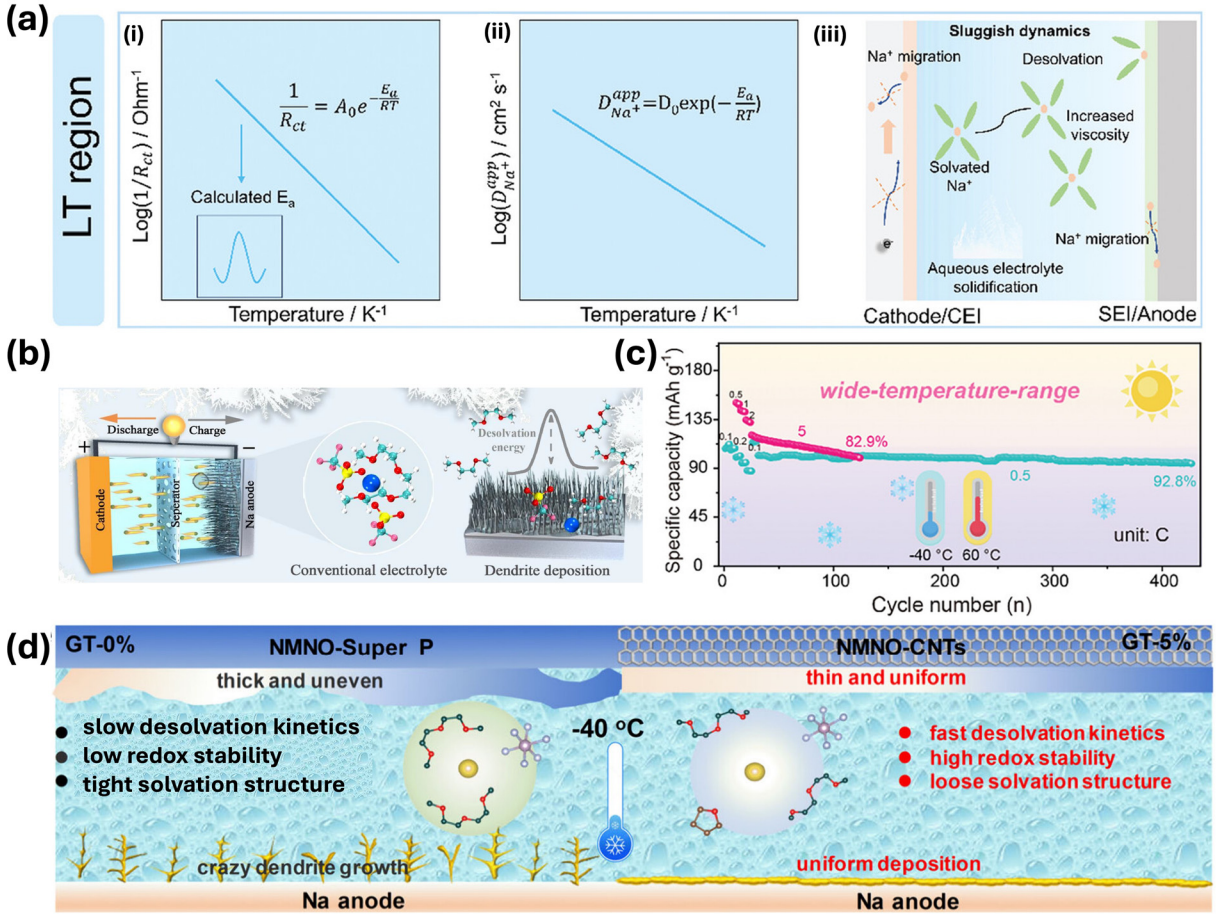

Fig. 3 (a) Temperature-dependent trends in (i) charge resistance, (ii) intrinsic ion diffusion coefficient, and (iii) highlighting low-temperature challenges in SIBs.[25] (b) Illustration of high-rate SIB operation at low temperatures (LT), where conventional electrolytes promote dendrite formation under high current densities.[31] (c) Rate capacity and cycling stability of SIBs under extreme temperatures (−40 °C to 60 °C).[32] (d) Schematic diagram of the conductive agent and electrolyte on the cathode and anode surfaces.[28]

risks like thermal runaway during nail penetration tests, underscoring the interplay of thermodynamic instability, kinetic sluggishness, and interfacial degradation in limiting LT SIB viability.

Mitigation strategies focus on electrolyte engineering and interfacial stabilization. Ether-based solvents (DEGDME/DOL) with NaOTf salts extend operational limits to −80 °C by reducing freezing points and forming NaF-rich SEIs.[10] Weakly solvating electrolytes lower desolvation energy by 40%, enabling 30C charging at −30 °C,[28] while co-solvent systems suppress salt precipitation and maintain ionic conductivity (>1 mS cm^{-1} at −80 °C). Electrode modifications, such as CNT agents, establish a continuous conductive network in the P2-$Na_{0.67}Mn_{0.67}Ni_{0.33}O_2$ electrode (Fig. 3(d)), enhancing conductivity, specific capacity, and voltage plateaus, while the THF additive restructures solvation clusters to form compact/robust interfacial films on cathode/anode surfaces, improving rate capability and cycling stability.[28] Mn^{2+}-doped cathodes and hard carbon anodes with pseudocapacitive storage improve structural stability and ion diffusion.[33,34] Despite progress, challenges persist, including dendrite growth risks at −60 °C, limited oxidative stability of ethers above 4.0 V,[35] and SEI repair failures below −50 °C.[13] Full cells with optimized electrolytes achieve 94% capacity retention after 100 cycles at −40 °C,[10] but inconsistencies in field performance underscore the need for standardized testing and advanced diagnostics to bridge laboratory advances with real-world reliability.

2.2. Electrode material challenges

Cathode materials for SIBs face distinct challenges at low temperatures that limit their performance capabilities. The development of cathode materials for LT-SIBs is hindered by intrinsic and temperature-exacerbated limitations. Polyanionic compounds, such as NASICON-type $Na_3V_2(PO_4)_3$ (NVP), provide stable frameworks and rapid Na^+ diffusion but suffer from inherently low electronic conductivity,[36] which becomes pronounced at sub-zero temperatures, necessitating conductive coatings[37] or nanostructuring.[38] However, these modifications often compromise energy density and long-term stability due to coating degradation. Transition metal oxides (TMOs), particularly layered P2/O3-type structures, face irreversible phase transitions under deep desodiation, leading to

© 2025 The Author(s). Published by the Royal Society of Chemistry

Open Access Article. Published on 20 August 2025. Downloaded on 18.02.26 05:05:09.
This article is licensed under a Creative Commons Attribution 3.0 Unported Licence.

volume expansion (up to 23%) and intracrystalline cracking, while diminished ionic conductivity at LT amplifies kinetic barriers.[39,40] Although strategies like high-valence cation doping stabilize Na^+ occupancy,[41,42] the formation of metastable phases during cycling remains a critical issue. Prussian blue analogs (PBAs), despite their open frameworks and minimal volume changes (<1%), exhibit structural voids and interstitial water from rapid crystallization, degrading capacity retention at LT.[43,44] Additionally, their poor electronic conductivity exacerbates polarization, requiring conductive composites like Prussian blue (PB)/CNT, yet challenges persist in balancing conductivity with structural integrity. For all cathode materials, irreversible phase transitions and particle cracking under thermal stress during deep cycling remain unresolved, underscoring the need for hierarchical architectures and advanced computational design to optimize LT performance.

Anode materials for LT-SIBs face equally significant challenges, particularly sluggish Na^+ kinetics and structural instability. Hard carbon (HC), though promising for its high capacity (~300 mA h g^{-1}), suffers from severe polarization effects and premature voltage cut-offs at LT, exacerbated by thick SEI layers formed on high surface area open pores, which reduce initial coulombic efficiency (ICE) and accelerate capacity fade.[45,46] The strategies such as sulfuric acid hydrolysis and hydrothermal carbonization (HTC) pretreatment enable controlled tuning of pores, heteroatom content, and

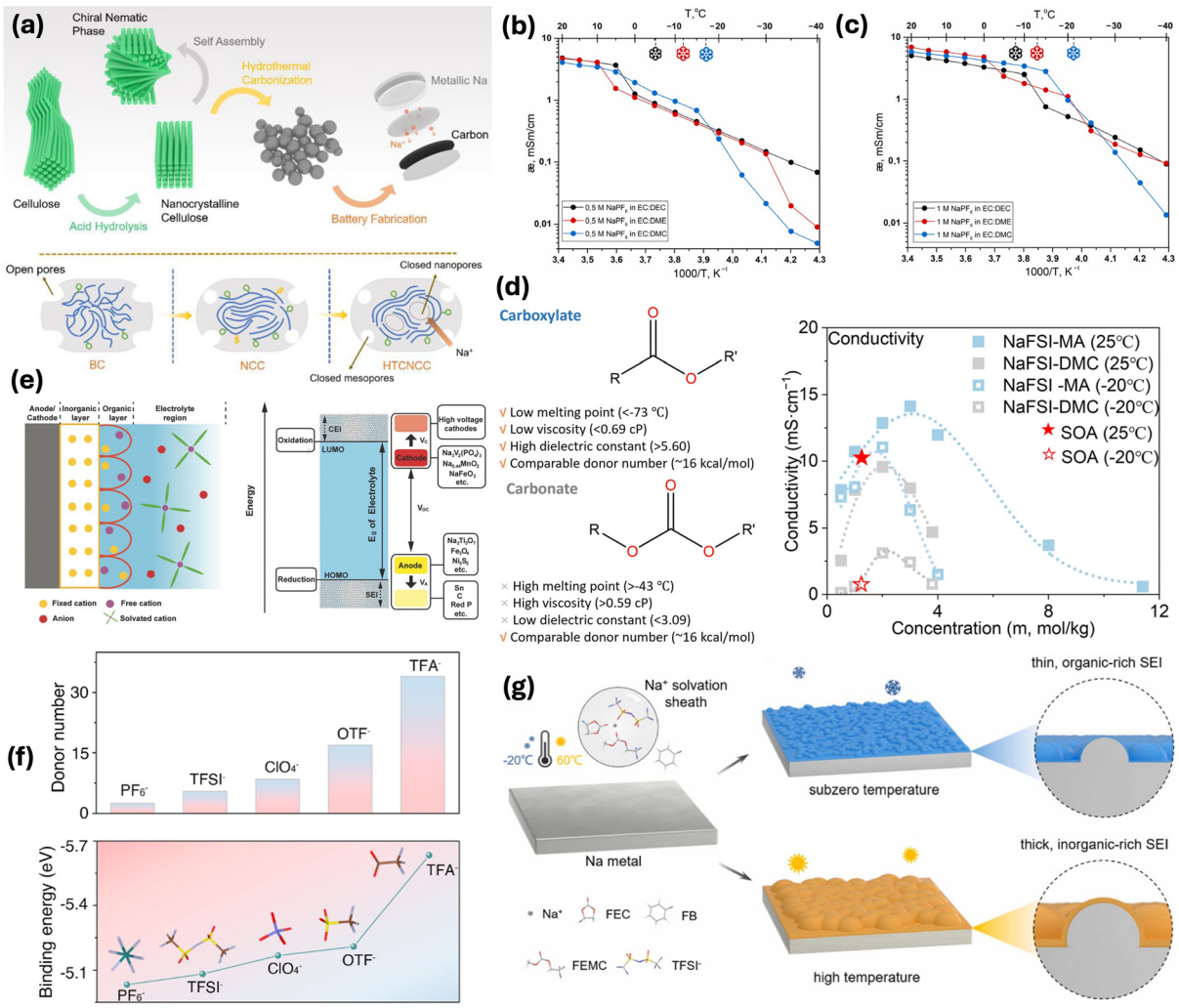

Fig. 4 (a) Schematic illustration of the synthesis strategy and microstructure regulation for achieving high ICE (BC: bulk cellulose; HTC: hydrothermally carbonized; NCC: nanocrystalline cellulose).[45] Temperature-dependent specific conductivity of (b) 0.5 M $NaPF_6$, (c) 1 M $NaPF_6$ in binary mixtures (1 : 1 v/v) from +20 °C to −40 °C. Snowflake symbols on the temperature axis indicate the onset of "wet snow" conditions.[56] (d) Solvent effects on bulk electrolyte conductivity: comparison of NaFSI–DMC and NaFSI–MA electrolyte systems.[58] (e) Interfacial structure and formation mechanisms of SEI/CEI in SIBs. The blue region shows the electrolyte's stability window (E_g); red and yellow squares mark cathode (V_C) and anode (V_A) potentials, with V_{OC} as the open-circuit voltage.[72] (f) Donor number of commonly used anions, and binding energy of Na^+ with anions.[11] (g) Schematic illustration of temperature-dependent Na deposition and SEI formation in the WT electrolyte, highlighting Na^+ coordination with fluorinated carbonates/$TFSI^-$, small spherical Na and thin organic-rich SEI at low temperature, and larger spherical Na with thick inorganic-rich SEI at high temperature.[15]

Open Access Article. Published on 20 August 2025. Downloaded on 18.02.26 05:05:09.
This article is licensed under a Creative Commons Attribution 3.0 Unported Licence.

defect density in the bulk cellulose (BC) precursor (Fig. 4(a)). However, quantitatively correlating pores, heteroatoms, and defects with the electrochemical performance, particularly the ICE of carbon anodes, remains challenging, and tailoring the microstructure through precursor pretreatment and modification is essential for enhancing ICE. Moreover, a deeper understanding of the relationship between microstructural features and sodium storage behavior is crucial for rational electrode design. Titanium-based anodes, such as $Na_2Ti_3O_7$ and $NaTi_2(PO_4)_3$, offer structural resilience but are limited by poor electronic/ionic conductivity,[47] necessitating pseudocapacitive engineering[34] or heteroatom doping[48] to enhance kinetics, approaches that struggle to offset the intrinsic limitations at extreme temperatures. Conversion-type materials such as $MoSe_2$, FeS exhibit high theoretical capacities but undergo drastic volume expansion during redox reactions, leading to electrode pulverization, while LT conditions further slow reaction kinetics and destabilize electrode–electrolyte interfaces.[49] Alloy-based anodes, despite high capacities (>400 mAh g^{-1}), face severe volume changes (>250%) and Na^+ transport barriers due to electrolyte thickening and sluggish desolvation at LT, which limit practical deployment.[31,50] Even with carbon–matrix composites,[51] the interplay between nanostructuring and tap density reduction complicates scalability.[52] Across all anode categories, the combined effects of reduced ion mobility, unstable SEI layers, and irreversible structural degradation at LT highlight the critical need for integrated solutions, including electrolyte optimization and morphology engineering, to enable reliable low-temperature operation.

2.3. Electrolyte and SEI limitations

Electrolyte systems represent perhaps the most critical limitation for low-temperature SIB operation[10,53] for three reasons: (1) governing free ion concentration and mobility, which dictates overall electrolyte conductivity; (2) determining the composition of the cathode/solid electrolyte interphase (CEI/SEI) through decomposition products, thereby controlling interphase resistance; and (3) regulating solvent–cation interactions, which directly influence the de-solvation energy barrier during interfacial charge transfer.

Limitations in the low-temperature functionality of present SIB electrolytes arise from shortcomings in their bulk material properties and interfacial behavior. At low temperatures, increased electrolyte viscosity hampers ionic conductivity and slows Na^+ migration kinetics, while also exacerbating electrode–electrolyte incompatibility, leading to higher charge transfer resistance. Therefore, optimizing the selection and combination of electrolyte solvents, salts, and additives is crucial for enhancing the performance of SIBs under low-temperature conditions. A significant rise in electrolyte resistance occurs with decreasing temperature, primarily due to the elevated freezing/melting points of nonaqueous carbonate solvents and the diminished solubility of conductive salts.[54,55] Conventional formulations based on carbonate solvents exhibit drastically reduced ionic conductivity as temperatures drop, as presented in Fig. 4(b and c), eventually reaching their freezing points below −20 °C and causing catastrophic battery failure.[56,57] The increased viscosity of these electrolytes at low temperatures directly impacts sodium-ion transport, while simultaneously raising the energetic barrier for desolvation at electrode interfaces. In contrast, carboxylate-based electrolytes offer superior ionic conductivity at low temperatures due to their low viscosity and high dielectric constant, outperforming traditional carbonates (Fig. 4(d)). However, their high reactivity hinders stable interphase formation, and while high salt concentrations can promote anion-derived SEI for improved cycling, excessive decomposition raises interfacial resistance, limiting low-temperature performance.[58]

The SEI is a passivation layer formed *via* electrolyte decomposition on electrode surfaces, plays a crucial role in stabilizing SIBs, but undergoes significant structural and compositional alterations at low temperatures. Comprising an inorganic-rich inner layer and an organic-dominated outer layer, the SEI ideally acts as an electronic insulator while maintaining high ionic conductivity.[59–61] However, the formation dynamics, including solvent reduction, growth, and deposition, are governed by electrolyte composition. This modulates interfacial impedance and promotes electrolyte degradation, thereby shortening battery lifespan.[62,63] Characterization techniques like XPS, FTIR, SEM, and TEM, initially developed for LIBs, have been adapted for SIBs, while computational methods such as quantum chemical calculations and first-principles molecular dynamics provide deeper insights into SEI evolution.[64–67] Recent findings suggest SEI films formed under high vacuum are thinner and less dense than traditionally believed,[68] challenging classical SEI theories that fail to fully explain anomalies like graphite shedding[69] and coulombic efficiency decline[70] in electrode–electrolyte mismatches. In SIBs, the sodium-based SEI is more soluble than its lithium counterpart, leading to higher dissolution rates and impedance-induced degradation.[71,72] Fig. 4(e) presents a simplified schematic of the anode/cathode interfaces in SIBs, highlighting the formation of SEI and CEI layers. According to Goodenough's energy band model, the formation and stability of these interphases are governed by the electrolyte's electrochemical stability window, defined by its HOMO–LUMO gap (E_g). For a battery system to operate effectively, E_g must either encompass the electrochemical potentials of both electrodes or allow controlled decomposition of the electrolyte to form stable interphases. In high-energy systems like SIBs, where the cell voltage is pushed to extremes, the former condition is rarely met. Instead, practical electrode/electrolyte systems typically rely on the latter mechanism, forming a stable SEI on the anode and/or a CEI on the cathode to ensure long-term performance and stability.[72] At low temperatures, SEI stability further deteriorates due to sluggish formation kinetics, resulting in NaF-rich layers with increased porosity, micro-cracking, and ionic resistance exceeding 500 Ω cm^2.[10] Additionally, the SEI becomes more brittle, fracturing under volume changes during Na^+ insertion–extraction, triggering continuous SEI reformation and electrolyte consumption that accelerates capacity fade. While electrolyte additives like

© 2025 The Author(s). Published by the Royal Society of Chemistry

Open Access Article. Published on 20 August 2025. Downloaded on 18.02.26 05:05:09.
This article is licensed under a Creative Commons Attribution 3.0 Unported Licence.

fluoroethylene carbonate (FEC) and sodium nitrate ($NaNO_3$) improve SEI properties, their efficacy drops below −30 °C due to extremely slow reaction kinetics.[13] The structural and compositional evolution of SEI on Na metal electrodes remains poorly understood, necessitating further theoretical studies and alternative SEI models to address the performance limitations of SIBs in extreme environments.

Another critical challenge in SIBs is the high energy barrier for sodium ion desolvation at the electrode–electrolyte interface, which becomes increasingly energy-intensive at low temperatures and induces significant charge transfer impedance, thereby limiting battery performance in cold environments. The desolvation energy of Na^+ is governed by solvent and anion interactions, with the Gutmann donor number (DN) quantifying solvation capacity as presented in Fig. 4(f). High-DN solvents enhance salt dissolution but impede interfacial kinetics due to strong Na^+ coordination, while high-DN anions like trifluoroacetate (TFA^-, DN = 34.0 kcal mol^{-1}) competitively occupy the inner solvation sheath, reducing solvent coordination and desolvation barriers.[11] However, TFA^-'s strong Na^+ binding in glyme-based (G2) electrolytes causes poor salt dissociation, yielding low ionic conductivity (0.20 mS cm^{-1} *vs.* 7.59 mS cm^{-1} for $NaPF_6$-G2) due to limited ion mobility. The solvation theory, first proposed by Miertuš *et al.*, has been revisited to refine the understanding of electrolyte behavior in SIBs.[73] Since 2015, research has identified EC–PC binary mixtures as optimal solvents for SIBs, benefiting from weaker Na^+–solvent interactions compared with Li^+, thus enhancing ion transport dynamics.[74–76] However, at low temperatures, desolvation resistance and SEI impedance remain debated as primary limitations,[77] with conventional electrolyte formulations struggling to balance stability across broad temperature ranges. The solvation structure, dictated by ion–ion, ion–dipole, and dipole–dipole interactions, plays a crucial role in electrolyte performance,[78,79] yet its temperature dependence remains largely unexplored.

Moreover, the temperature-dependent chemical structure of the SEI directly governs the electrochemical reversibility of sodium anodes at low temperatures through distinct mechanistic pathways. At subzero temperatures (−20 °C), the SEI formed in the wide-temperature electrolyte exhibits an organic-rich composition (higher C content: 18.8% *vs.* 7.8% at RT) with reduced inorganic fluoride content (15.7% *vs.* 29.2% at RT), creating a thinner interfacial layer with enhanced sodiophilicity. This organic-dominated SEI structure, shown in Fig. 4(g), facilitates rapid Na^+ diffusion through weak interfacial forces and pore diffusion mechanisms, directly correlating with the observed 16-fold impedance reduction (from ~31 000 Ω to ~1830 Ω) and improved coulombic efficiency (83.9%). Conversely, at elevated temperatures (60 °C), the SEI transitions to an inorganic-rich structure (34.5% F content) dominated by thermally stable compounds like NaF and Na_2CO_3, which provides robust passivation against high-temperature parasitic reactions but exhibits higher ionic resistances.[15] The mechanistic basis for this temperature-responsive behavior lies in the altered thermodynamic reaction pathways: low temperatures favor organic species formation through fewer reaction steps, while elevated temperatures promote multi-step inorganic compound formation and organic species dissolution.

Additionally, Wang *et al.* designed a temperature-adaptive electrolyte (SMTA) by dissolving $NaPF_6$ in a mixture of MeTHF, THF, and Anisole (AN), where AN modulated solvent interactions to suppress side reactions at high temperatures and prevent salt precipitation at subzero conditions.[80] This approach enabled stable electrochemical performance across a wide temperature range (−60 to 55 °C) by leveraging dipole–dipole interactions, offering a new paradigm for wide-temperature electrolyte design. Despite these insights, both models oversimplify the issue, neglecting key factors such as interfacial double layers, concentration gradients, and anion effects, while conventional characterization techniques fail to capture transient solvation dynamics. Furthermore, the inclusion of sodium metal-related studies in low-temperature sodium-ion battery research serves as the most fundamental platform for understanding interfacial phenomena that directly translate to practical SIB systems. Unlike insertion-type anodes where SEI formation is complicated by host structure interactions, sodium metal provides an ideal model system for isolating and characterizing temperature-dependent SEI chemistry, electrolyte decomposition mechanisms, and interfacial kinetics. These fundamental insights are directly applicable to emerging anode-free SIB configurations and inform the design of electrolyte formulations, SEI-modifying additives, and interfacial engineering strategies for conventional hard carbon anodes operating under low-temperature conditions where interfacial resistance becomes the dominant performance limitation. Advancements in AI and machine learning, alongside novel spatiotemporal interface characterization methods, may offer deeper insights into solvation and SEI behavior, enabling the development of improved low-temperature electrolyte formulations for SIBs.[81]

At low temperatures, both electrolyte ionic conductivity and interfacial resistance critically influence sodium-ion battery performance, but interfacial resistance often becomes the dominant limiting factor due to the formation of thicker, more resistive SEI layers that impede Na^+ charge transfer despite moderate bulk ionic conductivity; electrolyte formulations that optimize solvent composition and additives to form thin, inorganic-rich SEI can substantially reduce this interfacial barrier. Simultaneously, electrode materials govern LT cycling through their intrinsic Na^+ diffusion kinetics, structural stability, and surface chemistry. Materials with open frameworks, doping strategies, and nanostructuring facilitate faster ion transport and minimize mechanical degradation, while favorable electrode–electrolyte interfacial compatibility enhances SEI stability and mitigates impedance growth. Therefore, a holistic approach optimizing both electrolyte interphase properties and electrode design is essential to achieve robust and efficient sodium-ion battery operation under subzero conditions.

Open Access Article. Published on 20 August 2025. Downloaded on 18.02.26 05:05:09.
This article is licensed under a Creative Commons Attribution 3.0 Unported Licence.

3. Strategies for improving low-temperature performance

LT SIBs face significant thermodynamic and kinetic hurdles, including electrolyte freezing, sodium salt precipitation, and irreversible phase transitions in electrodes, which degrade ionic conductivity and structural stability. Sluggish Na^+ diffusion, exponential spikes in charge-transfer resistance, and brittle SEIs further impair performance below −20 °C, while real-world thermal shocks exacerbate capacity loss and safety risks. Electrolyte engineering emerges as a critical strategy, leveraging ether-based solvents, weakly solvating systems, and localized high-concentration formulations to enhance ionic mobility and SEI stability at subzero temperatures. Electrode modifications, such as doping, nanostructuring, and pseudocapacitive designs address kinetic barriers and structural strain, enabling faster ion transport and resilience against phase transitions. Fig. 5 summarizes the critical challenges and effective strategies for low-temperature SIBs.

3.1. Advanced electrolyte development

Electrolyte engineering represents the most direct approach for enhancing sodium-ion battery performance at low temperatures. To address this challenge, many strategies have been explored, including the use of multi-solvent systems, ionic liquids, and various additives, that play a crucial role in enhancing conductivity, SEI formation, and overall stability. Strategies like optimizing solvent selection, incorporating high-conductivity salts, and developing solid-state electrolytes are critical for enhancing SIB performance, especially in cold climates, ensuring better cycle life, and mitigating issues such as dendrite formation and SEI impedance.

3.1.1. Solvents for low-temperature electrolytes. The electrolyte solvent plays a crucial role, primarily by dissociating sodium salts to generate charge carriers, thereby influencing key battery properties. The solvent's impact on battery performance can be attributed to its ability to dissolve sodium salts, dictate ion solvation, participate in SEI formation, and ensure overall stability and safety. However, single-solvent systems often fail to meet operational demands under extreme conditions, such as low temperatures, necessitating the adoption of multi-solvent co-solutions. Given sodium's low reduction potential and the cathode's high oxidation potential, proton-type solvents are typically excluded. To achieve optimal low-temperature operation, an ideal solvent requires a low melting point (to avoid freezing), coupled with a high dielectric constant and minimal viscosity (to maximize ionic conductivity), alongside a low donor number (DN) to minimize solvent–cation interactions and enable rapid charge transfer kinetics.[58] Among various low-temperature-resistant co-solvents, organic (non-aqueous) co-solvents have shown the most promising development due to three key characteristics: low viscosity to maintain ion mobility in cold conditions, high sodium salt solubility facilitated by a high dielectric constant for efficient salt dissociation, and excellent chemical and electrochemical stability for constructing high-energy-density, high-voltage batteries. These attributes collectively enhance the commercial viability of SIBs, especially in low-temperature environments, where electrolyte optimization is critical for improving conductivity, SEI formation, and overall cycle life. Fig. 6 provides a comparison of selected solvents' physical properties.

Carbonate-based solvents are widely utilized in SIB electrolytes due to their strong ability to dissociate sodium salts.

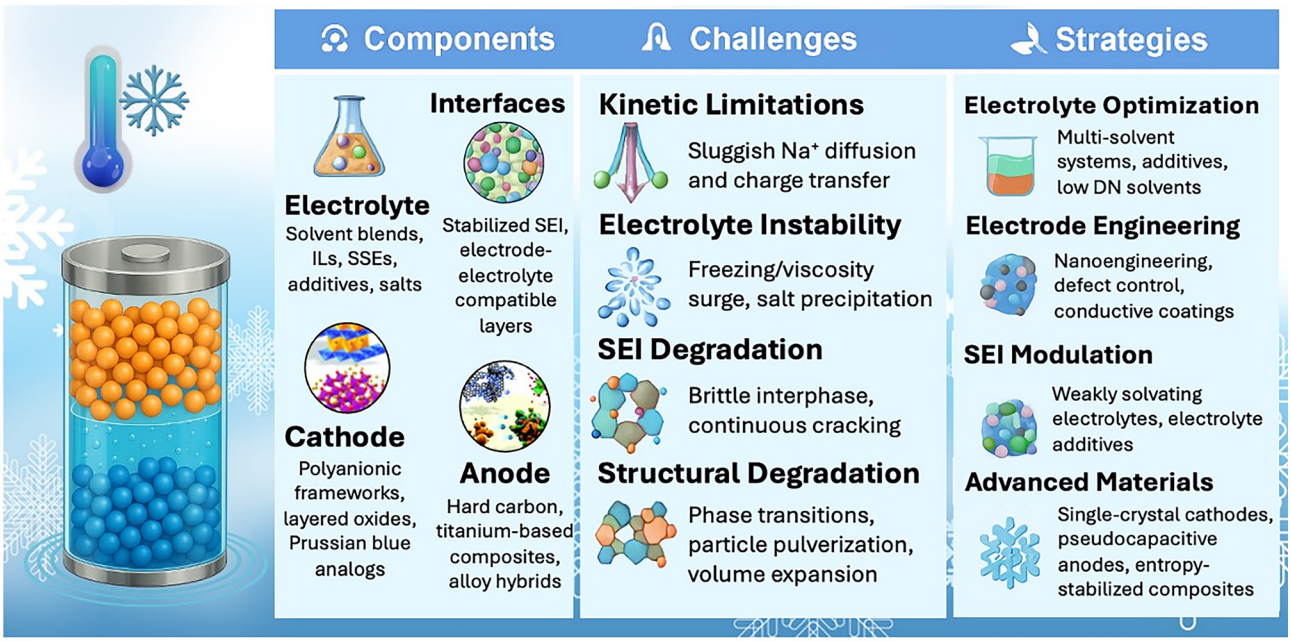

Fig. 5 Key challenges and strategic solutions for low-temperature SIBs.

© 2025 The Author(s). Published by the Royal Society of Chemistry

Open Access Article. Published on 20 August 2025. Downloaded on 18.02.26 05:05:09.
This article is licensed under a Creative Commons Attribution 3.0 Unported Licence.

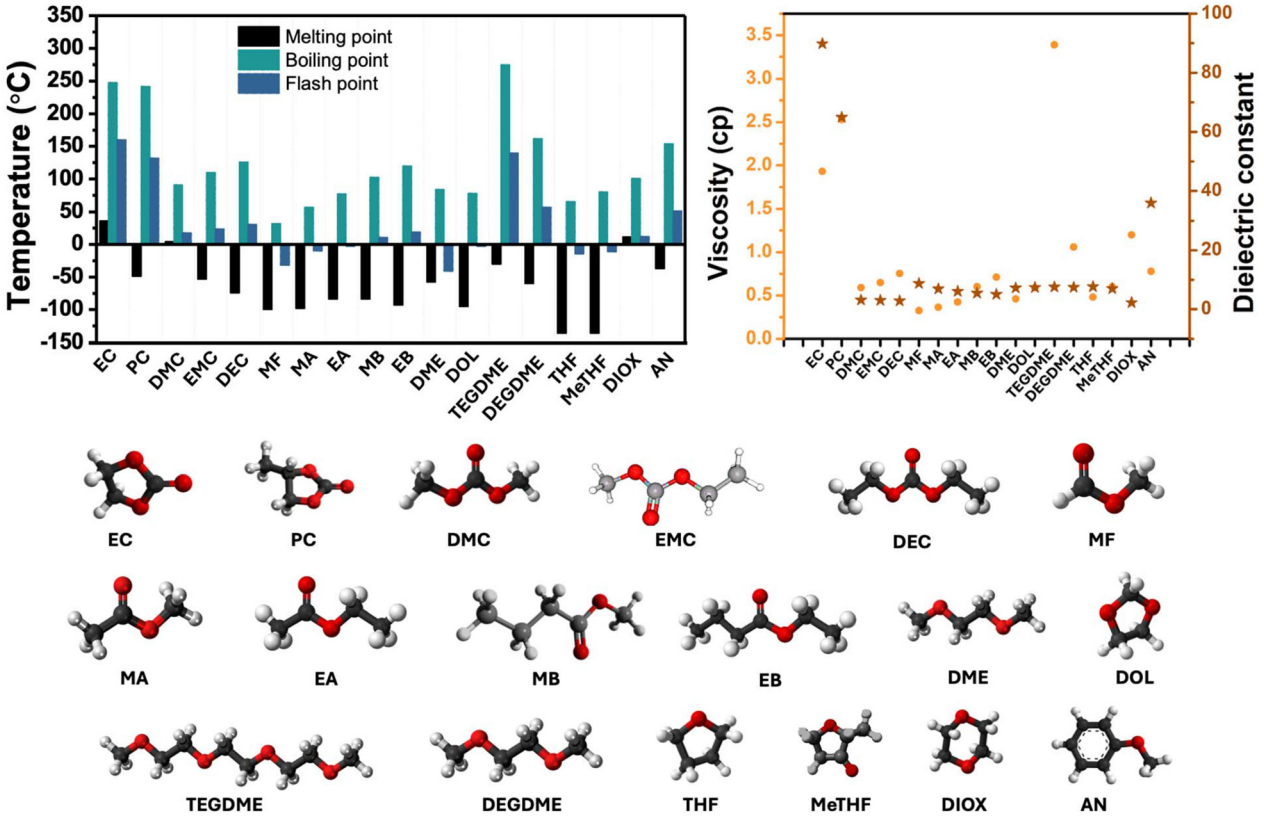

Fig. 6 Comparison of physical properties of selected solvents.

Ester-based solvents primarily consist of carbonate esters, including ethylene carbonate (EC), propylene carbonate (PC), dimethyl carbonate (DMC), diethyl carbonate (DEC), and ethyl methyl carbonate (EMC). The detailed physicochemical properties of these solvents have been extensively documented in the study by Zhu *et al.*[82] Notably PC, with a low melting point of −48.8 °C and minimal viscosity change at low temperatures, offers distinct advantages for low-temperature applications.[83] However, its poor electrode compatibility and high SEI resistance necessitate the incorporation of co-solvents.[84] Conversely, EC plays a crucial role in forming a stable SEI on the anode. However, its high melting point of approximately 36.4 °C poses a challenge for its application in low-temperature environments. Blending PC with EC balances their respective strengths, improving conductivity and electrode stability, as shown in Fig. 7(a and b).[83,85] Furthermore, PC–EC mixtures show stable electrochemical performance at subzero temperatures. At 0 and −25 °C, the PB/CNT composite cathode retains 81% (93 mA h g^{-1}) and 86% (76 mA h g^{-1}) of its capacity over 1000 cycles (Fig. 7(c)), with coulombic efficiencies ranging from 99.4% to 100.2% at −25 °C.[86] The high Fermi level of the Na metal anode, combined with the low LUMO energy of the EC–PC solvent, leads to the formation of a thick and resistive SEI on the anode surface. Furthermore, the strong coordination between EC/PC and Na^+ at low temperatures hinders efficient sodium-ion transport within the electrolyte and across the electrode–electrolyte interface, adversely affecting battery performance under such conditions.[87] Additionally, EMC, DMC, and DEC are frequently introduced into PC and EC-based systems to mitigate SEI impedance and enhance interface stability. Five 0.8 M $NaPF_6$ electrolytes with 2 wt% FEC additives, formulated using PC/EMC, PC/DMC, EC/EMC, EC/DMC, and EC/DEC (2 : 3 cyclic/linear carbonate ratio), exhibit ionic conductivity inversely correlated with viscosity, ranked as EC/DMC > PC/DMC > EC/EMC > PC/EMC > EC/DEC (Fig. 7(d)).

Temperature-dependent ionic conductivity, modeled *via* the Vogel–Tamman–Fulcher equation, reveals EC/DMC freezing at −30 °C, while PC/EMC maintains amorphous stability (−40 °C) with minimal conductivity loss, outperforming others in low-temperature resilience (Fig. 7(e and f)). While EC-based electrolytes offer stability advantages, their conductivity declines sharply below −30 °C due to crystallization.[88] To address these limitations and achieve superior electrochemical performance under extreme conditions, mixed solvent systems have been investigated beyond binary solvents.[89] Incorporating a co-solvent with a low melting point and low viscosity (such as methyl formate (MF), methyl acetate (MA), ethyl acetate (EA), ethyl propionate (EP), and ethyl butyrate (EB)) into multi-component electrolyte formulations mitigates electrolyte freezing and improves ionic conductivity at low temperatures.[57,90] Fig. 7(g) reveals the temperature-dependent bulk ionic conduc-

© 2025 The Author(s). Published by the Royal Society of Chemistry

Open Access Article. Published on 20 August 2025. Downloaded on 18.02.26 05:05:09.
This article is licensed under a Creative Commons Attribution 3.0 Unported Licence.

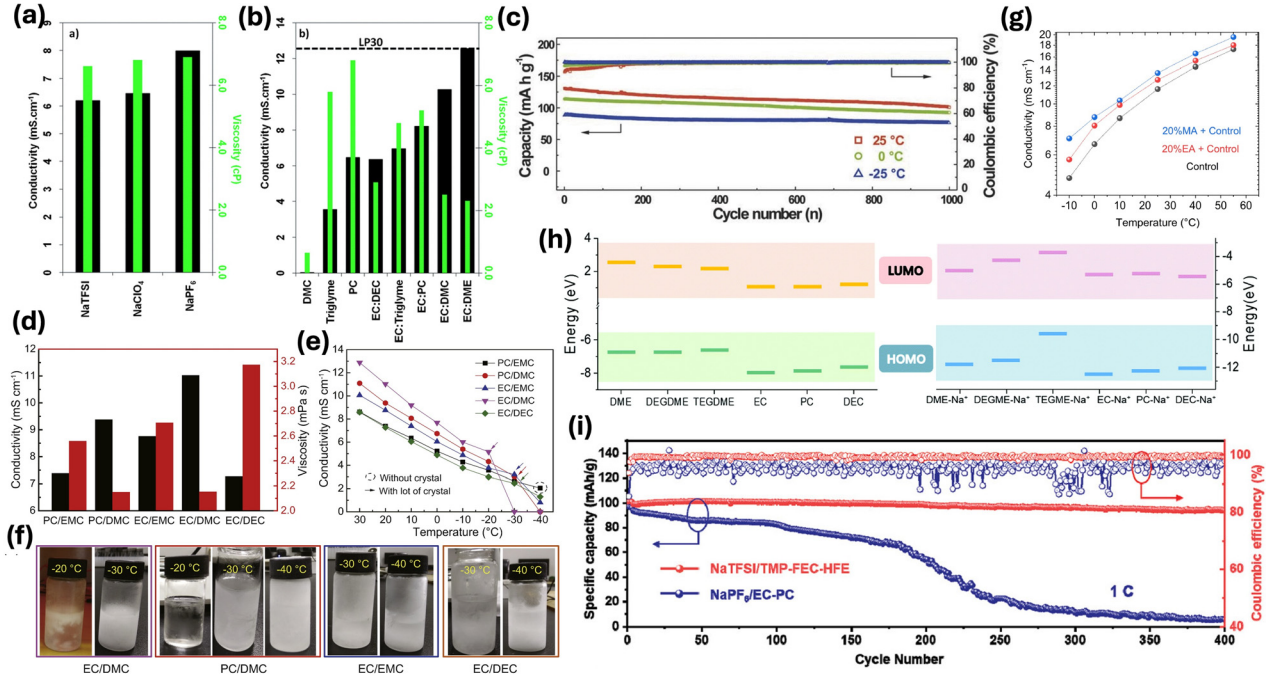

Fig. 7 Conductivity and viscosity of (a) PC-based electrolytes with 1 M of different Na salts, and (b) 1 M $NaClO_4$ in various solvents and solvent mixtures.[83] (c) Rate capabilities and long-term cycling performance at 2.4C of the PB/CNT cathode across various temperatures.[86] (d) Conductivity and viscosity of 0.8 M $NaPF_6$ electrolytes at 20 °C, (e) temperature-dependent conductivity of these electrolytes, and (f) visual appearance of the electrolytes at low temperatures.[88] (g) Temperature-dependent ionic conductivity of control (1 M $NaPF_6$ in EC–PC–DMC 1 : 1 : 2 vol%) and its 20% MA- or EA-modified variants.[91] (h) HOMO and LUMO energy levels of ether solvents and carbonate solvents, along with their respective solvent–ion complex.[95] (i) Electrochemical performance of Na/NVP full cells in $NaPF_6$/EC–PC and NaTFSI/TMP-FEC-HFE electrolytes.[100]

tivity of the control electrolyte (1 M $NaPF_6$ in EC–PC–DMC 1 : 1 : 2 by vol%) with a co-solvent (EA, MA) addition. The addition of 20% MA to the control electrolyte significantly enhanced ionic conductivity, achieving 13.65 mS cm^{-1} at 25 °C and 7.07 mS cm^{-1} at −10 °C, while EA-blended electrolytes exhibited intermediate conductivity due to EA's higher viscosity (0.46 cP *vs.* MA's 0.40 cP at 25 °C). Despite both MA and EA having low dielectric constants (6.68 and 6.0, respectively), MA's lower viscosity enables superior charge transport efficiency in low-temperature conditions.[91] While this design strategy improves low-temperature performance, it degrades electrolyte–electrode compatibility at elevated temperatures (45 °C). An alternative method employs weakly polar solvents[92–94] to minimize solvent–cation interactions and lower charge transfer resistance. Nevertheless, this approach suffers from inadequate salt dissociation[31] and diminished ionic conductivity resulting from reduced solvent polarity.

Beyond carbonates, ether-based solvents have recently gained attention due to their low viscosity, low melting point, high chemical stability, and thin, homogeneous SEI formation. Ether-based solvents mainly include linear ethylene glycol dimethyl ether (glyme), diethylene glycol dimethyl ether (DEGDME or diglyme), triethylene glycol dimethyl ether (triglyme), tetraethylene glycol dimethyl ether (TEGDME or tetraglyme), cyclic tetrahydrofuran (THF), and 1,3-dioxolane (DOL). Fig. 7(h) compares HOMO/LUMO levels of ethers (DME, DEGDME, TEGDME) and carbonates (EC, PC, DEC), revealing ethers' higher LUMO (enhanced reductive stability, thin SEI formation) and higher HOMO (weaker oxidative stability) *versus* carbonates. Ether solvents exhibit comparable HOMO/LUMO values among themselves, suggesting similar redox potentials and stability profiles during electrochemical processes.[95] Early studies challenged the assumption that graphite could not be used as an anode in SIBs,[96] demonstrating that ether electrolytes enable efficient sodium storage through the formation of ternary intercalation compounds.[97] Linear ethers, such as diglyme or tris(2,2,2-trifluoroethyl)phosphate (TFP), provide strong solvation capability,[98] while cyclic ethers like THF exhibit superior cryogenic properties due to weaker sodium-ion solvation energy.[99] Incorporating fluorinated solvents such as 1,1,2,2-tetra-fluoroethyl 2,2,3,3-tetrafluoropropyl ether (HFE) and FEC into trimethyl phosphate (TMP)-based electrolytes created a flame-retardant SMA-compatible system that displayed remarkable stability with capacity retention of 93.1% for over 400 cycles, massively outperforming the conventional EC–PC based and the diluent TMP-based counterparts, as shown in Fig. 7(i), *via* HFE-driven localized concentration elevation and suppressed TMP decomposition.[100] Furthermore, a low-solvation NaFSI/DMC : TFP electrolyte stabilized 4.2 V SIBs by suppressing SEI dissolution through the use of a low-polar TFP solvent, reducing free solvent *via* tailored solvation structures as illustrated in Fig. 8(a), and forming insoluble FSI^--derived SEI/CEI layers, which collectively mitigated interfacial degradation, transition metal dis-

© 2025 The Author(s). Published by the Royal Society of Chemistry

Open Access Article. Published on 20 August 2025. Downloaded on 18.02.26 05:05:09.
This article is licensed under a Creative Commons Attribution 3.0 Unported Licence.

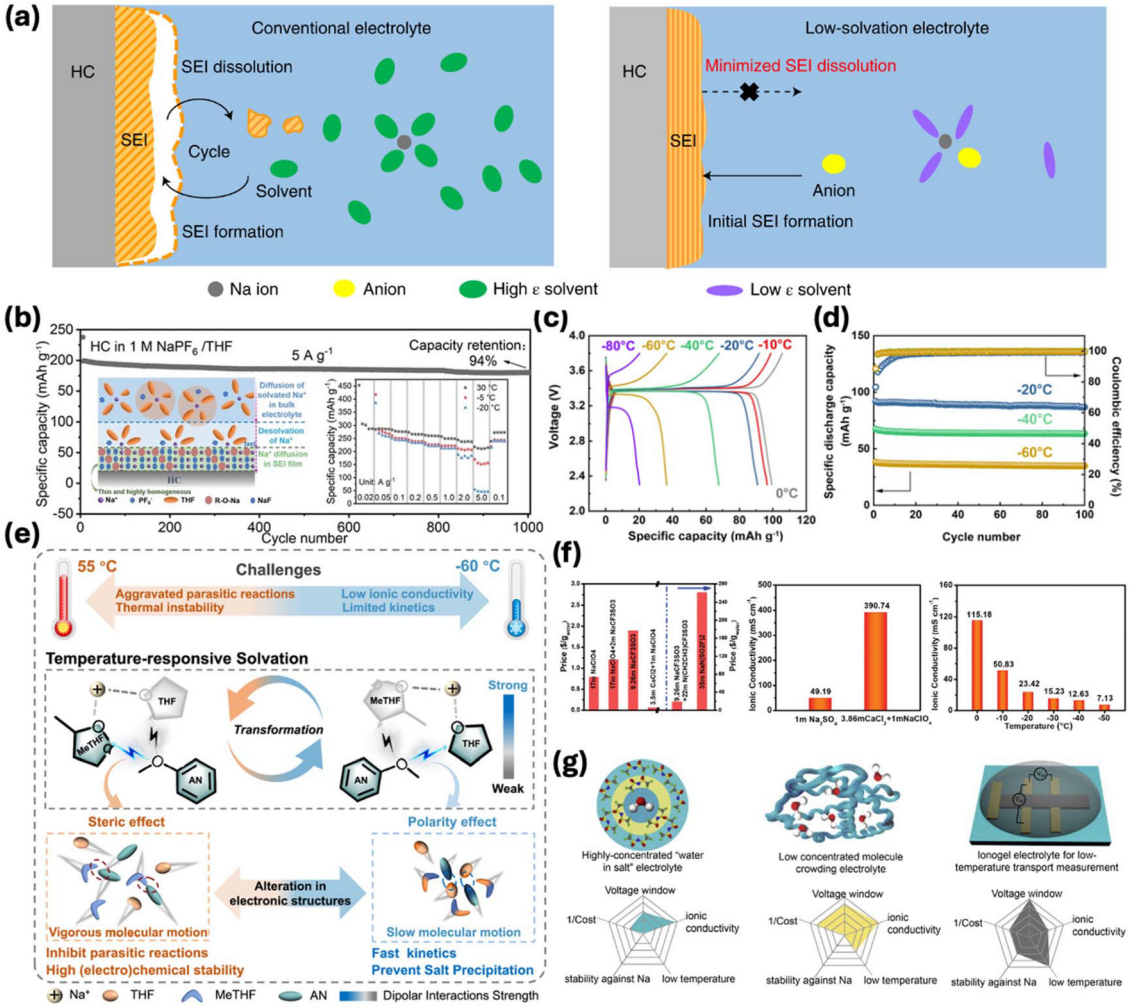

Fig. 8 (a) SEI behavior in conventional *vs.* low-solvation electrolytes.[63] (b) Long-term cycling performance in 1 M $NaPF_6$/THF.[92] (c) Galvanostatic charge–discharge voltage profiles at 22 mA g^{-1} from 0 °C to −80 °C, and (d) long-term cycling performance at 22 mA g^{-1} at −20 °C, −40 °C, and −60 °C.[10] (e) Schematic illustration depicting the challenges faced by wide-temperature electrolytes and the temperature-adaptive solvation structure transformation in the SMTA electrolyte.[80] (f) Electrolyte cost and conductivity comparison for ASIBs.[112] (g) Schematics and radar plots illustrating low-temperature transport properties of water-in-salt (WIS), molecular crowding, and conventional ionogel electrolytes.[113]

solution, and phase transitions for improved cycling stability.[63]

A weakly solvating electrolyte is highly suitable for low-temperature SIBs, as it facilitates faster ion desolvation by reducing the ion–solvent interaction strength, thereby lowering the desolvation energy barrier, the primary rate-limiting step at low temperatures. Additionally, the limited ability of the solvent to dissociate salt crystals promotes the formation of anion-rich solvation structures, leading to the preferential reduction of anions and the formation of an inorganic-rich SEI, which enhances ion transport across the interphase. Furthermore, the use of a low-polar solvent with weak solvent–solvent interactions results in a low freezing point and low viscosity, contributing to improved electrolyte performance under low-temperature conditions.[79] Commercial hard carbon delivers superior rate performance (212 mAh g^{-1} at 5 A g^{-1}) and low-temperature resilience (175 mAh g^{-1} at −20 °C, 74% of RT capacity) in weakly solvating THF electrolytes, outperforming carbonate-based systems with negligible capacity. This stability (90% retention after 1000 cycles) arises from THF-facilitated ion diffusion and a homogeneous SEI enriched with NaF/organic components, ensuring rapid Na^+ transport and interfacial durability as shown in Fig. 8(b).[92] Furthermore, Zhou *et al.* utilized a THF/DME cosolvent system to lower the Na^+ solvation kinetic barrier, enabling stable operation at −60 °C,[31] while Wang *et al.* incorporated DOL into DEGDME, achieving a highly stable Na||Na symmetric battery with a minimal 50 mV overpotential for over 2000 hours at −80 °C.[10] Remarkably, this electrolyte system maintained its liquid state even at −150 °C, and Na||$Na_3V_2(PO_4)_3$ showed significantly low temperature performance as shown in Fig. 8(c and d). Besides, Wang *et al.* introduced trimethylsilyl isocyanate (Si-NCO), an additive with a low LUMO level, to modify the solvation structure in a DEGDME/DOL-based electrolyte.[101] This modification

Open Access Article. Published on 20 August 2025. Downloaded on 18.02.26 05:05:09.
This article is licensed under a Creative Commons Attribution 3.0 Unported Licence.

enhanced PF_6^- anion involvement in the inner solvation shell, thereby improving electrolyte stability across a range of temperatures. As a result, the Na||HC half-cell retained 88.57% of its room-temperature capacity at −40 °C and maintained 94.50% capacity after 100 cycles. Despite the wide LT liquid windows of ether-based electrolytes, Na salt precipitation often occurs well above the solvent freezing point, drastically reducing ionic conductivity.

To address this limitation, Yang *et al.* developed a temperature-adaptive solvation structure by combining a strongly solvating solvent DEGDME, with a weakly solvating solvent THF.[102] As temperature decreases, THF increasingly participates in Na^+ solvation, shifting the solvation structure from DEGDME-dominant to THF-dominant, thereby preventing LT salt precipitation. Similarly, SMTA electrolyte leverages temperature-dependent dipole–dipole interactions, where AN preferentially interacts with MeTHF at elevated temperatures to suppress parasitic reactions and stabilize solvation structures, while binding strongly with THF at subzero temperatures to inhibit salt precipitation and enhance ion kinetics as shown in Fig. 8(e), enabling hard carbon anodes to operate stably from −60 °C to 55 °C.[80] However, although ether-based solvents excel in LT applications, their inherent poor oxidative stability and flammability constrain their operational voltage range. Integrating ester or fluorinated nitrile solvents offers a promising strategy to enhance oxidative resistance and improve high-voltage stability in composite electrolyte systems. The introduction of fluorinated ether solvents into carbonate systems has been shown to reduce solvation energy, enhance electrolyte stability, and support high-capacity retention at extremely low temperatures.[103,104] These innovations contribute to the development of robust low-temperature SIB electrolyte systems with improved cycle life and fast-charging capabilities.

Ionic liquids (ILs) have emerged as promising electrolyte components; they consist of organic anions and metal cations, with the ability to remain liquid even at low temperatures, such as −96 °C. Originally known as molten salts, they were renamed after their unique property of maintaining a liquid state at low temperatures.[105] Ionic liquids possess an asymmetric structure that allows them to dissolve a variety of high-concentration metal salts, offering several advantages over other electrolytes. ILs composed entirely of ions offer promising features for battery electrolytes, such as flame retardancy, broad electrochemical stability, and high ionic conductivity across wide temperature ranges, yet their performance is strongly influenced by ion pairing chemistry, with limitations including high viscosity, reduced molar conductivity at low temperatures, and the frequent use of highly fluorinated anions.[106] Further research demonstrated that FSI anions promote stable SEI formation, facilitating reversible sodium intercalation. Additionally, a composite electrolyte combining ionic liquids with ether was shown to prevent metallic sodium dendrite growth at −40 °C, resulting in high reversible capacity and excellent cycling stability.[107]

Aqueous or inorganic liquid solvents are advantageous due to their low cost, minimal pollution, and high conductivity compared with organic electrolytes.[108] However, traditional electrolytes suffer from poor conductivity at low temperatures, limiting their use in low-temperature electrochemical energy storage devices.[109] To address this, high-concentration aqueous electrolytes have been explored to improve electrochemical stability window and cycling stability. For instance, a high-concentration sodium salt solution (17 M $NaClO_4$ in water) exhibited excellent energy density and stable performance at −40 °C. Moreover, to address the limited solubility of single sodium salts, researchers have explored innovative electrolyte systems with sodium bisalt mixtures (*e.g.*, $NaClO_4$ + NaOTF, NaTFSI + NaOTF), dual-cation solutions (*e.g.*, 32 M KAc + 8 M NaAc), and inert cation-assisted highly concentrated electrolytes (*e.g.*, 9 M NaOTF + 22 M TEAOTF). These advanced formulations not only enhance salt solubility but also expand the electrochemical stability window, enabling improved performance in SIBs by mitigating precipitation issues and increasing available charge carriers. Despite this, the high cost of such electrolytes remains a challenge.[110,111] To mitigate this, inexpensive inorganic antifreeze solutions, such as a mixture of 3.86 M $CaCl_2$ and 1 M $NaClO_4$, have been used to enhance conductivity (7.13 mS cm^{-1} at −50 °C). $CaCl_2$ exhibits strong interactions with water molecules, disrupting the native hydrogen-bonding network and effectively lowering the freezing point of the optimized electrolyte.[112] The economic comparison of various electrolytes used in aqueous sodium ion batteries (ASIBs), as shown in Fig. 8(f), highlights the optimized electrolyte's cost-effectiveness, with a low price of $0.059 per g (per gram of water), underscoring its suitability for large-scale applications. Additionally, a molecular crowding aqueous electrolyte utilizing a poly(ethylene glycol) (PEG) network effectively confines water molecules and enables high-voltage operation, yet its freezing point (4 °C–8 °C) limits low-temperature applications. To overcome this, a water-in-ionogel (WIG) electrolyte (Fig. 8(g)) has emerged as a superior alternative, combining a high operational voltage (3.0 V) with low-temperature resilience by confining water molecules (10 wt%) in an ionogel network *via* hydrogen bonding, while maintaining low salt concentration (2 M NaTFSI) for cost-effective, high-energy, and freeze-resistant aqueous batteries, enabling operation at −25 °C.[113] Furthermore, multi-component solvent systems, such as the multi-component aqueous electrolyte (MCAE) solution with urea, DMF, and water, have shown promise by reducing water content and improving cycling stability.[114] These advances lead to more environmentally friendly, safe, and recyclable batteries, promoting large-scale energy storage applications.

Solid-state electrolyte (SSE) technologies offer advantages for cold-climate applications, particularly in transportation and energy, where safety risks due to rising electrolyte temperatures in accidents are a concern. Solid electrolytes can inhibit sodium dendrite growth, and among them, gel polymer electrolytes are gaining attention for their higher ionic conductivity and better interface properties, offering flexibility and mechanical softness.[115,116] Research has shown that polymer-based solid-state electrolytes (named PFSA-Na

© 2025 The Author(s). Published by the Royal Society of Chemistry

Open Access Article. Published on 20 August 2025. Downloaded on 18.02.26 05:05:09.
This article is licensed under a Creative Commons Attribution 3.0 Unported Licence.

membranes), exhibit excellent cycling performance and high coulombic efficiency at temperatures as low as −35 °C. These membranes also enhance the interface compatibility over cycles.[117] Multifunctional phosphate gel electrolytes (MTP92) demonstrate exceptional performance across a broad temperature range (−20 °C to 70 °C), achieving a wide electrochemical stability window of 5.1 V (*vs.* Na^+/Na) and maintaining high ionic conductivity (>1.0×10^{-3} S cm^{-1}) even at −20 °C, attributed to their stable hydrogen-bonded polymer network. Moreover, the $Na_3V_2(PO_4)_3$||MTP92||Na cell showcases outstanding cycling stability, retaining 93.2% capacity after 3000 cycles at room temperature, and 97.6% after 1200 cycles at −10 °C.[118] Additionally, polyether solid electrolytes, enhanced by additives like $NaPF_6$ and fluorine doping, have improved ionic conductivity and stabilized the interface.[119,120] Studies also indicate that modifying the crystalline–amorphous transition of solid electrolytes and adjusting their crystalline forms can further enhance ion transport, reduce interfacial resistance, and improve sodium metal deposition uniformity, thus advancing the performance of solid sodium-ion batteries (SSIBs) in low-temperature environments.[121]

Moreover, high-entropy electrolytes (HEEs) exhibit exceptional electrochemical and thermal stability, enabling their application in diverse high-energy battery systems (Li, Na, Mg, Zn) and promoting lighter, cheaper, and more reliable devices.[122] The concept of entropy, central to the second law of thermodynamics, quantifies disorder in a system and governs electrolyte stability through Gibbs free energy ($\Delta G = \Delta H - T\Delta S$). HEEs exploit this principle by integrating multiple components to maximize configurational entropy (S_{conf}), thereby reducing ΔG and enhancing stability. In HEEs, increased S_{conf} disrupts ordered structures (*e.g.*, crystallinity in salts or solvent networks), promoting ionic mobility and solubility. Excess entropy (S_{ex}) further influences properties like solvent–solute interactions and ion dynamics in liquid systems. Rational tuning of these entropic contributions including S_{conf}, S_{ex}, mixing entropy (S_{mix}), and reaction entropy enables tailored electrolyte performance.[123,124]

HEEs are categorized into four types: non-aqueous liquid, aqueous liquid, polymer (solid/gel), and all-solid inorganic electrolytes.[122,125] In liquid HEEs, multi-solvent or multi-salt formulations increase S_{conf}, weakening ion–solvent interactions and suppressing crystallization. This enhances ionic conductivity *via* diverse solvation structures and LT operation through eutectic effects. Polymer HEEs utilize entropy-driven designs like copolymer matrices or filler additives to inhibit crystallization, improving mechanical strength and ion transport. Inorganic solid HEEs (*e.g.*, oxides, sulfides, halides) leverage entropy stabilization to achieve disordered structures that lower ion migration barriers, boosting ionic conductivity and reducing sintering temperatures. HEEs offer significant merits over conventional electrolytes: (1) enhanced salt solubility due to disrupted crystallization; (2) improved ionic conductivity *via* S_{ex}-driven ion collision networks and low-activation-energy pathways; (3) optimized LT performance from widened liquid ranges and modified interfacial kinetics; and (4) tunable stability windows and electrode compatibility. However, challenges persist in predicting HEE behavior due to compositional complexity, achieving long-term stability, and bridging laboratory designs with scalable applications. Despite these hurdles, HEEs represent a paradigm shift in electrolyte engineering, merging thermodynamic principles with materials innovation to advance energy storage.

3.1.2. Sodium salts for low-temperature electrolytes. Sodium salts play a critical role in electrolytes for SIBs working at low temperatures, which must exhibit high solubility, chemical stability, and a wide electrochemical stability window (ESW) to ensure efficient ion transport and cell performance. Anion selection critically influences these properties: electron-withdrawing ligands such as PF_6^-, BF_4^- enhance Na^+ mobility by delocalizing negative charge, while their size and dissociation ability govern conductivity and SEI stability.[81] The interplay between salt properties such as lattice energy ($NaPF_6$ > $NaClO_4$ > NaTFSI/NaOTf/>$NaBF_4$) and HOMO levels (NaOTf > $NaClO_4$ > NaTFSI > $NaBF_4$ > $NaPF_6$) dictates oxidation tendencies and electrolyte compatibility, narrowing viable candidates to those balancing ESW, thermal stability, and toxicity, though their performance in LT conditions remains underexplored. For instance, $NaPF_6$, with its large anion radius and weak Na^+ interactions, excels in carbonate-based electrolytes due to high conductivity and stable operation,[126] whereas $NaBF_4$'s small volume and rapid dissociation favor LT kinetics despite limited standalone SEI-forming capability. $NaClO_4$, though cost-effective and beneficial in aqueous systems for reducing hydrogen bonding and enhancing solvation,[110] poses safety risks due to oxidative instability.[83] Ionic liquids paired with $NaClO_4$ achieve low viscosity and high conductivity, outperforming NaTFSI,[127] while fluorinated dual-salt systems ($NaOTf/NaBF_4$) improve coulombic efficiency and electrode stability.[128] However, it should be noted that using BF_4^- standalone use remains limited due to insufficient SEI formation capability. Moreover, the density functional theory (DFT) can compute reduction potentials of sodium salts, correlating them with SEI quality. The salts with low-reduction potentials (NaTFSI) impede inorganic-rich SEI formation, causing high overpotentials, while high-reduction potential salts (NaFSI, $NaClO_4$) form nonuniform SEI layers due to excessive reactivity. Intermediate-reduction potential salts like NaOTf (1.02 V) and $NaPF_6$ (0.75 V) balance reactivity and solubility, enabling smooth, uniform SEI formation, with NaOTf particularly suited for low-temperature applications due to favorable solubility and moderate reduction kinetics.[10]

Electrolyte salt concentration further affects LT performance as illustrated in Fig. 9(a).[81] Conventional electrolytes (~1 M) balance ionic conductivity and moderate voltage stability but suffer from solvent/anion decomposition at high voltages, limiting their electrochemical window. In contrast, highly concentrated electrolytes reduce free solvents, forming anion-rich solvation structures that suppress solvent decomposition and enable wider voltage windows, yet their high viscosity and cost hinder practical use. Conversely, ultralow-concentration electrolytes (ULCE) reduce both cost and temperature sensitivity.

Open Access Article. Published on 20 August 2025. Downloaded on 18.02.26 05:05:09.
This article is licensed under a Creative Commons Attribution 3.0 Unported Licence.

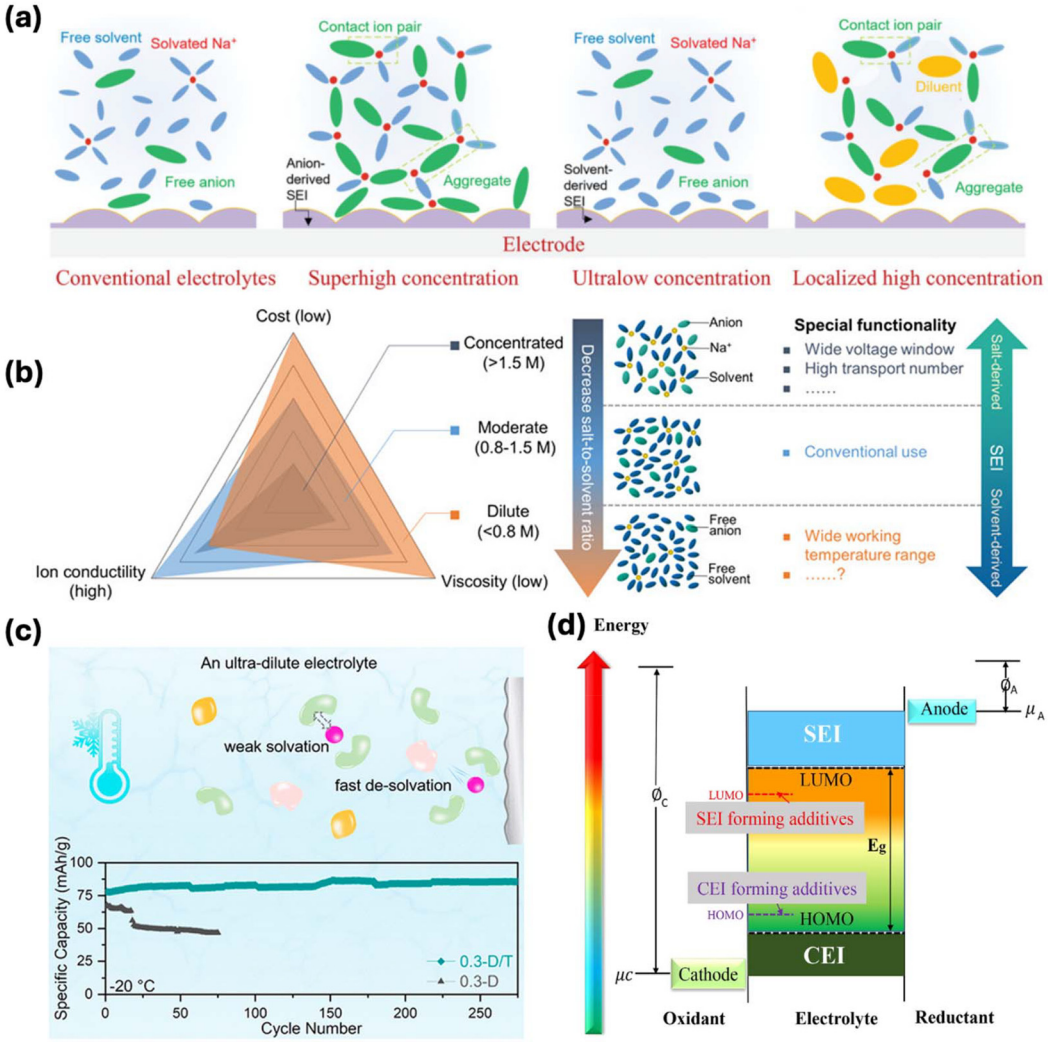

Fig. 9 (a) Solvation and interfacial models for different electrolyte concentrations.[81] (b) Overview of electrolyte concentration effects on physicochemical properties, molecular interactions, and interfacial components.[129] (c) LT (−20 °C) cycle performance of Na/NVP cells with 0.3 M $NaPF_6$ in DEGDME (0.3-D) and 0.3 M $NaPF_6$ in DEGDME/THF electrolyte (0.3-D/T).[130] (d) Schematic open-circuit energy diagram of functional electrolytes with SEI and CEI additives, showing electrolyte stability window (E_g), electrode functions (ϕ_A, ϕ_C), and chemical potentials (μ_A, μ_C).[133]

Research comparing conventional 1 M $NaPF_6$ electrolytes with 0.3 M $NaPF_6$ (ULCE) in EC/PC (1 : 1, volume ratio) has shown that ULCE provides superior capacity retention and kinetic performance at subzero temperatures, attributed to the formation of an organic-rich SEI and enhanced Na^+ transfer Fig. 9(b).[129] Similarly, dilute ether-based electrolytes (0.3 M $NaPF_6$ dissolved in DEGDME/THF) have demonstrated lower impedance and polarization voltage at LT by weakening Na^+–solvent interactions, facilitating faster ion transport. The dilute electrolyte showed lower impedance (10 Ω), reduced polarization (~0.01 V), and improved Na deposition at −20 °C, enabling the Na/NVP cell to deliver ~80 mAh g^{-1} with low overpotential as shown in Fig. 9(c).[130] However, excessively low salt concentrations reduce the number of charge carriers, narrowing the voltage window and promoting cation–solvent co-intercalation. Localized high-concentration electrolytes (LHCE) are emerging as a promising alternative,[131] balancing high ionic conductivity with low viscosity through a unique solvated structure, thereby optimizing Na^+ transport and SEI stability.[132] The synergy between electrolyte salt composition, concentration, and solvation structure holds the key to advancing LT performance in SIBs,[81] enabling improved energy density and long-term cycling stability under extreme conditions.

3.1.3. Additives for low-temperature electrolytes. Electrolyte additives offer a promising approach; though present in small amounts, they significantly enhance the performance of SIBs, especially at low temperatures. These additives facilitate the stable formation of the SEI by participating in chemical and electrochemical reactions at the electrode/electrolyte interface. They also modify the solvation structure of sodium ions, improving electrolyte properties such as viscosity, conductivity, and electrochemical stability, thus expanding the voltage window, increasing battery capacity, and enhancing ICE. Certain additives can reduce side reactions at

© 2025 The Author(s). Published by the Royal Society of Chemistry

Open Access Article. Published on 20 August 2025. Downloaded on 18.02.26 05:05:09.
This article is licensed under a Creative Commons Attribution 3.0 Unported Licence.

low temperatures, promoting safe battery operation by preventing sodium evolution and offering flame-retardant or overcharge protection. Fluoride-based additives, particularly fluorinated carbonates like FEC, are commonly used to stabilize SEI films and protect electrodes, although their concentration must be carefully controlled to prevent degradation. Both SEI and CEI additives stabilize electrode–electrolyte interfaces by aligning their electrochemical stability windows within the electrolyte's HOMO–LUMO gap, as presented in Fig. 9(d). SEI additives, with lower LUMO levels, reduce first to form an anode-protective layer, while CEI additives, with higher HOMO levels, oxidize preferentially to create a cathode-stabilizing layer, preventing electrolyte degradation.[133,134] Sulphide and nitrile additives, such as dimethyl sulfoxide (DMSO)[135] and adiponitrile (ADN),[136] can further improve low-temperature performance by enhancing ion migration and preventing dendrite formation. Other additives, including organic solvents like methanol[137] and inorganic salts like $CaCl_2$,[112] help mitigate electrolyte freezing and improve ionic conductivity at low temperatures. Furthermore, the combination of these additives optimizes the SEI structure, reduces interfacial impedance, and enhances the overall cycling stability and performance of SIBs under extreme conditions. Studies show that FEC, when combined with adiponitrile (ADN), enhances SEI composition by promoting NaF and NaCN complex formation, reducing side reactions, and improving cycling stability.[136] Additionally, modifying the electrolyte's solvation structure can facilitate Na^+ desolvation at LT, addressing sluggish ion transport. For instance, adding 6 vol% ethyl sulfate (ES) to a 1.0 M NaFSI in EC/PC/DEC (1/1/4, v/v/v) (denoted as BLTE) electrolyte system alters Na^+ coordination, weakening its interaction with solvent molecules and enhancing desolvation kinetics, enabling stable operation even at −40 °C.[138] Similarly, fluorinated carbonate and low-melting-point fluorobenzene additives lower electrolyte viscosity at subzero temperatures, mitigating solvent–Na^+ affinity and accelerating desolvation, thereby preserving battery capacity retention and cycling stability at −20 °C. These advancements highlight electrolyte additives as a key strategy for improving LT SIB performance by optimizing SEI properties and ion transport mechanisms.[15]

Improving the low-temperature performance of SIBs hinges on the optimization and the development of novel electrolytes and additives that enhance conductivity, stability, and SEI formation. Multi-solvent and hybrid electrolyte systems, along with ionic liquids and solid-state alternatives, offer promising solutions. The incorporation of carefully selected additives also contributes significantly to improving ion transport and preventing undesirable side reactions. Collectively, these advancements pave the way for more efficient and durable SIBs in cold-climate applications.

3.2. Cathode engineering approaches

The selection of cathode materials for LT-SIBs is governed by several key factors to ensure optimal performance. A suitable cathode material must exhibit a high redox potential to maintain a high discharge voltage, along with rapid Na^+ diffusion and electron transport capabilities to mitigate polarization effects under LT conditions. Additionally, a stable bulk structure is essential to accommodate Na^+ insertion and extraction while minimizing internal structural stress, which becomes more challenging at low temperatures. Furthermore, the material should possess strong environmental adaptability and be feasible for large-scale production. Current research on LT cathode materials primarily focuses on polyanionic compounds, TMOs, and PBAs, each offering distinct advantages in terms of electrochemical stability and structural robustness under extreme conditions.

3.2.1. Polyanion-type electrode materials. Polyanion-type electrode materials, composed of tetrahedral anion units $(XO_4)^{n-}$ or their derivatives $(X_mO_{3m}+1)^{n-}$ (X = S, P, Si, As, Mo, W), feature strong covalent bonding between MO_x polyhedra and transition metals, imparting high thermal stability and making them ideal for applications where safety is a priority.[139] Characterized by their robust 3D framework of polyhedral anionic units, they provide stable Na^+ diffusion channels that enhance cycling stability at high potentials, making them promising cathode candidates for SIBs.[140] However, their inherently low electronic conductivity limits specific capacity, especially under low-temperature (LT) conditions. To address these drawbacks, researchers have employed strategies such as element doping, carbon coating, and particle size reduction to improve conductivity and Na^+ transport rates. Among polyanionic materials, Na Super Ionic Conductor (NASICON)-type compounds (with $Na_3M_2(XO_4)_3$ formula wherein M denotes V, Fe, Ni, Mn, Ti, and others, and X denotes P, S, Si, and others), particularly $Na_3V_2(PO_4)_3$ (NVP), are extensively studied due to their stable open framework composed of corner-sharing PO_4 tetrahedra and VO_6 octahedra, facilitating Na^+ mobility even at LT. Nevertheless, NVP suffers from poor intrinsic conductivity, prompting modifications like carbon coating[36,38] and hybridization with conductive nanostructures such as graphene oxide (GO)[141] and carbon nanotubes (CNTs),[142] which significantly enhance electronic connectivity and LT cycling performance.

For instance, a tailored NASICON-type carbon-coated NVP (NVP@C) nanocomposite demonstrates outstanding rate capability over a broad temperature range (−20 to 55 °C). In particular, at −20 °C and a high rate of 10C, the NVP@C cathode retains a discharge capacity of 91.3 mAh g^{-1}, corresponding to 85.2% of its room-temperature performance as shown in Fig. 10(a and b), while delivering an average output voltage of 2.86 V *vs.* Na^+/Na.[38] Similarly, NVP@rGO composites enable rapid charge transfer, achieving discharge capacities of 112 mAh g^{-1} at 0 °C and 91.3 mAh g^{-1} at −20 °C. Multi-component coatings, such as $Na_3V(PO_4)_2$, V_2O_3, and reduced graphene oxide on NVPOF cathode ($Na_3V_2(PO_4)_2O_2F$), have been engineered to improve interfacial compatibility, accelerate Na^+ transport, and reduce interfacial resistance, and have excellent low temperature applicability (88 mA h g^{-1} at 0.2C and long cycling for 500 cycles at 3C) at −40 °C.[37] The fluorine-free $Na_3V(PO_4)_2$ phase, known for its high ionic conductivity and stability, facilitates rapid Na^+ diffusion, while the high electronic conductivity of V_2O_3 and rGO enhances electron trans-

Open Access Article. Published on 20 August 2025. Downloaded on 18.02.26 05:05:09.
This article is licensed under a Creative Commons Attribution 3.0 Unported Licence.

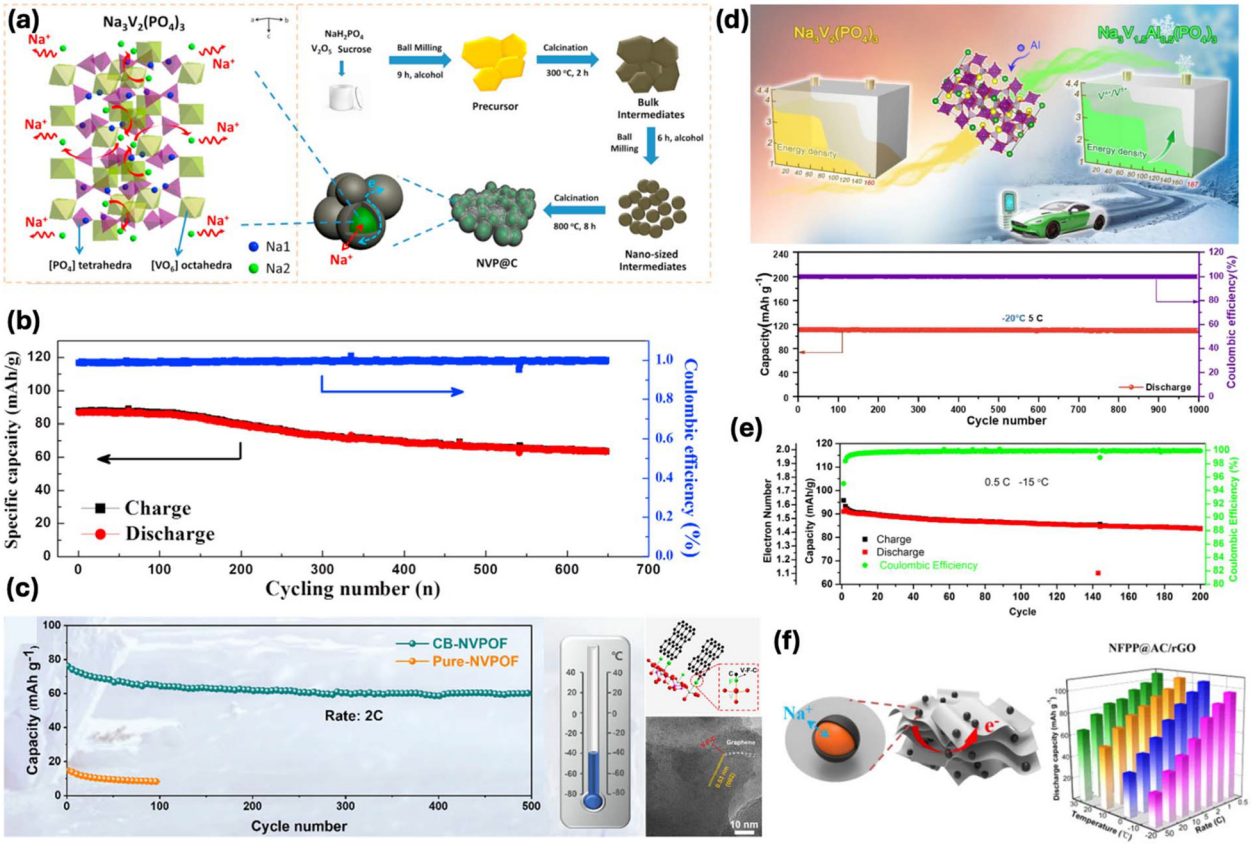

Fig. 10 (a) Schematic representation of Na^+ transport *via* hopping mechanism within the crystalline lattice, and synthesis route of the NVP@C nanocomposite. (b) Extended cycling stability of NVP@C evaluated at −20 °C.[38] (c) Cycling performance of the pure NVPOF and CB-NVPOF at −40 °C.[143] (d) Long-term cycling stability of $Na_3V_{1.5}Al_{0.5}(PO_4)_3$ at a rate of 5.[145] (e) Cycling performance of NVCP at 0.5C and −15 °C in a three-electrode setup.[146] (f) Bar graph showing NFPP@AC/rGO discharge capacities across various rates and temperatures.[148]

port across the electrode. Similarly, the incorporation of interfacial chemical bonding, such as V–F–C bonds formed through ball-milling NVPOF with graphene (CB-NVPOF), enhances electronic conductivity, facilitates Na^+ diffusion, and improves interfacial stability at −40 °C, while delivering 56 mA h g^{-1} at a high rate of 10C, and the capacity retention is ~80% after 500 cycles at 2C as shown in Fig. 10(c).[143] Despite these advantages, surface coatings can stabilize phase transitions and sustain cycling performance at low temperatures, but they often compromise energy density. Moreover, their long-term instability and susceptibility to fracture can degrade performance over extended cycling, highlighting the need for further advancements in coating design for durable SIB operation in extreme conditions.

Furthermore, nanostructuring represents another powerful approach for addressing diffusion limitations in cold environments. By reducing the characteristic dimensions of active materials, the diffusion path lengths for sodium ions decrease quadratically, partially offsetting the reduced diffusion coefficients at low temperatures. While nanostructuring is effective, it introduces a critical drawback in the form of poor tap density, which suppresses the attainable volumetric energy density. Additionally, strategies such as anionic substitution (*e.g.*, replacing PO_4^{3-} with F^- or O^{2-})[144] and cation doping (*e.g.*, V^{3+} with Al^{3+}, Mn^{2+}, Cr^{3+}, Sc^{4+})[33,145,146] have successfully increased discharge voltage, boosting energy density beyond 500 Wh kg^{-1} while improving cycling stability. For instance, Al^{3+} substitution for V^{3+} in the NASICON structure enables the V^{4+}/V^{5+} redox at 4.0 V *vs.* Na^+/Na, allowing full V^{2+}–V^{5+} redox activity and three-electron transfer. This results in a reversible capacity of 163 mAh g^{-1} with 98.9% retention after 1000 cycles at 5C and −20 °C (Fig. 10(d)).[145] Similarly, $Na_3VCr(PO_4)_3$, utilizing highly reversible 1.5-electron redox reactions ($V^{3+}/V^{4+}/V^{5+}$), exhibits excellent cycling stability at −15 °C and 0.5C, retaining 95% of its initial discharge capacity after 200 cycles as shown in Fig. 10(e).[146] These advancements underscore the importance of tailored material engineering in enhancing the viability of polyanionic cathodes for next-generation SIBs. The high cost and toxicity of vanadium have driven interest in Fe-based alternatives such as $Na_4Fe_3(PO_4)_2(P_2O_7)$ (NFPP), which offer superior structural stability and cost-effectiveness for low-temperature applications.[84,147] The NFPP@AC/rGO composite synergistically integrates amorphous carbon-coated NFPP nanoparticles within cross-linked rGO networks, combining NFPP's intrinsic 3D ion channels with the enhanced electrical conductivity and dispersion provided by the AC/rGO matrix as

© 2025 The Author(s). Published by the Royal Society of Chemistry

Open Access Article. Published on 20 August 2025. Downloaded on 18.02.26 05:05:09.
This article is licensed under a Creative Commons Attribution 3.0 Unported Licence.

illustrated in Fig. 10(f), thereby enabling ultrafast and temperature-resilient sodium storage (78 mAh g^{-1} at 20C and 30 °C, 42 mAh g^{-1} at 20C, and −15 °C) through stabilized charge transport and reduced polarization.[148] Mn^{2+}-doped NFPP, further enhanced with graphene modifications, has demonstrated promising electrochemical performance, delivering a discharge capacity of 85.3 mAh g^{-1} at 0.2C with 96.8% capacity retention rate after 180 cycles at 0.5C at −20 °C. The incorporation of Mn^{2+} effectively lowers the Na^+ migration energy barrier and narrows the lattice bandgap, thereby improving Na^+ diffusion kinetics and electrical conductivity, making it a viable candidate for practical SIB applications in extreme conditions.[149]

3.2.2. Layered transition metal oxide (TMO). Layered TMO cathodes offer significant advantages, including cost-effective and abundant precursors, simple synthesis, high power density, and environmental sustainability. Their general formula, Na_xTMO_2 ($0 < x \leq 1$, TM = Mn, Cr, Co, Ni, Fe, V, Cu, *etc.*), can be divided into layered ($x > 0.5$) and tunnel ($x < 0.5$) structured based on the crystal characteristics, allowing for extensive tunability.[140,150] In the layered structure, sodium ions are alternately distributed between MO_2 layers, which consist of stacked metal–oxygen octahedra. These cathodes are classified as P-type or O-type based on Na^+ occupation in prismatic or octahedral sites, respectively, with the thermodynamically stable P2- and O3-type structures, referring to the ABBA and ABCABC oxygen stacking, gaining attention due to their favorable electrochemical properties.[151] P2-type oxides exhibit superior Na-ion conductivity and structural stability compared with their O3-type counterparts, enhancing power density and cycling performance. However, their lower initial Na content reduces storage capacity relative to O3 materials, and structural O–P phase transitions during (de)intercalation often compromise cycling stability. Furthermore, the layered TMO materials at low temperatures face challenges like irreversible phase transitions, particle cracking, transition metal dissolution, and diminished ionic conductivity.

To improve LT performance, strategies focusing on bulk and interfacial reaction optimization, such as ionic doping, crystal structure control, and constructing P/O biphasic

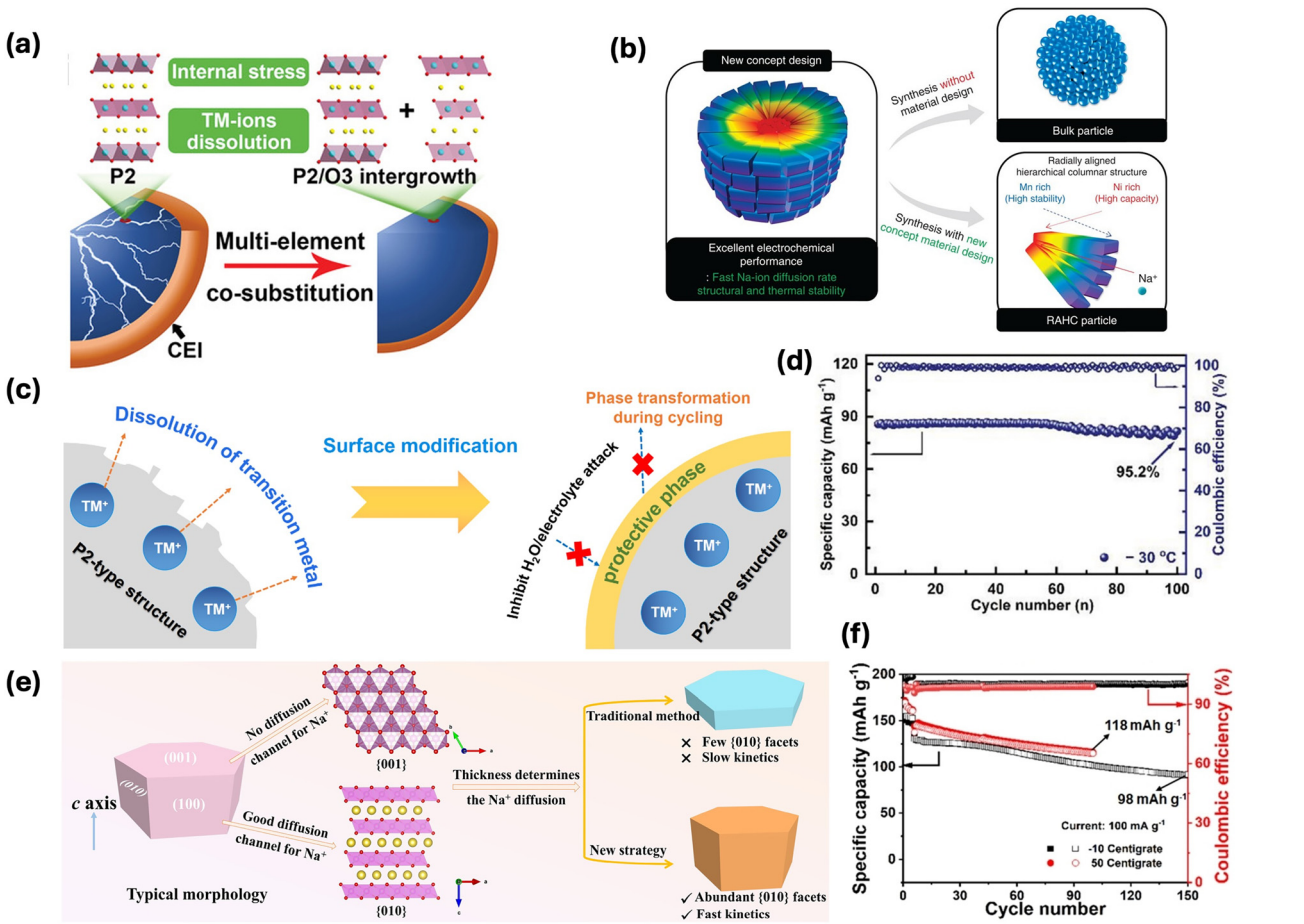

Fig. 11 (a) Schematic showing cathode structural evolution with and without multi-element co-substitution during cycling.[152] (b) Schematic illustration of the novel cathode concept (left) *versus* conventional bulk (top right) and engineered radially aligned columnar microstructure (bottom right).[153] (c) Protective effect on the bulk structure.[41] (d) Cycling stability of $Na_{0.696}Ni_{0.329}Mn_{0.671}O_2$ at −30 °C.[154] (e) Design principle for enhancing Na^+ diffusion kinetics in Na-based LTMOs without compromising volumetric energy density.[156] (f) The stable long-term cycling at −10 °C and 50 °C with 100 mA g^{-1} of crystalline MnHCF-S-170.[163]

Open Access Article. Published on 20 August 2025. Downloaded on 18.02.26 05:05:09.
This article is licensed under a Creative Commons Attribution 3.0 Unported Licence.

materials show promising potential. Fig. 11(a) shows a multi-element co-substitution strategy that enhances structural stability and mechanical integrity of a layered oxide cathode, enabling superior Na storage performance.[152] The major drawback of these materials is the occurrence of irreversible structural phase transitions (*e.g.*, P2–OP4 or P2–O2) under deep desodiation, leading to volume expansion of up to 23% and intracrystalline cracking, ultimately degrading capacity retention and cycling stability.[39,152] While ion doping and surface coatings have mitigated these issues at room temperature, low-temperature operation presents additional challenges, including sluggish Na^+ diffusion kinetics and irreversible phase transformations, making the practical application of layered transition metal oxide cathodes in SIBs highly challenging. P2-type layered oxides, such as $Na_{0.67}Ni_{0.1}Co_{0.1}Mn_{0.8}O_2$, have been optimized by substituting Mn sites with Co/Ni, reducing electrostatic interactions and enhancing Na^+ ion diffusion.[40] In addition, Hwang *et al.* presented a high-density spherical particle composed of radially assembled columnar structures with a gradient chemical composition: a Ni-rich inner core ($Na[Ni_{0.75}Co_{0.02}Mn_{0.23}]O_2$) transitioning to a Mn-rich outer shell ($Na[Ni_{0.58}Co_{0.06}Mn_{0.36}]O_2$). This unique structure (referred to as RAHC), shown in Fig. 11(b), facilitates the redox activity of $Ni^{2+/3+/4+}$ primarily within the material, minimizing direct contact with the electrolyte and suppressing undesirable side reactions. As a result, the RAHC material exhibits superior cycle retention under prolonged cycling at −20 °C (RAHC: 80.0% *vs.* bulk: 49.2% for 300 cycles).[153]

Moreover, elemental doping can suppress phase transitions and mitigate surface degradation in TMOs at low temperatures, as evidenced by the surface-enriched niobium-doped P2-type $Na_{0.78}Ni_{0.31}Mn_{0.67}Nb_{0.02}O_2$, which exhibited exceptional rate capability (65 mAh g^{-1} at 50C, 25 °C) and ultra-low temperature endurance (70 mAh g^{-1} after 1800 cycles at −40 °C with 76% retention).[41] The preconstructed surface layer stabilizes P2-NaMNNb by suppressing the P2–P2′ phase transition, inhibiting surface degradation, and blocking water ingress as shown in Fig. 11(c), thereby enhancing rate performance and cycling stability. Nb^{5+} doping also modulates Na^+ occupancy in P2-type cathodes, favoring the Na_e site with a lower ion diffusion energy barrier, a mechanism similarly observed with Sb^{5+} doping,[42] where high-valence cation substitution induces coulombic repulsion, prompting Na^+ migration to Na_e sites and potentially enhancing LT performance. Furthermore, a P2-type $Na_{0.696}Ni_{0.329}Mn_{0.671}O_2$ with a high Na_e/Na_f ratio by increasing Na^+ content achieved stable cycling (~95.2% capacity for 100 cycles) at −30 °C (Fig. 11(d)).[154] Another approach by introducing the nanostructuring concept, the O3-type $NaCrO_2$ synthesized *via* electrospinning, yields ultralong nanowires with improved electronic/ionic transport pathways and structural resilience during sodiation–desodiation cycles.[155] However, the use of nanomaterials reduces tap density, necessitating new crystal design strategies to boost diffusion kinetics and tap density for commercial viability particularly in LTMOs, where tailoring hexagonal prism thickness along the Na^+-diffusive {010} facets can simultaneously optimize ion transport and tap density, as illustrated in Fig. 11(e). A large-size single-crystalline O3-type $NaCrO_2$ cathode with an exposed (010) active facet, prepared using an acetate-assisted solid-phase reaction, leveraged special crystal modulation and single-crystal properties to achieve a remarkable capacity retention of 97.2% after 100 cycles at 1C, even under harsh conditions like −20 °C.[156]

Similarly, a hysteresis-abated P2-type $NaCoO_2$ cathode demonstrated high-rate, stable charge–discharge cycles.[157] This highlights the potential of tailored crystal structures for enhancing performance while addressing the challenges associated with nanomaterials. Ultimately, advancements in TMO synthesis at low temperatures emphasize the integration of P2 and O3 phases to enhance energy density and cycling stability in SIBs. By adjusting transition metal cation potentials and sodium ion content, these cathodes exhibit superior electrochemical characteristics compared with single-phase materials. Recent advancements include the creation of P2/O3 high-entropy mixed-phase oxides by incorporating fluorine codoped with copper, iron, and titanium (NaMnNiCuFeTiOF), maintaining 97.3% of initial capacity at −20 °C over 300 cycles, with a wide temperature (−40 to 50 °C) cycling performance at 200 mA g^{-1}.[158] Additionally, a Ni/Cu codoped P2/O3 $Na_{0.75}Mn_{1-y}Ni_{y-z}Cu_zO_2$ cathode demonstrated capacity of 58.2 mAh g^{-1} after 300 cycles at −40 °C without capacity fading.[159] In addition, the incorporation of LiF into $Na_{0.67}Mn_{0.5}Co_{0.5}O_2$ resulted in the formation of a biphasic P3/O3 cathode, significantly enhancing cycling stability, with ~85% capacity retention after 100 cycles at 0.2C (30 mA g^{-1}), compared with just 54% for the unmodified cathode. Moreover, at −20 °C, the modified cathode retained 70% of its room-temperature capacity (92 mAh g^{-1} at 0.1C/15 mA g^{-1}) and showed 94% capacity retention over 100 cycles.[160] The unique phase structure modulation of these biphasic materials presents significant potential for practical applications.

3.2.3. Prussian blue (PB) and Prussian blue analogs (PBAs). Prussian blue ($Fe[Fe(CN)_6]_3{\cdot}xH_2O$) and Prussian blue analogs ($Na_{2-x}M[Fe(CN)_6]_{1-y}\square y{\cdot}nH_2O$) ($x$ = 0–2, M are usually single or multitransition metals such as Fe, Mn, Co, Ni, *etc.*, □ signifies the vacancies occupied with coordinated water)[161] have gained significant attention as promising cathode materials for SIBs due to their minimal volume changes (<1%) during cycling, high energy densities (~500–600 Wh kg^{-1}), and excellent rate performance at room temperature.[43,162] The open framework of PBAs provides broad Na^+ diffusion channels, with DFT calculations indicating that the 24d site is the most energetically favorable position for Na^+, enabling efficient transport through ⟨100⟩ channels with a 3.59 Å diameter. The weak interaction between Na^+ and CN^- further enhances Na^+ mobility, but PB-type materials suffer from low electronic conductivity, necessitating strategies to maintain good electrical contact between electrode particles and current collectors. Composite PB/CNT materials have demonstrated improved electrochemical performance, retaining 81% and 86% of capacity after 1000 cycles at 0 °C and −25 °C, respectively.[86] Unlike conventional high-temperature calcined cathodes, PBAs are synthesized *via* water-based coprecipitation,

© 2025 The Author(s). Published by the Royal Society of Chemistry

Open Access Article. Published on 20 August 2025. Downloaded on 18.02.26 05:05:09.
This article is licensed under a Creative Commons Attribution 3.0 Unported Licence.

though rapid crystallization introduces structural voids and interstitial water, which degrade capacity and cycle life at LT.[44] To address these challenges, electrostatic spray-assisted coprecipitation has been used to synthesize high-crystal-quality $Na_{1.86}Ni[Fe(CN)_6]_{0.88}\cdot 1.88H_2O$, retaining 87% of capacity after 440 cycles at 0 °C and delivering 54 mAh g^{-1} at −25 °C.[89] Further innovations, such as the "water-in-salt" nanoreactor strategy[163] and chelator-assisted coprecipitation,[164] have yielded PBAs with enhanced stability. The $Na_{2-x}MnFe(CN)_6$ (MnHCF-S-170) exhibited a high specific capacity of 164 mAh g^{-1} at 10 mA g^{-1} and impressive all-climate performance ranging from −10 °C to 50 °C, as shown in Fig. 11(f) for Na ion storage,[163] while $Na_2Co_{0.7}Ni_{0.3}[Fe(CN)_6]$ ($Co_{0.7}Ni_{0.3}HCF$) maintained 109 mAh g^{-1} at −30 °C without activation.[164] Despite their advantages, PBAs require careful handling due to the potential release of free cyanide ions, and their poor ion/electron conductivity at LT exacerbates polarization, necessitating conductive composite materials to balance conductivity and capacity.[165] The development of high-crystallinity PBAs and dehydration treatments is critical for further improving LT performance. As cathode materials significantly influence battery cost (up to 60%) and energy density, layered cathodes and PBAs present compelling choices for SIBs, with polyanionic frameworks offering enhanced stability but lower capacities. Layered oxides, which can be adapted to LIB production lines, hold strong commercialization potential. Despite these advances, significant challenges remain in cathode development for low-temperature applications. Irreversible phase transitions still occur in many materials during deep cycling at sub-zero temperatures, and particle cracking from thermal stress continues to limit long-term durability. Future research directions point toward hierarchical architectures that combine nanoscale primary particles into microscale secondary structures, *in situ* doping techniques that create compositional gradients, and increasingly sophisticated computational approaches using machine learning to identify promising new material compositions with inherently favorable low-temperature characteristics.

3.3. Anode material modifications

The development of anode materials for SIBs has progressed alongside cathode advancements, with carbonaceous materials, TMOs or transition metal sulfides (TMSs), and intermetallic and organic compounds emerging as key candidates.[166] Based on the sodiation/desodiation mechanism, these materials can be classified into insertion, conversion, and alloying reaction types. Insertion anodes, such as carbon-based materials and titanium-based oxides, enable Na^+ intercalation,[167,168] while conversion-type anodes, including TMOs and TMSs, undergo redox-driven phase transformations to store sodium.[169] Alloying reaction anodes, primarily Na–Me (Me = group 14 or 15 metals) compounds, offer high capacities[170,171] but suffer from severe volume expansion and self-pulverization.[169] The alloying-, conversion-, and conversion–alloying-type electrode materials, along with schematic representations of their respective reaction mechanisms, are illustrated in Fig. 12(a). A major limitation in SIB anodes is the sluggish reaction kinetics caused by the large ionic radius of Na^+ (1.02 Å), which hinders fast ion diffusion and storage.[166,172] To enhance performance, ideal anode materials should exhibit stable redox potentials, structural integrity, high electronic and ionic conductivity, and simple, resource-efficient synthesis. Unlike LIBs, graphite is unsuitable for SIBs due to its insufficient Na^+ storage capability, and Na metal anodes pose significant safety concerns. For LT-SIBs, anode materials are similarly categorized into insertion/intercalation, conversion, and alloying types, yet must also overcome additional challenges such as sluggish Na^+ diffusion and reduced electrochemical activity at sub-zero conditions. Addressing these limitations requires further research into electrode design, surface engineering, and electrolyte optimization to enhance Na^+ storage and cycling stability in both ambient and low-temperature environments.

3.3.1. Insertion materials

3.3.1.1. Carbon-based materials. Carbonaceous and titanium-based oxides have been extensively explored as anode materials for SIBs due to their ability to accommodate Na^+ ions through an insertion mechanism. Among carbon-based materials, both graphitic and non-graphitic carbons have been investigated,[167,173,174] with hard carbon emerging as a promising candidate due to its relatively high capacity (~300 mAh g^{-1}) and low operating potential (~0 V *vs.* Na^+/Na).[175,176] Despite its advantages, the precise Na^+ storage mechanism in disordered carbon structures remains debated.[177–180] Meanwhile, titanium-based oxides offer an alternative due to their low operational voltage and cost-effectiveness.[168]

Hard carbon (HC) is considered one of the most promising anode materials for SIBs due to its low embedded sodium platform, higher capacity, ample interlayer spacing, and abundant sodium storage sites.[181] Researchers have categorized HC's capacity–voltage curves into two distinct regions: a sloping region above 0.1 V and a plateau region below 0.1 V,[182] with nanopore filling occurring during the low-potential plateau.[183] HC's nanopores, including both open and closed pores, play a critical role in sodium storage, with closed pores providing additional active sites and promoting the formation of quasi-metallic clusters that enhance both storage capacity and plateau capacity.[184–186] Conversely, open pores increase the surface area exposed to the electrolyte, leading to thick SEI films that reduce the initial coulombic efficiency (ICE), while closed pores also contribute to SEI formation, as evidenced by *in situ* small-angle neutron scattering studies.[187,188] Fig. 12(b) schematically illustrates how alkali metal ions (Li^+, Na^+) are stored in hard carbon (HC). Current sodium storage mechanisms encompass three primary behaviors: sodium adsorption on defects/graphite surfaces, intercalation within graphite layers, and nanopore filling, described by proposed models including "adsorption–insertion", "insertion-filling", "adsorption-filling", and "multistep processes".

These mechanistic distinctions are electrochemically discernible through their characteristic voltage profiles, manifesting as either plateaus or sloping regions during operation.

Open Access Article. Published on 20 August 2025. Downloaded on 18.02.26 05:05:09.
This article is licensed under a Creative Commons Attribution 3.0 Unported Licence.

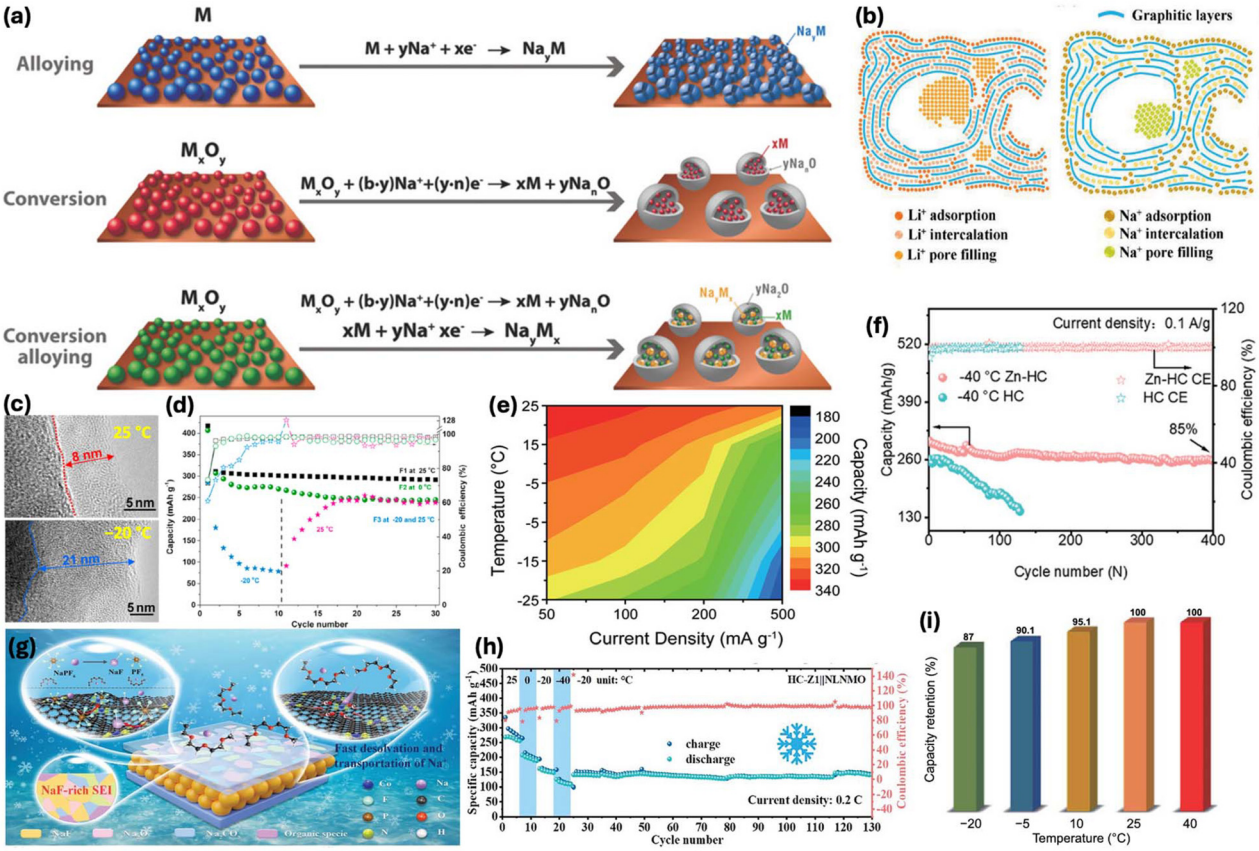

Fig. 12 (a) Schematic reaction mechanisms of alloying, conversion, and conversion–alloying.[215] (b) Schematic illustrations of Li^+, and Na^+ storage in HC.[189] (c) TEM images of cycled hard carbon at 25 °C and −20 °C; (d) capacity retention and coulombic efficiency of $Na_{3.5}V_2(PO_4)_2F_3$/HC full cells at −20 °C, 0 °C, and 25 °C.[85] (e) Capacity retention across temperatures at different current densities.[192] (f) Cycling stabilities of Zn-HC and HC at −40 °C.[196] (g) Schematic of Na^+ storage kinetics at low temperature. (h) Electrochemical performance and cycling stability of HC-Z1||NLNMO under low-temperature conditions.[197] (i) Temperature-dependent capacity retentions of modified HC anode.[198]

Moreover, storage depends on factors such as interlayer spacing, ion size, and graphite intercalation compound (GIC) stability. Li^+ readily forms stable LiC_6, while Na^+ intercalation is limited due to its larger size and unstable Na-GICs. Capacity also arises from ion adsorption at defects and edges, and metal clustering in closed pores. Understanding these mechanisms is crucial for linking HC structure to performance.[189] Furthermore, HC suffers from slow charge transfer dynamics, low-voltage operation, and severe low-temperature polarization effects that accelerate capacity loss. Under such conditions, hysteresis dynamics result in premature cut-off voltages, limiting effective capacity, while surface sodium metal deposition at potentials above the sodium deposition potential further exacerbates irreversible capacity loss.[45,46,189] These combined factors restrict HC's development as a high-performance anode material for SIBs in cold environments. For instance, biomass-derived HC exhibits a drastic capacity drop due to the formation of unstable SEI at low temperature (−20 °C) compared with room temperature (Fig. 12(c and d)), highlighting HC's inefficiency in LT environments.[85,190] Additionally, low ICE, typically around 80% for commercial HC materials, results from excessive active Na consumption during SEI formation, prompting strategies such as precycling with Na, though practical implementation remains difficult. However, direct ball milling or ultrasonic dispersion of molten sodium metal in mineral oil has proved to be a viable commercial method for pre-sodiating anodes or cathodes, offering compatibility with existing battery manufacturing processes without requiring major modifications.[191]

Structural modifications, such as preoxidation to create a flexible and self-supporting HC paper derived from tissue, have improved ICE and enhanced cycling stability at LT in ether electrolyte through the "adsorption–intercalation" process. Fig. 12(e) shows high sodium storage capacity retention as temperature decreases, with reversible capacities of approximately 97.3%, 94.7%, 92.8%, 90.6%, and 89.0% at 15, 5, −5, −15, and −25 °C, respectively, at 50 mA g^{-1}.[192] Additionally, surface carbon coating has been shown to suppress side reactions and elevate HC's reversible capacity at −15 °C. While a carbon-coated HC anode exhibited improved ICE (70% *vs.* 55% for uncoated HC) and stable cycling at −15 °C with 265 mAh g^{-1},[193] challenges such as coating degradation and electrolyte incompatibility persist. To address HC's low-rate capability, heteroatom doping (N, P, S, O) can opti-

© 2025 The Author(s). Published by the Royal Society of Chemistry

Open Access Article. Published on 20 August 2025. Downloaded on 18.02.26 05:05:09.
This article is licensed under a Creative Commons Attribution 3.0 Unported Licence.

mize defect structures and interlayer spacing, but excessive doping risks lattice distortions that degrade electrode stability.[194,195] A notable advancement is the Zn-HC composite in the $NaPF_6$/diglyme electrolyte, where atomic zinc expands interlayer spacing, enhances Na^+ storage kinetics, and catalyzes SEI formation, resulting in exceptional 85% capacity retention (258 mAh g^{-1} after 400 cycles) and rate performance at extreme LT conditions, with capacities of 443 mAh g^{-1} at 50 mA g^{-1} under −40 °C as presented in Fig. 12(f).[196] Additionally, localized electric field induction using transition metals like CoN_4 further enhances Na^+ kinetics and interfacial electrochemistry, achieving 288.7 mAh g^{-1} with 89% retention at −20 °C. The full cell delivered a capacity of 105 mAh g^{-1} at −40 °C, showcasing its potential for cold-climate energy storage as shown in Fig. 12(g and h).[197] Physical vapor deposition for uniform carbon coating has also proved effective, enhancing ICE from 55% to 70% and ensuring stable cycling at −20 °C.[193] Engineering nanostructures by tailoring carbon's pore size has further optimized Na^+ storage, where micropores (>1 nm) converted to ultra-micropores (<0.5 nm) improve Na^+ concentration and diffusion. Chen *et al.* enhanced ultra-microporosity in carbon materials through molten diffusion of aromatic hydrocarbons followed by carbonization, effectively suppressing electrolyte decomposition and achieving an initial coulombic efficiency (ICE) of ~80.6%. This approach delivered high areal capacities of 6.14 mAh cm^{-2} at 25 °C and 5.32 mAh cm^{-2} at −20 °C. Fig. 12(i) shows the 87% capacity retention at −20 °C compared with 25 °C, underscoring the critical role played by Na^+ transport kinetics in low-temperature performance.[198] However, challenges persist, including coating layer instability, incompatibility with electrolytes, and long-term cycling degradation. Thus, selecting optimal coating materials and refining surface modification strategies remain critical for enhancing HC's viability in LT SIBs.

3.3.1.2. Titanium-based materials. Ti-based anodes are considered highly promising for LT-SIBs due to their stable frameworks, higher redox potential (which minimizes the risk of Na dendrite formation), lower lattice strain, and efficient ion diffusion channels. These properties contribute to their exceptional safety, cycling stability, and rate performance, making them ideal for low-temperature applications in SIBs. These materials can be classified into three categories: TiO_2 polymorphs, $Na_2O{\cdot}nTiO_2$, and layered Na/Ti-containing oxides.[199] Fig. 13(a) illustrates the crystal structures of Ti-based compounds for Na storage. TiO_2 polymorphs, such as anatase and TiO_2-B, consist of TiO_6 octahedra connected differently, forming distinct structures like 3D frameworks or monoclinic open channels. $Na_2Ti_3O_7$ and $Na_2Ti_6O_{13}$, part of the $Na_2O{\cdot}nTiO_2$ system, feature 2D sheets with edge-sharing octahedral chains, while Na_xTiO_2 layered oxides ($Na_xTi_yTM_{1-y}O_2$; TM = Li, Cr, Co, or Ni) benefit from transition metal doping at the Ti site, which reduces lattice strain and enhances long-cycle stability.

However, Ti-based materials face limitations at low temperatures due to poor ionic and electronic conductivity, as well as slow transport kinetics.[47,200] Strategies like leveraging pseudocapacitive effects, structural modifications like carbon coating, and heterogeneous element doping are employed to enhance their performance by improving conductivity and anion transport, thus optimizing their efficiency in low-temperature applications. The pseudocapacitive effect mitigates sluggish kinetics and polarization, improving rate capability at low temperatures.[34] Deng *et al.* synthesized TiO_2@rGO heterostructures, where abundant heterojunctions facilitated rapid Na^+ insertion/extraction, leading to a capacity of 118.2 mAh g^{-1} at 5C (−20 °C) and 100 mAh g^{-1} over 1500 cycles at −40 °C (Fig. 13(b and c)).[201] Meng *et al.* developed ultrathin nanosheet-covered hollow $Na_2Ti_3O_7$ microspheres (H-NTO) with oxygen vacancies and NTO/C(N) bonding interfaces as illustrated in Fig. 13(d), enhancing Na^+ diffusion and structural stability.[202] A NaF-rich SEI layer protected H-NTO from degradation, enabling stable cycling for 200 days (3000 cycles) at −40 °C (Fig. 13(e)). Similarly, Li *et al.* synthesized $Na_2Ti_3O_7$ nanotubes with excellent rate performance, achieving 60% capacity retention at −20 °C when paired with ultrathin $VOPO_4$ cathodes.[203] Furthermore, Hu *et al.* improved $Na_2Ti_6O_{13}$ by Nb^{5+} doping. High-valence Nb^{5+} doping in NTO broadens ion migration channels, redistributes charge density, and modulates oxygen vacancies, synergistically enhancing long-cycle stability and low-temperature performance by boosting electrical conductivity and ion diffusion kinetics. First-principles studies revealed preferential substitution at Ti^3 sites, while *in situ* Raman identified a Nb-stabilized "spring effect" in chemical bonds, enabling reversible structural recovery during Na^+ migration, critical for sustained electrochemical stability, as shown in Fig. 13(f).[48] The optimized $Na_2Ti_{5.92}Nb_{0.08}O_{13}$ ($NTONb_{0.08}$) exhibited a Na^+ diffusion coefficient ten times higher than the undoped sample, delivering 103 mAh g^{-1} after 200 cycles at −15 °C (Fig. 13(g)). Additionally, the $NTONb_{0.08}$|| NVP full cell demonstrated superior LT cycling stability with a substantial capacity of 143 mAh g^{-1} at −15 °C, highlighting its potential for next-generation LT SIBs. Furthermore, Zhou *et al.* developed a high-crystallinity anode material with a post-spinel structure ($NaV_{1.25}Ti_{0.75}O_4$) that exhibited excellent low-temperature performance due to its stable 1D Na^+ transport channels.[204] These channels, formed by edge- or vertex-shared VO_6 and TiO_6 octahedra, facilitate fast Na^+ diffusion while a stable SEI layer enhances kinetics at low temperatures. The $NaV_{1.25}Ti_{0.75}O_4$/$Na_{0.8}Ni_{0.4}Ti_{0.6}O_2$ full cell retained 84% capacity after 200 cycles (Fig. 13(h)) at −20 °C, confirming the long-term stability of the high-crystallinity post-spinel $NaV_{1.25}Ti_{0.75}O_4$ anode at sub-zero temperatures.

$NaTi_2(PO_4)_3$ (NTP) with a NASICON structure offers large ion channels and rich sodium insertion sites, enhancing its electrochemical performance at low temperatures. However, its low electrical conductivity and ion diffusion coefficient limit its applicability in electric vehicles. To address this, carbon coating is commonly used to improve conductivity, reduce particle size, and prevent metal ion oxidation.[205,206] Hu *et al.* synthesized NTP@C-2 by mixing NTP with NVP and coating it with graphene-like layers, achieving superior electrochemical performance with specific capacities of 102 mAh g^{-1} at −20 °C

Open Access Article. Published on 20 August 2025. Downloaded on 18.02.26 05:05:09.
This article is licensed under a Creative Commons Attribution 3.0 Unported Licence.

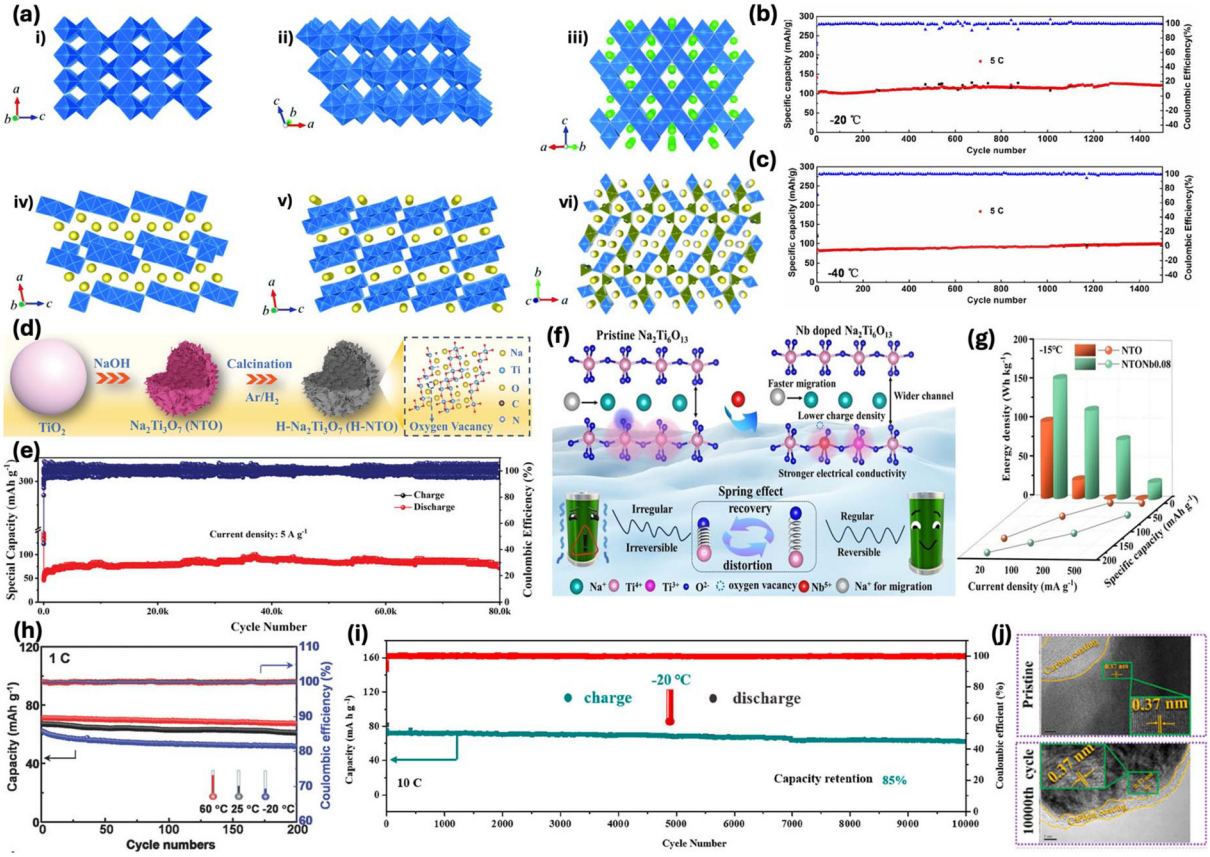

Fig. 13 (a) Schematic crystal structures of typical Ti-based compounds for sodium storage: (i) anatase TiO_2, (ii) TiO_2-B, (iii) spinel $Li_4Ti_5O_{12}$, (iv) $Na_2Ti_3O_7$ (zig-zag), (v) $Na_2Ti_6O_{13}$ (zig-zag), and (vi) tunnel-type $Na_4Mn_4Ti_5O_{18}$. TiO_6 octahedra and MnO_5/MnO_6 polyhedra are shown in blue and olive, with Li and Na as green and yellow spheres.[199] Charge–discharge capacities of TiO_2@rGO at 5C for (b) −20 °C, and (c) −40 °C over cycling.[201] (d) Schematic of the synthesis route and (e) long-term cycling performance of H-NTO microspheres at 5 A g^{-1}.[202] (f) Schematic illustration of crystal structure evolution in NTO before and after Nb doping. (g) Rate performance and energy density comparison of NTO and $NTO_{0.08}Nb$ at 100 mA g^{-1} under −15 °C.[48] (h) Cycling stability of $NaV_{1.25}Ti_{0.75}O_4/Na_{0.8}Ni_{0.4}Ti_{0.6}O_2$ full cells at 1C.[204] (i) Extended cycling of $NaTi_2(PO_4)_3/Ni(OH)_2$ at −20 °C and 10C rate; (j) TEM images of NTP@C electrode at initial and 10 000th cycle.[209]

(0.2C).[207] Similarly, Reber *et al.* developed an NTP-based full cell with an ionic liquid electrolyte, demonstrating ideal LT performance.[208] Nian *et al.* coated NTP with carbon, enhancing Na^+ transport and fast reaction kinetics, enabling a dual-ion reaction in a full cell with a $Ni(OH)_2$ cathode and 2 M $NaClO_4$ electrolyte.[209] Fig. 13(i) shows the full cell retains 85% capacity at 10C after 10 000 cycles at −20 °C, indicating excellent low-temperature stability. The HR-TEM image in Fig. 13(j) reveals clear lattice fringes (d = 0.37 nm) corresponding to the (113) planes, confirming that NTP@C maintained its crystal structure after prolonged cycling. Furthermore, a CNT-decorated $NaTi_2(PO_4)_3$@C nanocomposite demonstrated a specific capacity of 62.2 mAh g^{-1} at 10C under −20 °C, leveraging the advantages of both the CNT network and the NASICON framework.[210] Additionally, $KTiOPO_4$, known for its high ionic conductivity, exhibited remarkable stability in Na/K ion batteries at low temperatures, showing no capacity degradation after 550 cycles at 3C under −35 °C.[211] Despite these advancements, the challenge of low discharge capacity and electronic conductivity continues to limit the full potential of titanium-based compounds in SIBs. To enhance low-temperature performance, Ti_3C_2 MXene was modified by tailoring nitrogen terminals (Ti_3C_2-N_{fuct}) to improve ion diffusion kinetics and reduce dendrite formation.[212] This modification redistributes charge, reduces the bandgap, and lowers the diffusion barrier, promoting fast charging at low temperatures. Ti_3C_2-N_{fuct} retained 80.9% capacity after 5000 cycles at −25 °C, demonstrating its excellent low-temperature performance, which is largely attributed to improved Na^+ diffusion kinetics driven by high ionic and electronic conductivity. Furthermore, Li *et al.* developed a 3D a-$KTiO_x/Ti_2CT_x$ heterostructure, integrating 1D nanoribbons with 2D MXene nanosheets to enhance ion diffusion and charge storage at low temperatures.[213] This structure maintained a reversible capacity of 112.6 mAh g^{-1} after 100 cycles at −25 °C. Additionally, a $WS_2/Ti_3C_2T_x$ heterojunction with a built-in electric field (BIEF) was engineered to improve reaction kinetics and electrochemical activity. This heterostructure achieved 293.5 mAh g^{-1} at 0.1 A g^{-1} after 100 cycles at −20 °C.[214]

3.3.2. Conversion materials. Conversion-type anode materials including transition metal oxides, chalcogenides

© 2025 The Author(s). Published by the Royal Society of Chemistry

Open Access Article. Published on 20 August 2025. Downloaded on 18.02.26 05:05:09.
This article is licensed under a Creative Commons Attribution 3.0 Unported Licence.

(M_xO_y or M_xS_y where M is Fe, Co, Cu, Mn, Ni, and Mo), nitrides, and phosphides, have emerged as promising candidates for SIBs due to their high theoretical capacities enabled by multi-electron redox reactions. Unlike graphite and carbon-based anodes that rely primarily on intercalation, these compounds store sodium through reversible conversion reactions that yield metallic species and corresponding Na-containing compounds.[215–217] However, transition metal oxides often suffer from poor reversibility and low coulombic efficiency due to the high electronegativity of oxygen, which forms highly stable Na–O bonds, making the regeneration of active materials (Na_2O) challenging.[49] This results in voltage hysteresis and inefficient charge/discharge processes. To overcome these limitations, researchers have increasingly focused on transition metal sulfides and selenides, which possess lower electronegativity and higher electronic conductivity, enabling more reversible redox reactions and better coulombic efficiency.[218,219] Furthermore, their layered structures with expanded interlayer spacings facilitate easier Na^+ diffusion and accommodate volume changes more effectively. Among these, selenides stand out for offering larger interlayer distances and superior conductivity than their oxide and sulfide counterparts, making them particularly suitable for LT-SIB applications. Nevertheless, all conversion-type materials still face issues such as significant volume expansion, structural degradation, and sluggish kinetics at low temperatures, which impair cycle life and capacity retention.[220–223] To address these challenges, advanced strategies such as nanostructuring, carbon compositing, introducing pseudocapacitance effects, and elemental doping are widely adopted to improve electronic conductivity, buffer volume changes, and accelerate reaction kinetics under harsh conditions.

Fan *et al.* designed FeS@g-C composites with a graphitic carbon coating that enhanced electrical conductivity and minimized diffusion barriers, resulting in superior performance at −25 °C.[224] The synergistic interactions in binary metal sulfides, such as $CuGaS_2$/graphene[225] and $CoGa_2S_4$/graphene,[226] further improved ionic conductivity, ensuring excellent sodium storage capabilities in subzero environments. Jiang *et al.* demonstrated that the key to improving the Na storage performance of $MoSe_2$ lies in its ability to regenerate $MoSe_2$ from Mo and Na_2Se, a process that can be controlled by tuning structural strain.[223] Fig. 14(a) shows the rate performance of TS-$MoSe_2$ (TS: applying tensile constraints) from 50 to −30 °C, highlighting its strong temperature adaptability. At −30 °C, TS-$MoSe_2$ retains a high reversible capacity of 380 mAh g^{-1} at 0.1 A g^{-1} after 100 cycles (Fig. 14(b)), significantly outperforming $MoSe_2$, which delivers only 128 mAh g^{-1} under the same conditions. Furthermore, ZnSe@NCNF[227] and $FeSe_2$/rGO[228] demonstrated stable sodium storage at extreme temperatures. For instance, Ultrafine ZnSe nanoparticles embedded in N-doped porous carbon nanofibers (ZnSe@NCNFs) were synthesized from PAN@ZIF-8 *via* pyrolysis and selenization as illustrated in Fig. 14(c). As an anode, ZnSe@NCNFs delivered excellent sodium storage (119.7 mAh g^{-1} at 0.2 A g^{-1} under −40 °C) and operated efficiently at −20 to −40 °C, as shown in Fig. 14(d).[227]

Additionally, the incorporation of pseudocapacitance effects has proved to be a critical strategy for LT SIBs, as surface-controlled redox reactions enable rapid ion adsorption and diffusion. Tian *et al.* leveraged this approach by designing $FeSe_2$ nanoparticles embedded in rGO, forming a conductive network that accelerated charge transfer and minimized volume expansion, allowing the material to function effectively even at ultra-low temperatures. The use of dual-anion doping, as seen in MoSSe@rGO, further optimized Na^+ transport kinetics, retaining 87.8% capacity at 0 °C,[229] and NbSSe achieved 136 mAh g^{-1} at 0.2C under 0 °C with 92.67% capacity retention after 500 cycles.[230] Double transition-metal selenides, such as $Ni_{1.8}Co_{1.2}Se_4$/NDDC[231] and $Ni_{1.5}CoSe_5$/NC,[232] exhibit excellent low-temperature SIB performance when paired with $Na_3V_2(PO_4)_2O_2F$ cathodes. $Ni_{1.8}Co_{1.2}Se_4$@NDDC (NCS@NDDC), featuring a 3D conductive N-doped dual carbon (NDDC) network, enhanced electron/ion transport and buffered volume changes. The GCD curves from Fig. 14(e) show two distinct plateaus at all temperatures, indicating excellent kinetics. As the temperature dropped from 25 to −25 °C, the NCS@NDDC//NVPOF retains 97–83% of its room-temperature capacity (Fig. 14(f)), reflecting weak temperature dependence.[231] In addition, sulfur-rich materials like $(NH_4)_2Mo_3S_{13}$ facilitated the formation of a 3D ion pathway, enhancing diffusion kinetics and sustaining high capacities at subzero temperatures.[233] These advancements highlight the necessity of combining strain engineering, conductive coatings, pseudocapacitive mechanisms, and multivalent interactions to develop next-generation conversion-reaction anodes for LT SIBs, paving the way for efficient energy storage solutions in extreme environments.

3.3.3. Alloy-based materials. Alloy-based materials, such as Sn, Sb, Bi, Si, Ge, and P, are promising candidates for next-generation SIBs due to their ability to electrochemically alloy with Na^+, offering high theoretical capacities by accommodating a high stoichiometric ratio of Na^+ (general representation: $xNa^+ + xe^- + M = Na_xM$).[234] These materials, primarily from the IVA (*e.g.*, Ge, Sn, Pb) and VA (*e.g.*, P, Sb, Bi) groups of the periodic table, form Na-rich intermetallic compounds like NaGe, $Na_{15}Sn_4$, Na_3P, and Na_3Sb, which exhibit advantages such as high theoretical specific capacities (>400 mAh g^{-1}), appropriate working potentials (0.2–0.6 V), good conductivity, and ease of preparation due to the abundance of raw materials.[234,235] However, alloy-based anodes face significant challenges, including severe volume changes during alloying/dealloying processes and poor Na^+ kinetics, which hinder their practical application, particularly in LT-SIBs. At ultralow temperatures (−40 °C), the capacity of these batteries sharply decreases due to the thickening of the electrolyte and the slowed desolvation process of solvated Na^+ at the SEI, making Na^+ transport the rate-limiting step (RLS) of the electrochemical reaction.[31,50] To address these issues, strategies like nanotechnology, carbon coating, and introducing interior void space have been employed to enhance Na^+ kinetics and mitigate volume expansion. Despite these challenges, alloy-based anodes remain a research hotspot due to their high specific

Open Access Article. Published on 20 August 2025. Downloaded on 18.02.26 05:05:09.
This article is licensed under a Creative Commons Attribution 3.0 Unported Licence.

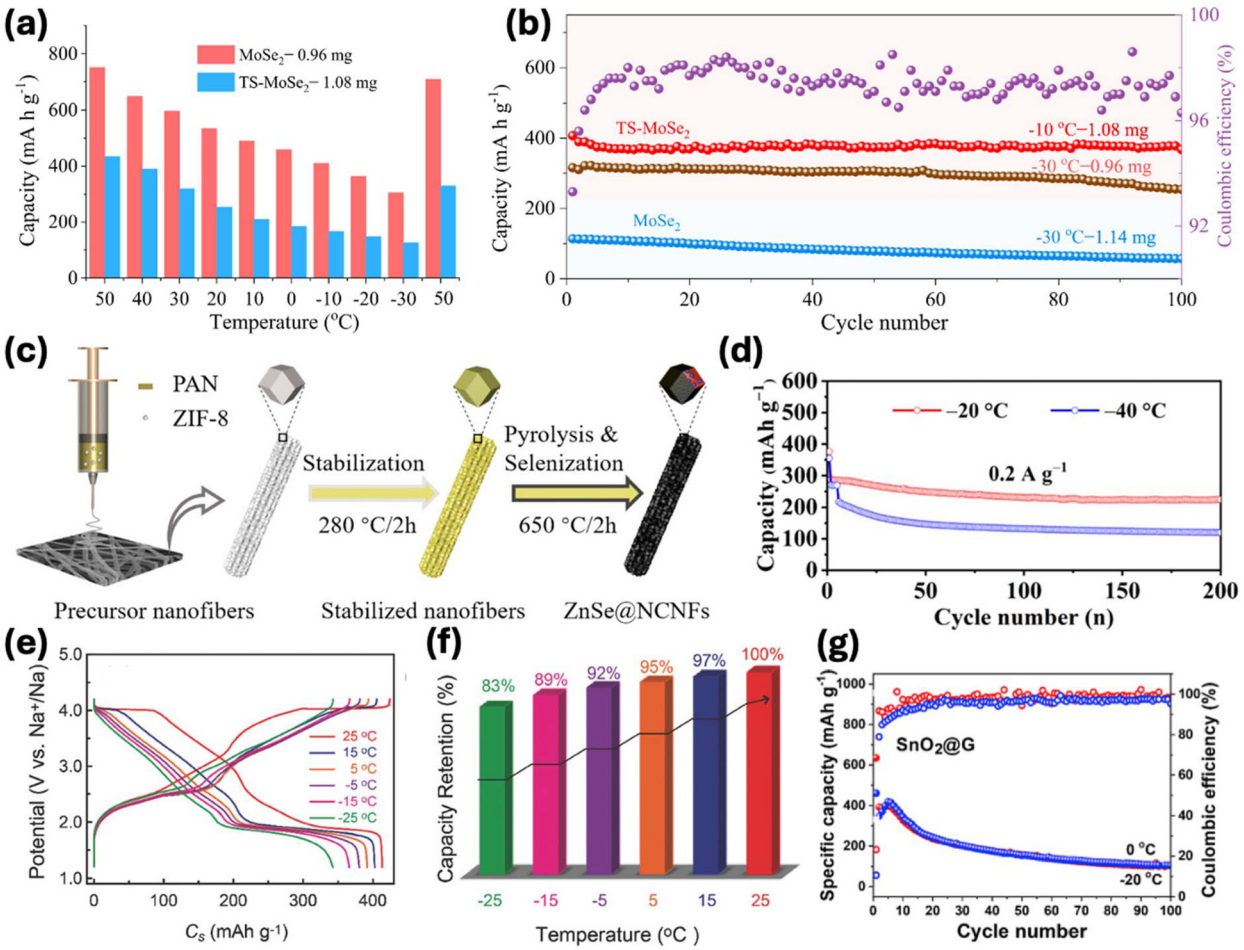

Fig. 14 (a) Cycling performance of TS-$MoSe_2$ and $MoSe_2$ across 50 to −30 °C; (b) performance of TS-$MoSe_2$ at −10 and −30 °C, and $MoSe_2$ at −30 °C.[223] (c) Schematic of the synthesis process and (d) cycling performance of ZnSe@NCNFs at 0.2 A g^{-1}.[227] (e) GCD profiles at 0.1 A g^{-1}, and (f) capacity retention of NCS@NDDC//NVPOF SIFC from RT to −25 °C.[231] (g) Low-temperature cycling performance of SnO_2@G.[239]

capacity and potential, outperforming carbon-based materials. However, their large volume changes during charge/discharge cycles lead to electrode pulverization and inferior cycling performance, particularly at LT, where low electrical conductivity further limits their specific capacity and rate performance.

To enhance LT sodium-ion kinetics, researchers have explored compositing alloy-based anode materials with carbon matrices to address poor electrical conductivity and severe volume changes during cycling. For instance, Chen *et al.* developed a bismuth-intercalated graphite (Bi@graphite) anode, where Bi nanoparticles were embedded between graphite layers, providing a buffer for volume changes and facilitating ion transport.[236] This composite demonstrated a capacity of 150 mAh g^{-1} at −20 °C and 160 mA g^{-1}. Furthermore, embedding ultrasmall Bi nanoparticles into a 3D porous carbon framework (EMP-Bi@3DCF) reduced ion diffusion paths and accommodated volume changes.[51] In contrast, Li *et al.* demonstrated a solvent co-intercalation process using an ether-based electrolyte, forming a coral-like porous Bi structure that enabled a remarkable capacity of 330 mAh g^{-1} at −60 °C.[50] These studies highlight the critical role played by LT Na^+ transport in determining electrochemical performance. Additionally, carbonaceous matrices have been combined with other materials, such as amorphous selenium coated with rGO,[237] Sb@graphene,[52] and SbO_x-GNP,[238] which exhibited capacities of 240–250 mAh g^{-1}, 472.5 mAh g^{-1}, and 550 mAh g^{-1}, respectively, at low temperatures. Metal-based compounds such as SnO_2@graphene have also been investigated, where the dominant conversion reaction, facilitated by ultrafine SnO_2 nanoparticles, offers new insights into sodium storage mechanisms. Even at reduced temperatures of 0 °C and −20 °C, the material maintained specific capacities of 100 mAh g^{-1} and 97 mAh g^{-1}, respectively, as shown in Fig. 14(g).[239] Despite these advancements, the significant volume expansion of alloying anodes, such as Bi, which exceeds 250%, remains a challenge. Strategies like designing micro/nanostructured composites such as layer-stacked Sb@graphene and using 3D porous carbon frameworks have shown promise in mitigating volume changes and improving cycling stability.[52] Chen *et al.* developed N/S codoped porous carbon microspheres coated

© 2025 The Author(s). Published by the Royal Society of Chemistry

Open Access Article. Published on 20 August 2025. Downloaded on 18.02.26 05:05:09.
This article is licensed under a Creative Commons Attribution 3.0 Unported Licence.

with Sb composite material that maintained excellent high-rate cycling at 5 °C.[240] Overall, combining carbon-based materials with alloy anodes, along with innovative morphology design, surface modification, and electrolyte optimization, represents a promising pathway to enhance LT sodium-ion battery performance.

4. Advancements, applications, and sustainability of LT-SIBs

4.1. Low-temperature testing and performance metrics

Recent advancements in full-cell SIB configurations have demonstrated significant improvements in low-temperature performance, making them promising candidates for energy storage in extreme environments. Innovations in electrolyte optimization, such as the use of sodium salts, additives, and multi-solvent systems, have enhanced ionic conductivity, reduced viscosity, and improved ion mobility, thereby stabilized the SEI and enhanced LT performance. However, challenges like balancing sodium salt solubility, managing additive concentrations to avoid side reactions, and addressing the increased weight and cost of multi-solvent systems remain critical barriers to practical applications. Additionally, the solvation structure within the electrolyte plays a pivotal role in ensuring battery efficiency and reliability. On the electrode front, modified materials such as high-capacity alloy metals, transition-metal chalcogenides, and titanium-based compounds have shown remarkable LT performance. While half-cell configurations have been instrumental in basic research, the convergence of scientific and industrial advancements has shifted focus to sodium-ion full batteries (SIFBs), showcasing their potential for low-temperature applications and driving further innovation in both research and practical implementation. Aqueous sodium-ion full batteries (ASIFBs)[241,242] and antifreezing hydrogel electrolytes[243] have further expanded adaptability. Despite these advancements, issues such as low mass loadings (<3.0 mg cm^{-2}) and the need for optimized binders and conductive agents hinder industrialization.

Furthermore, SSIBs are emerging as a promising alternative, offering improved safety and stability, though they still face limitations in LT ionic conductivity and interfacial resistance. Advances in polymer-based electrolytes, such as PFSA-Na membranes,[117] and roughened β″-alumina substrates[244] have shown potential, but further optimization of electrode–electrolyte interfaces is essential. Thermal management innovations, including self-heating mechanisms and phase-change materials,[245–247] offer promising solutions for maintaining operational efficiency in sub-zero temperatures, though they require careful energy balance considerations. Additionally, a deeper understanding of the SEI microscopic formation mechanism and LT solvation effects is critical, with advanced characterization techniques like cryo-electron microscopy and *in situ* spectroscopy providing valuable insights.[59] Computational simulations and machine-learning models are also expected to play a pivotal role in predicting optimal materials and electrolytes. Moreover, Artificial Intelligence (AI) is employed to overcome costly traditional methods, pursuing three primary objectives: performance optimization *via* predictive models establishing Quantitative Structure–Property Relationships (QSPRs), inverse design of novel materials with specified functionalities, and mechanism exploration to uncover fundamental physical and chemical principles governing battery behavior. Overcoming data scarcity, quality, and model interpretability challenges is critical for deploying AI-driven autonomous systems in battery material discovery as illustrated in Fig. 15(a). This necessitates high-throughput platforms for large-scale datasets and standardized protocols for seamless lab integration, alongside encoding domain knowledge (*e.g.*, electrochemistry, thermodynamics) into AI models *via* theory-guided regularization to ensure physical plausibility and enable hypothesis generation.[248–252] By addressing challenges and leveraging emerging technologies, SIBs can be scaled up to meet the demands of next-generation energy storage systems for harsh environments, paving the way for their real-world application in industries ranging from electric vehicles to grid storage.

4.2. Low-temperature battery safety

When a battery experiences abnormal conditions, such as external heating, overcharging, over-discharging, short circuits, or mechanical damage, it can trigger failures like thermal runaway (TR). During TR, continuous exothermic side reactions generate excessive heat and flammable gases, often leading to venting, jet flames, or explosions, posing serious threats to battery modules and energy storage systems. Thus, assessing the risks associated with TR and fire is crucial for ensuring the safety and reliability of batteries. SIBs comprising an electrolyte, anode, and cathode, face significant safety and performance challenges rooted in the intrinsic properties and interactions of these components.[253–255] Key safety risks arise from organic electrolyte flammability, reactivity, and corrosiveness. Concurrently, anode degradation manifests through sodium dendrite growth, SEI instability/decomposition, and parasitic side reactions, while cathode failure involves thermal decomposition and structural collapse. Critically, these issues are interdependent and can cascade into TR: initial overheating from external/internal triggers (*e.g.*, Na dendrites, cathode damage, collector corrosion) decomposes the SEI; the exposed, reactive anode then violently reacts with the flammable electrolyte, releasing heat and gas; this subsequently drives oxygen-releasing cathode decomposition, further accelerating exothermic reactions until combustion or explosion occurs.

LT operation severely degrades SIB performance due to reduced electrolyte ionic conductivity and increased viscosity (governed by Arrhenius kinetics), sluggish Na^+ diffusion/desolvation at interfaces, and exacerbated Na dendrite growth from plating and high SEI ion-diffusion barriers. An unstable SEI can impair ion transport, lead to spiking cell impedance, and promote localized heating and further side reactions, putting additional stress on the battery and raising the probability of hazardous failure if a short circuit occurs. During low-tempera-

Open Access Article. Published on 20 August 2025. Downloaded on 18.02.26 05:05:09.
This article is licensed under a Creative Commons Attribution 3.0 Unported Licence.

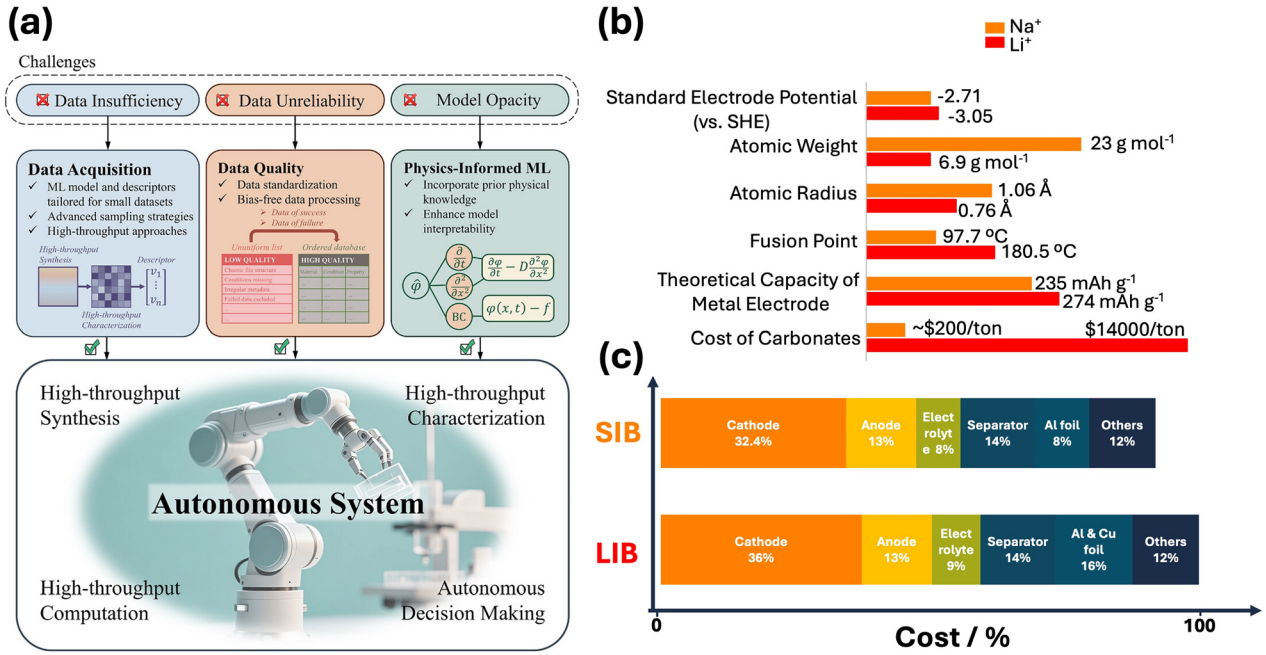

Fig. 15 (a) Overcoming key challenges and realizing opportunities through AI in rechargeable battery materials design.[250] (b) Comparison of sodium and lithium properties, and (c) the manufacturing costs for LIB and SIB cell components.

ture operation, deposited sodium tends to grow in a directional manner, forming dendrites that can potentially pierce the separator and increase the risk of thermal runaway. Although SIBs offer better low-temperature performance than LIBs,[256] both suffer significant losses in capacity, voltage, and rate capability in such conditions. However, the metallic sodium electrodes rely on an electroplating/stripping mechanism with minimal solid-state diffusion, making them better suited for low-temperature and fast-charging applications compared with Li metal electrodes. Moreover, the gas release and the severity of heat release is comparatively limited at lower temperatures, reducing catastrophic outcome risks even if failure is triggered.[257] Many organic electrolytes showed wide-temperature operation and longevity in SIBs due to their thermal/chemical stability,[258] yet persistent safety risks and side reactions limit their viability.

Improving the safety of SIBs focuses on developing non-flammable electrolytes through the use of stable sodium salts and highly concentrated formulations, which enhance thermal stability and reduce flammability, though these often require costly fluorinated ether cosolvents to address viscosity issues. Furthermore, to improve both electrochemical performance and safety at low temperatures, a promising approach involves adopting a high-entropy (HE) strategy.[122] By increasing the ΔS, this method helps preserve ionic conductivity in cold conditions, mitigates solubility limitations, and extends the operational temperature range of the electrolyte.[259] Likewise, in electrode materials, the HE approach enhances electronic conductivity, minimizes irreversible phase transitions, boosts redox activity, and refines Na^+ ion diffusion pathways.[260,261]

Additional strategies include employing nonflammable solvents such as ionic liquids or phosphates and incorporating cost-effective flame-retardant or overcharge additives along with antifreeze additives.[262] However, achieving a stable electrode–electrolyte interphase remains a major challenge due to its complex and variable composition, which is influenced by multiple electrolyte and electrode configurations and its sensitivity that complicates characterization, and the difficulty of optimizing beneficial inorganic components (like fluorides and oxides) without compromising performance. Employing a weakly solvated electrolyte with low solvation energy for Na^+ ions, along with forming an artificial SEI, helps facilitate smooth Na^+ ion transport across the Na metal/electrolyte interface.[263] Moreover, additive strategies, particularly synergistic combinations, represent a promising approach for targeted interphase engineering, though they demand deeper fundamental understanding. In addition, SSEs including polymer, sulfide, and ceramic types,[264–266] are emerging as critical solutions to overcome these challenges, enhancing safety and compatibility for next-generation LT-SIBs.

Furthermore, smart thermal management designs, including internal self-heating mechanisms and optimized cell architectures, reduce uneven temperature gradients within battery packs, mitigating the risk of local hot spots that could otherwise trigger thermal incidents. In SIBs, innovations in both the electrode structure and electrolyte formulation counteract much of this effect, but ongoing monitoring is necessary to prevent excessive heat buildup during rapid charge–discharge cycles. Effective battery management systems (BMS) continuously track internal resistance and temperature to coordinate charge protocols and avoid zones where safety margins could

© 2025 The Author(s). Published by the Royal Society of Chemistry

Open Access Article. Published on 20 August 2025. Downloaded on 18.02.26 05:05:09.
This article is licensed under a Creative Commons Attribution 3.0 Unported Licence.

be compromised. Moreover, the safety and reliability of SIBs under mechanical abuse remain uncertain, hindering commercialization. Combining both experimental and multiphysics computational models enables us to understand the mechanical–electrochemical–thermal behavior under extreme conditions.[267]

Despite the recognized safety risks of LT operation, a significant knowledge gap persists, as comprehensive experimental data are lacking on how thermal abuse specifically impacts critical safety mechanisms like valve cracking, deflagration, and fire characteristics in SIBs under realistic LT, non-adiabatic conditions. This gap is critical as SIBs advance towards practical use. To ensure reliable and secure performance in harsh environments, future efforts must prioritize designing intrinsically safe cell components and implementing rigorous, LT-tailored safety testing protocols. Crucially, understanding the TR and fire behavior resulting from rapid LT charging/discharging at various rates is essential for safe application. Future testing must therefore include controlled overcharging, induced internal short circuits, and accelerated thermal stress to evaluate venting and TR thresholds across temperature extremes. Ultimately, developing safe, efficient, and adaptable battery modules requires a comprehensive assessment of behavior under diverse operating conditions, aging states, and extreme environments.

4.3. Sustainability and scalability considerations

SIBs offer significant environmental and economic advantages that extend beyond their superior low-temperature performance, positioning them as a compelling alternative to LIBs across multiple sectors. One of the key benefits of SIBs is the abundance of sodium, which constitutes approximately 2.3% of Earth's crust, vastly exceeding lithium's availability (20 ppm). This abundance ensures a more stable and cost-effective supply chain, reducing dependence on geopolitically sensitive lithium and cobalt sources while addressing ethical concerns associated with their extraction. The widespread geographical distribution of sodium further mitigates supply concentration risks that currently challenge LIB production. Additionally, SIBs leverage the same fundamental working principles and manufacturing infrastructure as LIBs, allowing for large-scale production without significant capital investment. In 2024, the price of lithium carbonate was estimated at \$14 000 per metric ton, a significant decline from its peak of \$78 000 per ton in 2022 (Fig. 15(b)). Despite this reduction, sodium carbonate remains far more cost-effective and ranges from \$150 to \$250 per metric ton, highlighting the substantial economic advantage of SIB materials over lithium-based alternatives. Beyond affordability, SIBs offer notable safety advantages, as their cathode and anode materials can be developed without lithium and cobalt, relying instead on inexpensive and abundant elements. Furthermore, sodium's lack of reactivity with aluminum under standard operating conditions allows for the exclusive use of aluminum as the current collector, simplifying material requirements and further reducing costs.[166,268,269] The Fig. 15(c) shows the cost breakdown of each cell component in sodium-ion and lithium-ion batteries. Economic projections indicate favorable cost trajectories for sodium-ion technologies. Production expenses are forecast to decrease below \$51 per kWh by 2030,[17] driven by manufacturing optimizations including anode-free designs that eliminate copper current collectors and aqueous electrode processing techniques that reduce solvent requirements and associated environmental impacts.[270] These combined attributes make SIBs not only a sustainable and scalable energy storage solution but also a practical alternative for cold-climate applications including electric vehicles and grid-level storage, reinforcing the potential role they can play in diversifying and securing the global battery supply chain.

Recycling infrastructure, while still in early developmental stages for SIB technology, demonstrates promising technical feasibility.[271] Hydrometallurgical processes have demonstrated sodium recovery rates approaching 95%, though industrial-scale implementation currently lags behind the more established lithium-ion recycling ecosystem.[272,273] Unlike LIBs, which offset recycling costs through high-value metal recovery, SIBs' reliance on abundant, low-cost sodium and transition metals like iron and manganese reduces material valuation, undermining profitability and industrial recycling incentives. Environmental risks persist due to toxic fluorinated compounds and heavy metals in spent SIBs, necessitating pre-emptive design strategies, such as standardized, easily separable components and degradable binders to streamline recycling processes and minimize operational costs.[274,275] Early integration of circular economy principles, including closed-loop material regeneration and policy-driven collection systems, is critical to enhancing sustainability and avoiding the accumulation of hazardous waste. Addressing these challenges during SIB commercialization could position them as a cornerstone of eco-friendly energy storage, balancing performance with recyclability through innovations in material chemistry and scalable recycling frameworks.

Lifecycle assessment studies provide additional sustainability validation for SIB technology in cold-environment applications.[275–277] Carbon footprint analyses indicate the lower emissions compared with lithium-ion alternatives when deployed in cold storage applications, primarily due to reduced mining impacts and simplified thermal management requirements.[278,279] These environmental benefits align with increasingly stringent regulatory frameworks, particularly in European markets where battery passport systems[280] will soon require detailed carbon footprint declarations and material sourcing transparency. As sustainability metrics gain importance in procurement decisions across public and private sectors, these inherent advantages may accelerate market adoption despite lingering performance gaps in certain metrics.

5. Conclusions and perspectives

The comprehensive analysis of LT SIBs reveals a transformative technology poised to address critical energy storage challenges in extreme environments. Through systematic investigation of

Open Access Article. Published on 20 August 2025. Downloaded on 18.02.26 05:05:09.
This article is licensed under a Creative Commons Attribution 3.0 Unported Licence.

Fig. 16 Perspectives on advancing the performance of LT SIBs.

electrode materials, electrolyte formulations, and interfacial phenomena, significant progress has been achieved in understanding and mitigating the fundamental limitations that hinder SIB performance at sub-zero temperatures. This review presents a roadmap for transitioning from fundamental research breakthroughs to practical industrial applications, highlighting the unique advantages of sodium-ion technology in cold-climate energy storage scenarios. Perspectives on advancing the performance of LT SIBs are visually summarized in Fig. 16. This illustration provides a roadmap for overcoming current challenges and guiding future research directions to enable reliable operation in harsh and extreme environments.

Key scientific achievements and breakthroughs

1. Fundamental understanding of low-temperature mechanisms

Recent research has established a comprehensive framework for understanding the complex interplay between thermodynamic and kinetic factors that govern SIB performance at low temperatures. The identification of sluggish Na^+ diffusion kinetics, unstable electrode–electrolyte interfaces, and brittle SEI formation as primary limiting factors has enabled targeted material design strategies. Advanced characterization techniques, including cryogenic transmission electron microscopy and *in situ* spectroscopy, have provided unprecedented insights into the dynamic evolution of interfacial structures under extreme conditions.

2. Electrode materials: from understanding to engineering excellence

The evolution of LT SIB cathodes has progressed through three generations of understanding and engineering. Polyanionic compounds, especially NASICON-type materials, are leading candidates due to their robust 3D frameworks enabling fast Na^+ transport even under extreme cold; their performance is further enhanced by composite modifications like

© 2025 The Author(s). Published by the Royal Society of Chemistry

Open Access Article. Published on 20 August 2025. Downloaded on 18.02.26 05:05:09.
This article is licensed under a Creative Commons Attribution 3.0 Unported Licence.

surface coatings, nanosizing, and doping, which boost conductivity while preserving structural integrity. Layered transition metal oxides have been improved *via* interlayer doping to suppress detrimental phase transitions and metal dissolution, while the development of P2/O3 biphasic structures with compositional gradients offers exceptional wide temperature cycling stability, marking a shift toward multi-phase optimization. Prussian blue analogs show promise through refined synthesis reducing $Fe(CN)_6$ vacancies and lattice water, thereby enhancing sub-zero stability and electrochemical performance, where optimizing crystallinity and framework integrity remains crucial.

Research into LT operable anode materials focuses on three core categories, each addressed through distinct engineering strategies. Carbon-based anodes, particularly hard carbon, are optimized *via* microstructural engineering, such as controlled closed pore creation and heteroatom doping to enhance Na^+ storage kinetics and ICE. Titanium-based materials leverage pseudocapacitive engineering and high-valence element doping to enlarge ion migration channels and boost conductivity, with 3D nanoarchitectures combining titanium phases proving highly stable and rate-capable at LT. Conversion/alloy-type materials, despite their high theoretical capacity, require nanostructuring and integration into carbon matrices to mitigate severe LT volume expansion. Recent advances in strain engineering and interfacial design show promise in maintaining their structural integrity during cycling.

Moreover, the development of high-entropy electrode materials represents a paradigm shift in battery design philosophy, leveraging entropy stabilization effects to maintain structural integrity across wide temperature ranges.

3. Electrolyte engineering: the critical enabler

The understanding of LT electrolyte behavior has advanced significantly, evolving beyond basic freezing point depression to encompass sophisticated models of solvation structure dynamics and interfacial chemistry. Crucially, the discovery of temperature-dependent transitions in Na^+ coordination environments has driven the development of adaptive electrolyte formulations that sustain optimal performance across wide thermal ranges. Effective strategies include the strategic combination of cyclic and linear carbonates with specific ether co-solvents, which maintain ionic conductivity and prevent salt precipitation even at extremes. While solid-state and ionic liquid electrolytes showed promise for safety and stability, these systems still face challenges with slow Na^+ conductivity at low temperatures, requiring further research.

High-entropy electrolytes represent a frontier approach leveraging the eutectic effect to drastically lower melting points and enhance electrochemical stability *via* complex multi-component solvation structures. Complementing this, the development of localized high-concentration electrolytes has successfully balanced high ionic conductivity with reduced viscosity, overcoming a fundamental trade-off that historically limited LT performance. Furthermore, the strategic incorporation of functional additives has proved crucial for SEI engineering, enabling the formation of thin, inorganic-rich interphases that preserve ionic conductivity while ensuring electrochemical stability; the understanding of additive mechanisms has now advanced from empirical selection towards rational design based on molecular-level interactions.

Current challenges and future research priorities

1. Technical barriers

Despite significant progress, several technical challenges persist in the development of practical LT-SIBs. The formation of stable, ionically conductive SEI layers remains problematic at ultra-low temperatures, with brittleness and increased resistance limiting long-term cycling performance. Irreversible phase transitions in electrode materials during deep cycling continue to cause capacity degradation, particularly in layered oxide cathodes. The discrepancy between button cell performance and practical pouch cell behavior highlights the complexity of scaling laboratory innovations to commercial applications. The development of electrode materials with high mass loadings suitable for commercial applications while maintaining LT performance represents a critical challenge that requires continued innovation in materials design and processing. The optimization of inactive components, including binders, separators, and current collectors for LT operation, remains an underexplored area with significant potential for system-level improvements.

2. Advanced characterization and understanding

The complexity of LT electrochemical processes demands continued advancement in characterization techniques, particularly *in situ* and *operando* methods that can capture dynamic phenomena without disturbing the delicate interfacial chemistry. Cryogenic transmission electron microscopy and advanced spectroscopic techniques offer unprecedented opportunities to understand SEI formation mechanisms and ionic transport pathways at the molecular level. The development of predictive models that can accurately forecast LT performance based on fundamental materials properties remains a significant challenge that requires integration of experimental observations with advanced computational approaches. Machine learning algorithms trained on comprehensive datasets of LT performance metrics show promise for accelerating materials discovery and optimization.

3. Battery safety

Battery safety is a key concern for SIBs, particularly under LT conditions. While SIBs are inherently safer than LIBs due to sodium's lower reactivity, LT operation introduces challenges such as increased polarization, unstable interfaces, and fragile SEI formation that can lead to dendrite growth or short circuits. Ensuring safety requires the development of robust electrolytes, stable SEI layers, adoption of solid-state electrolytes, and reduced liquid electrolyte risks by implementing high-entropy concepts. Advancements in materials, interface engineering, and *in situ* diagnostics will be crucial to achieving both high performance and safety in extreme environments.

4. Manufacturing and scalability issues

The transition from laboratory-scale synthesis to industrial production presents significant challenges in maintaining material quality and performance consistency. Cost-effective

© 2025 The Author(s). Published by the Royal Society of Chemistry

Open Access Article. Published on 20 August 2025. Downloaded on 18.02.26 05:05:09.
This article is licensed under a Creative Commons Attribution 3.0 Unported Licence.

synthesis of nanostructured electrode materials and advanced electrolyte formulations remains a barrier to widespread commercialization. The development of standardized testing protocols for extreme-temperature conditions is essential for reliable performance evaluation and quality assurance.

Strategic research directions

1. Materials innovation and design philosophy

The future of LT-SIB development lies in the rational design of materials with inherent temperature resilience rather than post-synthesis modifications to address LT limitations. High-entropy electrode materials that leverage configurational entropy for enhanced structural stability represent a promising approach that has shown early success for maintaining performance across extreme temperature ranges. The development of amorphous and nanostructured materials with enriched interfaces can provide enhanced pseudocapacitive effects that are less temperature-dependent than traditional intercalation mechanisms. The strategic incorporation of defect engineering and interface optimization offers pathways to minimize energy barriers for ionic and electronic transport.

2. System-level integration

The development of integrated battery systems optimized for LT operation requires consideration of thermal management, cell architecture, and safety systems. Advanced battery management systems incorporating predictive algorithms and real-time diagnostics will be essential for safe and efficient operation in extreme environments. The standardization of testing protocols and performance metrics for LT batteries will facilitate technology transfer and commercialization. The establishment of safety standards and reliability assessments for extreme temperature operation will be crucial for regulatory approval and market acceptance.

Strategic application domains

The unique advantages of SIBs in LT environments position them advantageously for specialized applications where conventional lithium-ion technology fails. Arctic infrastructure, polar research installations, aerospace missions, and deep-sea exploration represent immediate deployment opportunities where the superior cold-weather performance and safety characteristics of SIBs justify premium pricing. Military and defense applications, including portable power systems and vehicle electrification in harsh climates, offer substantial market potential due to the enhanced supply chain security and reduced dependence on critical materials that SIBs provide. The integration of SIBs with renewable energy systems in cold climates could revolutionize grid-scale energy storage in northern regions.

Sustainability and circular economy considerations

The abundance and low cost of sodium resources, combined with the potential for aluminum-only current collectors, provide SIBs with significant economic advantages that become more pronounced as technology matures. The development of sustainable recycling processes specifically designed for sodium-ion chemistries will be essential for long-term environmental sustainability. The compatibility of SIB manufacturing with existing lithium-ion production infrastructure reduces barriers to large-scale deployment while enabling rapid scaling of production capacity. The reduced dependence on geopolitically sensitive materials enhances supply chain resilience and supports strategic national interests in energy security.

The convergence of fundamental scientific understanding, materials engineering innovations, and system-level optimization has created unprecedented opportunities for deploying reliable energy storage in extreme environments. While significant challenges remain in scaling laboratory breakthroughs to commercial reality, the strategic advantages of sodium-ion technology, including resource abundance, safety, and superior LT performance position it as a critical enabler of the global energy transition. The path forward requires sustained investment in fundamental research, materials innovation, and manufacturing capability development. Success will depend on close collaboration between academic researchers, industrial partners, and government agencies to address technical challenges while building the infrastructure necessary for widespread deployment. As the world increasingly relies on renewable energy and electrified transportation systems, LT SIBs will play an essential role in ensuring energy security and environmental sustainability in the planet's most challenging environments.

Author contributions

M. S. B. R.: data curation, conceptualization, writing – original draft; D. J.: writing – review & editing, S. A.: cowriting – review & editing, V. G. P.: conceptualization, supervision, writing – review & editing.

Conflicts of interest

There are no conflicts to declare.

Data availability

No primary research results, software or code have been included and no new data were generated or analysed as part of this review.

Acknowledgements

The authors acknowledge the Purdue university, USA, for providing the necessary research facilities. M.S.B.R. wolud like to thank the ANRF, Government of India, for the fellowship under the SERB-Overseas Visiting Doctoral Fellowship (OVDF) scheme with award number SB/S9/Z-03/2017-XV(2023), which supported his research at Purdue University, IN, USA.

References

1 J.-Y. Hwang, S.-T. Myung and Y.-K. Sun, *Chem. Soc. Rev.*, 2017, **46**, 3529–3614.

© 2025 The Author(s). Published by the Royal Society of Chemistry

Open Access Article. Published on 20 August 2025. Downloaded on 18.02.26 05:05:09.
This article is licensed under a Creative Commons Attribution 3.0 Unported Licence.

2 K. M. Abraham, *ACS Energy Lett.*, 2020, **5**, 3544–3547.
3 Z. Cui, C. Liu and A. Manthiram, *Adv. Mater.*, 2025, 2420463.
4 M. Ferraro and G. Tumminia, in *Emerging Battery Technologies to Boost the Clean Energy Transition*, ed. S. Passerini, L. Barelli, M. Baumann, J. Peters and M. Weil, Springer International Publishing, Cham, 2024, pp. 259–266.
5 J. F. Peters, A. Peña Cruz and M. Weil, *Batteries*, 2019, **5**, 10.
6 J. Wu, Y. Zheng, P. Zhang, X. Rao, Z. Zhang, J.-M. Wu and W. Wen, *Research*, 2024, **7**, 0461.
7 Y. Gao, H. Zhang, J. Peng, L. Li, Y. Xiao, L. Li, Y. Liu, Y. Qiao and S. Chou, *Carbon Energy*, 2024, **6**, e464.
8 Laserax., Sodium-Ion Battery *vs.* Lithium-Ion Battery: Which One is Better?, https://www.laserax.com/blog/sodium-ion-vs-lithium-ion-batteries.
9 M. D. Slater, D. Kim, E. Lee and C. S. Johnson, *Adv. Funct. Mater.*, 2013, **23**, 947–958.
10 C. Wang, A. C. Thenuwara, J. Luo, P. P. Shetty, M. T. McDowell, H. Zhu, S. Posada-Pérez, H. Xiong, G. Hautier and W. Li, *Nat. Commun.*, 2022, **13**, 4934.
11 X. Zhou, Y. Huang, B. Wen, Z. Yang, Z. Hao, L. Li, S.-L. Chou and F. Li, *Proc. Natl. Acad. Sci. U. S. A.*, 2024, **121**, e2316914121.
12 K. Chayambuka, G. Mulder, D. L. Danilov and P. H. L. Notten, *Adv. Energy Mater.*, 2018, **8**, 1800079.
13 S. Yang, K. Cheng and Z. Cao, *J. Mater. Chem. A*, 2024, **12**, 13059–13080.
14 H. Luo, Y. Wang, Y.-H. Feng, X.-Y. Fan, X. Han and P.-F. Wang, *Materials*, 2022, **15**, 8166.
15 X. Liu, X. Zheng, X. Qin, Y. Deng, Y. Dai, T. Zhao, Z. Wang, H. Yang and W. Luo, *Nano Energy*, 2022, **103**, 107746.
16 A. Gupta and A. Manthiram, *Adv. Energy Mater.*, 2020, **10**, 2001972.
17 A. Yao, S. M. Benson and W. C. Chueh, *Nat. Energy*, 2025, **10**, 404–416.
18 K. Chayambuka, G. Mulder, D. L. Danilov and P. H. L. Notten, *Adv. Energy Mater.*, 2020, **10**, 2001310.
19 J. Klemens, A.-K. Wurba, D. Burger, M. Müller, W. Bauer, S. Büchele, O. Leonet, J. Alberto Blázquez, I. Boyano, E. Ayerbe, H. Ehrenberg, H. Ehrenberg, A. Smith, P. Scharfer and W. Schabel, *Batteries Supercaps*, 2023, **6**, e202300291.
20 J. Tang, J. Barker and V. G. Pol, *Energy Technol.*, 2018, **6**, 213–220.
21 Y. He, W. Shang and P. Tan, *Carbon Neutralization*, 2024, **3**, 773–780.
22 D. Jeong, B. M. Tackett and V. G. Pol, *Commun. Chem.*, 2025, **8**, 170.
23 Y. Shang, Y. Huang, L. Li, F. Wu and R. Chen, *Chem. Rev.*, 2025, **125**, 5674–5744.
24 P. Li, N. Hu, J. Wang, S. Wang and W. Deng, *Nanomaterials*, 2022, **12**, 3529.
25 C. Che, F. Wu, Y. Li, Y. Li, S. Li, C. Wu and Y. Bai, *Adv. Mater.*, 2024, **36**, 2402291.
26 N. Ge, W. Gao and Y. Gan, *J. Power Sources*, 2024, **623**, 235377.
27 Z. Jian, W. Han, X. Lu, H. Yang, Y. Hu, J. Zhou, Z. Zhou, J. Li, W. Chen, D. Chen and L. Chen, *Adv. Energy Mater.*, 2013, **3**, 156–160.
28 P. Zhou, Z. Zhao, J. Weng, X. Wu, J. Zhou, Z. Niu, R. Feng, X. Zhou, J.-Z. Wang, S. Dou and L. Li, *ACS Energy Lett.*, 2025, **10**, 185–194.
29 P. Liu, L. Miao, Z. Sun, X. Chen and L. Jiao, *Adv. Mater.*, 2024, 2406058.
30 Z. Lu, C. Geng, H. Yang, P. He, S. Wu, Q.-H. Yang and H. Zhou, *Proc. Natl. Acad. Sci. U. S. A.*, 2022, **119**, e2210203119.
31 J. Zhou, Y. Wang, J. Wang, Y. Liu, Y. Li, L. Cheng, Y. Ding, S. Dong, Q. Zhu, M. Tang, Y. Wang, Y. Bi, R. Sun, Z. Wang and H. Wang, *Energy Storage Mater.*, 2022, **50**, 47–54.
32 M. Du, K. Li, N. Yu, Z. Hao, J. Guo, H. Liang, Z. Gu, X. Zhang, K. Zhang, Y. Liu, J. Yang, Y. Liu and X. Wu, *Adv. Mater.*, 2025, **37**, 2418219.
33 Z. Gu, J. Guo, Z. Sun, X. Zhao, X. Wang, H. Liang, B. Zhao, W. Li, X. Pan and X. Wu, *Small*, 2021, **17**, 2102010.
34 G. Fang, Z. Wu, J. Zhou, C. Zhu, X. Cao, T. Lin, Y. Chen, C. Wang, A. Pan and S. Liang, *Adv. Energy Mater.*, 2018, **8**, 1703155.
35 D. Ba, Q. Gui, W. Liu, Z. Wang, Y. Li and J. Liu, *Nano Energy*, 2022, **94**, 106918.
36 J. Hwang, K. Matsumoto and R. Hagiwara, *Adv. Sustainable Syst.*, 2018, **2**, 1700171.
37 K. Zheng, S. Xu, Y. Yao, D. Chen, L. Liu, C. Xu, Y. Feng, X. Rui and Y. Yu, *Chem. Commun.*, 2022, **58**, 10349–10352.
38 T. Liu, B. Wang, X. Gu, L. Wang, M. Ling, G. Liu, D. Wang and S. Zhang, *Nano Energy*, 2016, **30**, 756–761.
39 R.-M. Gao, Z.-J. Zheng, P.-F. Wang, C.-Y. Wang, H. Ye and F.-F. Cao, *Energy Storage Mater.*, 2020, **30**, 9–26.
40 Y. Li, Y. Zhao, X. Feng, X. Wang, Q. Shi, J. Wang, J. Wang, J. Zhang and Y. Hou, *Sci. China Mater.*, 2022, **65**, 328–336.
41 Q. Shi, R. Qi, X. Feng, J. Wang, Y. Li, Z. Yao, X. Wang, Q. Li, X. Lu, J. Zhang and Y. Zhao, *Nat. Commun.*, 2022, **13**, 3205.
42 Q. Wang, Z. Shadike, X. Li, J. Bao, Q. Qiu, E. Hu, S. Bak, X. Xiao, L. Ma, X. Wu, X. Yang and Y. Zhou, *Adv. Energy Mater.*, 2021, **11**, 2003455.
43 J. Qian, C. Wu, Y. Cao, Z. Ma, Y. Huang, X. Ai and H. Yang, *Adv. Energy Mater.*, 2018, **8**, 1702619.
44 A. Zhou, W. Cheng, W. Wang, Q. Zhao, J. Xie, W. Zhang, H. Gao, L. Xue and J. Li, *Adv. Energy Mater.*, 2021, **11**, 2000943.
45 F. Xie, Z. Xu, Z. Guo, A. C. S. Jensen, J. Feng, H. Luo, F. Ding, Y. Lu, Y. Hu and M. Titirici, *Carbon Energy*, 2022, **4**, 914–923.
46 Z. Tang, S. Zhou, Y. Huang, H. Wang, R. Zhang, Q. Wang, D. Sun, Y. Tang and H. Wang, *Electrochem. Energy Rev.*, 2023, **6**, 8.
47 Z. Bai, Q. Yao, M. Wang, W. Meng, S. Dou, H. K. Liu and N. Wang, *Adv. Energy Mater.*, 2024, **14**, 2303788.

© 2025 The Author(s). Published by the Royal Society of Chemistry

Open Access Article. Published on 20 August 2025. Downloaded on 18.02.26 05:05:09.
This article is licensed under a Creative Commons Attribution 3.0 Unported Licence.

48 C. Hu, Y. Li, D. Wang, C. Wu, F. Chen, L. Zhang, F. Wan, W. Hua, Y. Sun, B. Zhong, Z. Wu and X. Guo, *Angew. Chem., Int. Ed.*, 2023, **62**, e202312310.
49 S. Qiao, Q. Zhou, M. Ma, H. K. Liu, S. X. Dou and S. Chong, *ACS Nano*, 2023, **17**, 11220–11252.
50 Z. Li, Y. Zhang, J. Zhang, Y. Cao, J. Chen, H. Liu and Y. Wang, *Angew. Chem., Int. Ed.*, 2022, **61**, e202116930.
51 B. Wang, H. Yang, Y. Feng, S. Zeng, L. Tan, R. Xu, L. Wang, R. Hu and Y. Yu, *Mater. Today Energy*, 2021, **20**, 100627.
52 K.-C. Huang, J.-Z. Guo, H.-H. Li, H.-H. Fan, D.-H. Liu, Y.-P. Zheng, W.-L. Li, X.-L. Wu and J.-P. Zhang, *J. Alloys Compd.*, 2018, **731**, 881–888.
53 J. Holoubek, H. Liu, Z. Wu, Y. Yin, X. Xing, G. Cai, S. Yu, H. Zhou, T. A. Pascal, Z. Chen and P. Liu, *Nat. Energy*, 2021, **6**, 303–313.
54 S. S. Zhang, K. Xu and T. R. Jow, *J. Power Sources*, 2003, **115**, 137–140.
55 A. C. Thenuwara, P. P. Shetty and M. T. McDowell, *Nano Lett.*, 2019, **19**, 8664–8672.
56 D. S. Lutsenko, E. V. Belova, M. V. Zakharkin, O. A. Drozhzhin and E. V. Antipov, *Chemistry*, 2023, **5**, 1588–1598.
57 M. C. Smart, B. V. Ratnakumar and S. Surampudi, *J. Electrochem. Soc.*, 2002, **149**, A361.
58 Y. Qin, S.-G. Choi, L. Mason, J. Liu, Z. Li and T. Gao, *Chem. Sci.*, 2024, **15**, 9224–9239.
59 N. Takenaka, A. Bouibes, Y. Yamada, M. Nagaoka and A. Yamada, *Adv. Mater.*, 2021, **33**, 2100574.
60 K. Xu, *Chem. Rev.*, 2004, **104**, 4303–4418.
61 K. Xu, *Chem. Rev.*, 2014, **114**, 11503–11618.
62 S. J. An, J. Li, C. Daniel, D. Mohanty, S. Nagpure and D. L. Wood, *Carbon*, 2016, **105**, 52–76.
63 Y. Jin, P. M. L. Le, P. Gao, Y. Xu, B. Xiao, M. H. Engelhard, X. Cao, T. D. Vo, J. Hu, L. Zhong, B. E. Matthews, R. Yi, C. Wang, X. Li, J. Liu and J.-G. Zhang, *Nat. Energy*, 2022, **7**, 718–725.
64 S. Leroy, H. Martinez, R. Dedryvère, D. Lemordant and D. Gonbeau, *Appl. Surf. Sci.*, 2007, **253**, 4895–4905.
65 B. Xiang, L. Wang, G. Liu and A. M. Minor, *J. Electrochem. Soc.*, 2013, **160**, A415–A419.
66 Q. Liu, A. Cresce, M. Schroeder, K. Xu, D. Mu, B. Wu, L. Shi and F. Wu, *Energy Storage Mater.*, 2019, **17**, 366–373.
67 Y. Li and Y. Qi, *Energy Environ. Sci.*, 2019, **12**, 1286–1295.
68 Z. Zhang, Y. Li, R. Xu, W. Zhou, Y. Li, S. T. Oyakhire, Y. Wu, J. Xu, H. Wang, Z. Yu, D. T. Boyle, W. Huang, Y. Ye, H. Chen, J. Wan, Z. Bao, W. Chiu and Y. Cui, *Science*, 2022, **375**, 66–70.
69 J. Ming, Z. Cao, W. Wahyudi, M. Li, P. Kumar, Y. Wu, J.-Y. Hwang, M. N. Hedhili, L. Cavallo, Y.-K. Sun and L.-J. Li, *ACS Energy Lett.*, 2018, **3**, 335–340.
70 Q. Li, Z. Cao, W. Wahyudi, G. Liu, G.-T. Park, L. Cavallo, T. D. Anthopoulos, L. Wang, Y.-K. Sun, H. N. Alshareef and J. Ming, *ACS Energy Lett.*, 2021, **6**, 69–78.
71 R. Mogensen, D. Brandell and R. Younesi, *ACS Energy Lett.*, 2016, **1**, 1173–1178.
72 J. Song, B. Xiao, Y. Lin, K. Xu and X. Li, *Adv. Energy Mater.*, 2018, **8**, 1703082.
73 S. Miertuš, E. Scrocco and J. Tomasi, *Chem. Phys.*, 1981, **55**, 117–129.
74 G. Kamath, R. W. Cutler, S. A. Deshmukh, M. Shakourian-Fard, R. Parrish, J. Huether, D. P. Butt, H. Xiong and S. K. R. S. Sankaranarayanan, *J. Phys. Chem. C*, 2014, **118**, 13406–13416.
75 M. Shakourian-Fard, G. Kamath, K. Smith, H. Xiong and S. K. R. S. Sankaranarayanan, *J. Phys. Chem. C*, 2015, **119**, 22747–22759.
76 M. Okoshi, Y. Yamada, A. Yamada and H. Nakai, *J. Electrochem. Soc.*, 2013, **160**, A2160–A2165.
77 D. Hubble, D. E. Brown, Y. Zhao, C. Fang, J. Lau, B. D. McCloskey and G. Liu, *Energy Environ. Sci.*, 2022, **15**, 550–578.
78 K. Chen, X. Shen, L. Luo, H. Chen, R. Cao, X. Feng, W. Chen, Y. Fang and Y. Cao, *Angew. Chem., Int. Ed.*, 2023, **62**, e202312373.
79 R. Hou, S. Guo and H. Zhou, *Adv. Energy Mater.*, 2023, **13**, 2300053.
80 M. Wang, L. Yin, M. Zheng, X. Liu, C. Yang, W. Hu, J. Xie, R. Sun, J. Han, Y. You and J. Lu, *Nat. Commun.*, 2024, **15**, 8866.
81 Z. Tian, Y. Zou, G. Liu, Y. Wang, J. Yin, J. Ming and H. N. Alshareef, *Adv. Sci.*, 2022, **9**, 2201207.
82 X. Zhu and L. Wang, *EcoMat*, 2020, **2**, e12043.
83 A. Ponrouch, E. Marchante, M. Courty, J.-M. Tarascon and M. R. Palacín, *Energy Environ. Sci.*, 2012, **5**, 8572.
84 A. Liu, Q. Zhang, L. Li, L. Zhang, Z. Jin, C. Wang and Z. Su, *Chem. Eng. J.*, 2021, **405**, 126689.
85 X. Lin, X. Du, P. S. Tsui, J.-Q. Huang, H. Tan and B. Zhang, *Electrochim. Acta*, 2019, **316**, 60–68.
86 Y. You, H. Yao, S. Xin, Y. Yin, T. Zuo, C. Yang, Y. Guo, Y. Cui, L. Wan and J. B. Goodenough, *Adv. Mater.*, 2016, **28**, 7243–7248.
87 X. Zheng, L. Huang, X. Ye, J. Zhang, F. Min, W. Luo and Y. Huang, *Chem*, 2021, **7**, 2312–2346.
88 H. Che, X. Yang, Y. Yu, C. Pan, H. Wang, Y. Deng, L. Li and Z.-F. Ma, *Green Energy Environ.*, 2021, **6**, 212–219.
89 X.-H. Ma, Y.-Y. Wei, Y.-D. Wu, J. Wang, W. Jia, J.-H. Zhou, Z.-F. Zi and J.-M. Dai, *Electrochim. Acta*, 2019, **297**, 392–397.
90 M. C. Smart, B. V. Ratnakumar, K. B. Chin and L. D. Whitcanack, *J. Electrochem. Soc.*, 2010, **157**, A1361.
91 P. Desai, J. Abou-Rjeily, J.-M. Tarascon and S. Mariyappan, *Electrochim. Acta*, 2022, **416**, 140217.
92 Z. Tang, H. Wang, P. Wu, S. Zhou, Y. Huang, R. Zhang, D. Sun, Y. Tang and H. Wang, *Angew. Chem., Int. Ed.*, 2022, **61**, e202200475.
93 Z. Li, J. Liu, X. Bi, Y. Qin and T. Gao, *J. Mater. Chem. A*, 2023, **11**, 19996–20010.
94 Y. Mo, G. Liu, Y. Yin, M. Tao, J. Chen, Y. Peng, Y. Wang, Y. Yang, C. Wang, X. Dong and Y. Xia, *Adv. Energy Mater.*, 2023, **13**, 2301285.

© 2025 The Author(s). Published by the Royal Society of Chemistry

Open Access Article. Published on 20 August 2025. Downloaded on 18.02.26 05:05:09.
This article is licensed under a Creative Commons Attribution 3.0 Unported Licence.

95 Y. Li, F. Wu, Y. Li, M. Liu, X. Feng, Y. Bai and C. Wu, *Chem. Soc. Rev.*, 2022, **51**, 4484–4536.
96 K. Nobuhara, H. Nakayama, M. Nose, S. Nakanishi and H. Iba, *J. Power Sources*, 2013, **243**, 585–587.
97 B. Jache and P. Adelhelm, *Angew. Chem., Int. Ed.*, 2014, **53**, 10169–10173.
98 Y.-B. Niu, Y.-X. Yin, W.-P. Wang, P.-F. Wang, W. Ling, Y. Xiao and Y.-G. Guo, *CCS Chem.*, 2020, **2**, 589–597.
99 P. Peljo and H. H. Girault, *Energy Environ. Sci.*, 2018, **11**, 2306–2309.
100 X. Liu, X. Zheng, Y. Dai, W. Wu, Y. Huang, H. Fu, Y. Huang and W. Luo, *Adv. Funct. Mater.*, 2021, **31**, 2103522.
101 Y. Wang, J. Duan, Z. Zhu, X. Li, Q. Cheng, Y. Yang, S. Zhang, Y. Cao and S. Hou, *ACS Appl. Mater. Interfaces*, 2025, **17**, 30885–30894.
102 C. Yang, X. Liu, Y. Lin, L. Yin, J. Lu and Y. You, *Adv. Mater.*, 2023, **35**, 2301817.
103 J. Zhang, D. Wang, W. Lv, L. Qin, S. Niu, S. Zhang, T. Cao, F. Kang and Q. Yang, *Adv. Energy Mater.*, 2018, **8**, 1801361.
104 L. Yin, M. Wang, C. Xie, C. Yang, J. Han and Y. You, *ACS Appl. Mater. Interfaces*, 2023, **15**, 9517–9523.
105 D. Kruk, M. Jancelewicz, A. Klimaszyk, R. Markiewicz, Z. Fojud and S. Jurga, *Materials*, 2021, **15**, 216.
106 A. Basile, M. Hilder, F. Makhlooghiazad, C. Pozo-Gonzalo, D. R. MacFarlane, P. C. Howlett and M. Forsyth, *Adv. Energy Mater.*, 2018, **8**, 1703491.
107 X. Hu, E. Matios, Y. Zhang, C. Wang, J. Luo and W. Li, *Angew. Chem., Int. Ed.*, 2021, **60**, 5978–5983.
108 W. Ren, X. Chen and C. Zhao, *Adv. Energy Mater.*, 2018, **8**, 1801413.
109 P. Jiang, Z. Lei, L. Chen, X. Shao, X. Liang, J. Zhang, Y. Wang, J. Zhang, Z. Liu and J. Feng, *ACS Appl. Mater. Interfaces*, 2019, **11**, 28762–28768.
110 X. Wang, H. Huang, F. Zhou, P. Das, P. Wen, S. Zheng, P. Lu, Y. Yu and Z.-S. Wu, *Nano Energy*, 2021, **82**, 105688.
111 Z. Wang, Y. Xu, J. Peng, M. Ou, P. Wei, C. Fang, Q. Li, J. Huang, J. Han and Y. Huang, *Small*, 2021, **17**, 2101650.
112 K. Zhu, Z. Li, Z. Sun, P. Liu, T. Jin, X. Chen, H. Li, W. Lu and L. Jiao, *Small*, 2022, **18**, 2107662.
113 J.-Z. Rong, T.-X. Cai, Y.-Z. Bai, X. Zhao, T. Wu, Y.-K. Wu, W. Zhao, W.-J. Dong, S.-M. Xu, J. Chen and F.-Q. Huang, *Cell Rep. Phys. Sci.*, 2022, **3**, 100805.
114 H. Ao, C. Chen, Z. Hou, W. Cai, M. Liu, Y. Jin, X. Zhang, Y. Zhu and Y. Qian, *J. Mater. Chem. A*, 2020, **8**, 14190–14197.
115 J. Zheng, W. Li, X. Liu, J. Zhang, X. Feng and W. Chen, *Energy Environ. Mater.*, 2023, **6**, e12422.
116 S. Das, V. G. Pol and V. Adyam, *Energy Adv.*, 2024, **3**, 419–423.
117 G. Du, M. Tao, J. Li, T. Yang, W. Gao, J. Deng, Y. Qi, S. Bao and M. Xu, *Adv. Energy Mater.*, 2020, **10**, 1903351.
118 J. Zheng, J. Zhang, W. Li, J. Ge and W. Chen, *Chem. Eng. J.*, 2023, **465**, 142796.
119 T. Zhao, X. Zheng, D. Wang, L. Huang, B. Li, X. Liu, H. Yang, Y. Dai, Y. Huang and W. Luo, *Adv. Funct. Mater.*, 2023, **33**, 2304928.
120 Y. Pang, D. Zhang, H. Sun, X. Li, S. Xia, T. Yuan, T. Chen, J. Yang, J. Wang and S. Zheng, *Adv. Energy Mater.*, 2023, **13**, 2301637.
121 H. Liu, Y. Xing, N. Chen, J. Wu, Y. Li and C. Zhang, *Chem. Mater.*, 2023, **35**, 8686–8694.
122 X. Zhao, Z. Fu, X. Zhang, X. Wang, B. Li, D. Zhou and F. Kang, *Energy Environ. Sci.*, 2024, **17**, 2406–2430.
123 M. Wang, M. Zheng, J. Lu and Y. You, *Joule*, 2024, **8**, 2467–2482.
124 Y. Lin, S. Luo, W. Zhao, Q. Sun, J. Cong, P. Li, P. Li and S. Yan, *J. Energy Chem.*, 2024, **98**, 441–471.
125 K.-F. Ren, H. Liu, J.-X. Guo, X. Sun, F. Jiang, C. Guo, W. Bao, F. Yu, G. Kalimuldina, L. Kong, X.-B. Cheng and J. Li, *ACS Energy Lett.*, 2024, **9**, 2960–2980.
126 H. Che, S. Chen, Y. Xie, H. Wang, K. Amine, X.-Z. Liao and Z.-F. Ma, *Energy Environ. Sci.*, 2017, **10**, 1075–1101.
127 M. P. Do, N. Bucher, A. Nagasubramanian, I. Markovits, T. Bingbing, P. J. Fischer, K. P. Loh, F. E. Kühn and M. Srinivasan, *ACS Appl. Mater. Interfaces*, 2019, **11**, 23972–23981.
128 A. C. Thenuwara, P. P. Shetty, N. Kondekar, C. Wang, W. Li and M. T. McDowell, *J. Mater. Chem. A*, 2021, **9**, 10992–11000.
129 Y. Li, Y. Yang, Y. Lu, Q. Zhou, X. Qi, Q. Meng, X. Rong, L. Chen and Y.-S. Hu, *ACS Energy Lett.*, 2020, **5**, 1156–1158.
130 Z. Wang, X. Zheng, X. Liu, Y. Huang, L. Huang, Y. Chen, M. Han and W. Luo, *ACS Appl. Mater. Interfaces*, 2022, **14**, 40985–40991.
131 X. Cao, H. Jia, W. Xu and J.-G. Zhang, *J. Electrochem. Soc.*, 2021, **168**, 010522.
132 W. Van Ekeren, A. Hall, K. Lahtinen and R. Younesi, *ChemElectroChem*, 2024, **11**, e202400050.
133 B. Mosallanejad, S. S. Malek, M. Ershadi, A. A. Daryakenari, Q. Cao, F. Boorboor Ajdari and S. Ramakrishna, *J. Electroanal. Chem.*, 2021, **895**, 115505.
134 Z.-K. Han, D. Sarker, R. Ouyang, A. Mazheika, Y. Gao and S. V. Levchenko, *Nat. Commun.*, 2021, **12**, 1833.
135 Q. Nian, J. Wang, S. Liu, T. Sun, S. Zheng, Y. Zhang, Z. Tao and J. Chen, *Angew. Chem., Int. Ed.*, 2019, **58**, 16994–16999.
136 X. Song, T. Meng, Y. Deng, A. Gao, J. Nan, D. Shu and F. Yi, *Electrochim. Acta*, 2018, **281**, 370–377.
137 L. Chen, H. Li, H. Yoshitake, L. Qi, N. Gu and H. Wang, *Electrochim. Acta*, 2015, **157**, 333–344.
138 S. Zhong, Y. Yu, Y. Yang, Y. Yao, L. Wang, S. He, Y. Yang, L. Liu, W. Sun, Y. Feng, H. Pan, X. Rui and Y. Yu, *Angew. Chem., Int. Ed.*, 2023, **62**, e202301169.
139 N. Anantharamulu, K. Koteswara Rao, G. Rambabu, B. Vijaya Kumar, V. Radha and M. Vithal, *J. Mater. Sci.*, 2011, **46**, 2821–2837.
140 A. Joy, K. Kumari, F. Parween, M. S. Sultana and G. C. Nayak, *ACS Omega*, 2024, **9**, 22509–22531.
141 Y. Fang, L. Xiao, X. Ai, Y. Cao and H. Yang, *Adv. Mater.*, 2015, **27**, 5895–5900.

© 2025 The Author(s). Published by the Royal Society of Chemistry

Open Access Article. Published on 20 August 2025. Downloaded on 18.02.26 05:05:09.
This article is licensed under a Creative Commons Attribution 3.0 Unported Licence.

142 C. Wang, D. Du, M. Song, Y. Wang and F. Li, *Adv. Energy Mater.*, 2019, **9**, 1900022.
143 S. Xu, K. Yao, D. Yang, D. Chen, C. Lin, C. Liu, H. Wu, J. Zeng, L. Liu, Y. Zheng and X. Rui, *ACS Appl. Mater. Interfaces*, 2023, **15**, 14329–14338.
144 J. Guo, P. Wang, X. Wu, X. Zhang, Q. Yan, H. Chen, J. Zhang and Y. Guo, *Adv. Mater.*, 2017, **29**, 1701968.
145 C. Sun, Y. Zhao, Q. Ni, Z. Sun, X. Yuan, J. Li and H. Jin, *Energy Storage Mater.*, 2022, **49**, 291–298.
146 R. Liu, G. Xu, Q. Li, S. Zheng, G. Zheng, Z. Gong, Y. Li, E. Kruskop, R. Fu, Z. Chen, K. Amine and Y. Yang, *ACS Appl. Mater. Interfaces*, 2017, **9**, 43632–43639.
147 M. Chen, W. Hua, J. Xiao, D. Cortie, W. Chen, E. Wang, Z. Hu, Q. Gu, X. Wang, S. Indris, S.-L. Chou and S.-X. Dou, *Nat. Commun.*, 2019, **10**, 1480.
148 X. Ma, X. Wu and P. Shen, *ACS Appl. Energy Mater.*, 2018, **1**, 6268–6278.
149 X. Li, Y. Zhang, B. Zhang, K. Qin, H. Liu and Z.-F. Ma, *J. Power Sources*, 2022, **521**, 230922.
150 C. Delmas, C. Fouassier and P. Hagenmuller, *Physica B+C*, 1980, **99**, 81–85.
151 C. Zhao, Q. Wang, Z. Yao, J. Wang, B. Sánchez-Lengeling, F. Ding, X. Qi, Y. Lu, X. Bai, B. Li, H. Li, A. Aspuru-Guzik, X. Huang, C. Delmas, M. Wagemaker, L. Chen and Y.-S. Hu, *Science*, 2020, **370**, 708–711.
152 X. Liang and Y. Sun, *Adv. Funct. Mater.*, 2022, **32**, 2206154.
153 J.-Y. Hwang, S.-M. Oh, S.-T. Myung, K. Y. Chung, I. Belharouak and Y.-K. Sun, *Nat. Commun.*, 2015, **6**, 6865.
154 S. Liu, J. Wan, M. Ou, W. Zhang, M. Chang, F. Cheng, Y. Xu, S. Sun, C. Luo, K. Yang, C. Fang and J. Han, *Adv. Energy Mater.*, 2023, **13**, 2203521.
155 L. Liang, X. Sun, D. K. Denis, J. Zhang, L. Hou, Y. Liu and C. Yuan, *ACS Appl. Mater. Interfaces*, 2019, **11**, 4037–4046.
156 B. Peng, Z. Zhou, J. Xu, N. Ahmad, S. Zeng, M. Cheng, L. Ma, Y. Li and G. Zhang, *ACS Mater. Lett.*, 2023, **5**, 2233–2242.
157 V. R. R. Boddu, M. Palanisamy, L. Sinha, S. C. Yadav, V. G. Pol and P. M. Shirage, *Sustainable Energy Fuels*, 2021, **5**, 3219–3228.
158 P. Zhou, Z. Che, J. Liu, J. Zhou, X. Wu, J. Weng, J. Zhao, H. Cao, J. Zhou and F. Cheng, *Energy Storage Mater.*, 2023, **57**, 618–627.
159 J. Zhou, J. Liu, Y. Li, Z. Zhao, P. Zhou, X. Wu, X. Tang and J. Zhou, *J. Colloid Interface Sci.*, 2023, **638**, 758–767.
160 H. V. S. R. M. Koppisetti, H. Rao, H. V. Ramasamy, H. R. Inta, S. Das, S. Kim, Y. Zhang, H. Wang, V. Mahalingam and V. G. Pol, *ACS Appl. Mater. Interfaces*, 2023, **15**, 32291–32300.
161 W. Wang, Y. Gang, Z. Hu, Z. Yan, W. Li, Y. Li, Q.-F. Gu, Z. Wang, S.-L. Chou, H.-K. Liu and S.-X. Dou, *Nat. Commun.*, 2020, **11**, 980.
162 B. Xie, B. Sun, T. Gao, Y. Ma, G. Yin and P. Zuo, *Coord. Chem. Rev.*, 2022, **460**, 214478.
163 J. Peng, Y. Gao, H. Zhang, Z. Liu, W. Zhang, L. Li, Y. Qiao, W. Yang, J. Wang, S. Dou and S. Chou, *Angew. Chem., Int. Ed.*, 2022, **61**, e202205867.
164 J. Zhang, J. Wan, M. Ou, S. Liu, B. Huang, J. Xu, S. Sun, Y. Xu, Y. Lin, C. Fang and J. Han, *Energy Mater.*, 2023, **3**, 300008, DOI: 10.20517/energymater.2022.71.
165 L. Zhang, C. Wei, X. Fu, Z. Chen, B. Yan, P. Sun, K. Chang and X. Yang, *Carbon Energy*, 2021, **3**, 827–839.
166 Y. Kim, K. Ha, S. M. Oh and K. T. Lee, *Chem. – Eur. J.*, 2014, **20**, 11980–11992.
167 M.-S. Balogun, Y. Luo, W. Qiu, P. Liu and Y. Tong, *Carbon*, 2016, **98**, 162–178.
168 Y. Mei, Y. Huang and X. Hu, *J. Mater. Chem. A*, 2016, **4**, 12001–12013.
169 F. Klein, B. Jache, A. Bhide and P. Adelhelm, *Phys. Chem. Chem. Phys.*, 2013, **15**, 15876.
170 V. L. Chevrier and G. Ceder, *J. Electrochem. Soc.*, 2011, **158**, A1011.
171 M. Mortazavi, Q. Ye, N. Birbilis and N. V. Medhekar, *J. Power Sources*, 2015, **285**, 29–36.
172 S. P. Ong, V. L. Chevrier, G. Hautier, A. Jain, C. Moore, S. Kim, X. Ma and G. Ceder, *Energy Environ. Sci.*, 2011, **4**, 3680.
173 D. Zhou, M. Peer, Z. Yang, V. G. Pol, F. D. Key, J. Jorne, H. C. Foley and C. S. Johnson, *J. Mater. Chem. A*, 2016, **4**, 6271–6275.
174 V. G. Pol, E. Lee, D. Zhou, F. Dogan, J. M. Calderon-Moreno and C. S. Johnson, *Electrochim. Acta*, 2014, **127**, 61–67.
175 D. A. Stevens and J. R. Dahn, *J. Electrochem. Soc.*, 2000, **147**, 4428.
176 D. A. Stevens and J. R. Dahn, *J. Electrochem. Soc.*, 2001, **148**, A803.
177 E. Irisarri, A. Ponrouch and M. R. Palacin, *J. Electrochem. Soc.*, 2015, **162**, A2476–A2482.
178 C. Bommier, T. W. Surta, M. Dolgos and X. Ji, *Nano Lett.*, 2015, **15**, 5888–5892.
179 M. M. Doeff, Y. Ma, S. J. Visco and L. C. De Jonghe, *J. Electrochem. Soc.*, 1993, **140**, L169–L170.
180 P. Yadav, A. K. Das, A. Torris, K. Wasnik, H. V. S. R. M. Koppisetti, V. G. Pol, V. Shelke and M. Shelke, *Mater. Today Chem.*, 2024, **37**, 101978.
181 Q. Liu, R. Xu, D. Mu, G. Tan, H. Gao, N. Li, R. Chen and F. Wu, *Carbon Energy*, 2022, **4**, 458–479.
182 X. Yin, Z. Lu, J. Wang, X. Feng, S. Roy, X. Liu, Y. Yang, Y. Zhao and J. Zhang, *Adv. Mater.*, 2022, **34**, 2109282.
183 Q. Li, X. Liu, Y. Tao, J. Huang, J. Zhang, C. Yang, Y. Zhang, S. Zhang, Y. Jia, Q. Lin, Y. Xiang, J. Cheng, W. Lv, F. Kang, Y. Yang and Q.-H. Yang, *Natl. Sci. Rev.*, 2022, **9**, nwac084.
184 Z. Zheng, S. Hu, W. Yin, J. Peng, R. Wang, J. Jin, B. He, Y. Gong, H. Wang and H. J. Fan, *Adv. Energy Mater.*, 2024, **14**, 2303064.
185 Y. Huang, X. Zhong, X. Hu, Y. Li, K. Wang, H. Tu, W. Deng, G. Zou, H. Hou and X. Ji, *Adv. Funct. Mater.*, 2024, **34**, 2308392.
186 S. Zhang, N. Sun, X. Li, R. A. Soomro and B. Xu, *Energy Storage Mater.*, 2024, **66**, 103183.

© 2025 The Author(s). Published by the Royal Society of Chemistry

Open Access Article. Published on 20 August 2025. Downloaded on 18.02.26 05:05:09.
This article is licensed under a Creative Commons Attribution 3.0 Unported Licence.

187 Y. Li, A. Vasileiadis, Q. Zhou, Y. Lu, Q. Meng, Y. Li, P. Ombrini, J. Zhao, Z. Chen, Y. Niu, X. Qi, F. Xie, R. Van Der Jagt, S. Ganapathy, M.-M. Titirici, H. Li, L. Chen, M. Wagemaker and Y.-S. Hu, *Nat. Energy*, 2024, **9**, 134–142.
188 X. Feng, Y. Li, Y. Li, M. Liu, L. Zheng, Y. Gong, R. Zhang, F. Wu, C. Wu and Y. Bai, *Energy Environ. Sci.*, 2024, **17**, 1387–1396.
189 L. Zhao, Z. Hu, W. Lai, Y. Tao, J. Peng, Z. Miao, Y. Wang, S. Chou, H. Liu and S. Dou, *Adv. Energy Mater.*, 2021, **11**, 2002704.
190 M. Palanisamy, R. Perumal and V. G. Pol, *ACS Appl. Mater. Interfaces*, 2022, **14**, 684–697.
191 J. Tang, D. K. Kye and V. G. Pol, *J. Power Sources*, 2018, **396**, 476–482.
192 B. Hou, Y. Wang, Q. Ning, W. Li, X. Xi, X. Yang, H. Liang, X. Feng and X. Wu, *Adv. Mater.*, 2019, **31**, 1903125.
193 A. Ponrouch and M. R. Palacín, *Electrochem. Commun.*, 2015, **54**, 51–54.
194 Y. Yuan, Z. Chen, H. Yu, X. Zhang, T. Liu, M. Xia, R. Zheng, M. Shui and J. Shu, *Energy Storage Mater.*, 2020, **32**, 65–90.
195 A. Mehmood, G. Ali, B. Koyutürk, J. Pampel, K. Y. Chung and T.-P. Fellinger, *Energy Storage Mater.*, 2020, **28**, 101–111.
196 Z. Lu, J. Wang, W. Feng, X. Yin, X. Feng, S. Zhao, C. Li, R. Wang, Q. Huang and Y. Zhao, *Adv. Mater.*, 2023, **35**, 2211461.
197 M. Song, Z. Hu, C. Yuan, P. Dai, T. Zhang, L. Dong, T. Jin, C. Shen and K. Xie, *Adv. Energy Mater.*, 2024, **14**, 2304537.
198 J. Yang, X. Wang, W. Dai, X. Lian, X. Cui, W. Zhang, K. Zhang, M. Lin, R. Zou, K. P. Loh, Q.-H. Yang and W. Chen, *Nano-Micro Lett.*, 2021, **13**, 98.
199 S. Guo, J. Yi, Y. Sun and H. Zhou, *Energy Environ. Sci.*, 2016, **9**, 2978–3006.
200 Z. Liu, R. Du, X. He, J. Wang, Y. Qiao, L. Li and S. Chou, *ChemSusChem*, 2021, **14**, 3724–3743.
201 D.-R. Deng, X.-Y. Cui, Q.-H. Wu, M.-S. Zheng and Q.-F. Dong, *J. Alloys Compd.*, 2020, **835**, 155413.
202 W. Meng, Z. Dang, D. Li and L. Jiang, *Adv. Mater.*, 2023, **35**, 2301376.
203 H. Li, L. Peng, Y. Zhu, D. Chen, X. Zhang and G. Yu, *Energy Environ. Sci.*, 2016, **9**, 3399–3405.
204 Q. Li, K. Jiang, X. Li, Y. Qiao, X. Zhang, P. He, S. Guo and H. Zhou, *Adv. Energy Mater.*, 2018, **8**, 1801162.
205 T. Xu, M. Zhao, Z. Li, Z. Su, W. Ren, S. Yang and V. G. Pol, *Energy Technol.*, 2022, **10**, 2200970.
206 Y. He, Z. Zhang, G. Feng and H. Li, *Heliyon*, 2024, **10**, e23396.
207 Q. Hu, M. Yu, J. Liao, Z. Wen and C. Chen, *J. Mater. Chem. A*, 2018, **6**, 2365–2370.
208 D. Reber, R.-S. Kühnel and C. Battaglia, *ACS Mater. Lett.*, 2019, **1**, 44–51.
209 Q. Nian, S. Liu, J. Liu, Q. Zhang, J. Shi, C. Liu, R. Wang, Z. Tao and J. Chen, *ACS Appl. Energy Mater.*, 2019, **2**, 4370–4378.
210 L. Wang, B. Wang, G. Liu, T. Liu, T. Gao and D. Wang, *RSC Adv.*, 2016, **6**, 70277–70283.
211 Y. Qi, J. Li, W. Zhong, S. Bao and M. Xu, *Chem. Eng. J.*, 2021, **417**, 128159.
212 Y. Xia, L. Que, F. Yu, L. Deng, Z. Liang, Y. Jiang, M. Sun, L. Zhao and Z. Wang, *Nano-Micro Lett.*, 2022, **14**, 143.
213 J. Li, S. Tang, Z. Li, Z. Ding, T. Wang and C. Wang, *J. Colloid Interface Sci.*, 2023, **629**, 461–472.
214 J. Li, S. Tang, J. Hao, Q. Yuan, T. Wang, L. Pan, J. Li, S. Yang and C. Wang, *J. Energy Chem.*, 2024, **89**, 635–645.
215 H. Zhang, I. Hasa and S. Passerini, *Adv. Energy Mater.*, 2018, **8**, 1702582.
216 E. Goikolea, V. Palomares, S. Wang, I. R. De Larramendi, X. Guo, G. Wang and T. Rojo, *Adv. Energy Mater.*, 2020, **10**, 2002055.
217 S. Ghosh, Z. Qi, H. Wang, S. K. Martha and V. G. Pol, *Electrochim. Acta*, 2021, **383**, 138339.
218 X. Wei, X. Wang, X. Tan, Q. An and L. Mai, *Adv. Funct. Mater.*, 2018, **28**, 1804458.
219 Z. Huang, H. Hou, C. Wang, S. Li, Y. Zhang and X. Ji, *Chem. Mater.*, 2017, **29**, 7313–7322.
220 L. Fang, N. Bahlawane, W. Sun, H. Pan, B. B. Xu, M. Yan and Y. Jiang, *Small*, 2021, **17**, 2101137.
221 S. Dai, L. Wang, M. Cao, Z. Zhong, Y. Shen and M. Wang, *Mater. Today Energy*, 2019, **12**, 114–128.
222 Z. Ali, T. Zhang, M. Asif, L. Zhao, Y. Yu and Y. Hou, *Mater. Today*, 2020, **35**, 131–167.
223 M. Jiang, Y. Hu, B. Mao, Y. Wang, Z. Yang, T. Meng, X. Wang and M. Cao, *Nat. Commun.*, 2022, **13**, 5588.
224 H.-H. Fan, H.-H. Li, J.-Z. Guo, Y.-P. Zheng, K.-C. Huang, C.-Y. Fan, H.-Z. Sun, X.-F. Li, X.-L. Wu and J.-P. Zhang, *J. Mater. Chem. A*, 2018, **6**, 7997–8005.
225 Y. Song, Y. Li, L. Zhu, Z. Pan, Y. Jiang, P. Wang, Y.-N. Zhou, F. Fang, L. Hu and D. Sun, *J. Mater. Chem. A*, 2018, **6**, 1086–1093.
226 F. Mo, Z. Lian, B. Fu, Y. Song, P. Wang, F. Fang, Y.-N. Zhou, S. Peng and D. Sun, *J. Mater. Chem. A*, 2019, **7**, 9051–9058.
227 X. Wang, W. Zhao, W. Zhang, K. W. Wong, J. Wu, T. Chen and S. Huang, *ACS Sustainable Chem. Eng.*, 2021, **9**, 11705–11713.
228 Y. Tian, J. Lu, H. Tang, X. Wang, L. Zhang, P. Hu, L. Zhou, Y. Wang, Y. Guo, R. Khatoon, Q. Zhang, Q. He, Y. He, M. Qiu, Y. Hou and Z. Ye, *Chem. Eng. J.*, 2021, **422**, 130054.
229 Y. Huang, Z. Wang, M. Guan, F. Wu and R. Chen, *Adv. Mater.*, 2020, **32**, 2003534.
230 L.-F. Zhou, X.-W. Gao, T. Du, H. Gong, L.-Y. Liu and W.-B. Luo, *Chem. Eng. J.*, 2022, **435**, 134838.
231 B. Hou, Y. Wang, D. Liu, Z. Gu, X. Feng, H. Fan, T. Zhang, C. Lü and X. Wu, *Adv. Funct. Mater.*, 2018, **28**, 1805444.
232 Y.-Y. Wang, H. Fan, B.-H. Hou, X.-H. Rui, Q.-L. Ning, Z. Cui, J.-Z. Guo, Y. Yang and X.-L. Wu, *J. Mater. Chem. A*, 2018, **6**, 22966–22975.
233 S. Ding, B. Zhou, C. Chen, Z. Huang, P. Li, S. Wang, G. Cao and M. Zhang, *ACS Nano*, 2020, **14**, 9626–9636.

© 2025 The Author(s). Published by the Royal Society of Chemistry

Open Access Article. Published on 20 August 2025. Downloaded on 18.02.26 05:05:09.
This article is licensed under a Creative Commons Attribution 3.0 Unported Licence.

234 H. Tan, D. Chen, X. Rui and Y. Yu, *Adv. Funct. Mater.*, 2019, **29**, 1808745.
235 S. Liang, Y. Cheng, J. Zhu, Y. Xia and P. Müller-Buschbaum, *Small Methods*, 2020, **4**, 2000218.
236 J. Chen, X. Fan, X. Ji, T. Gao, S. Hou, X. Zhou, L. Wang, F. Wang, C. Yang, L. Chen and C. Wang, *Energy Environ. Sci.*, 2018, **11**, 1218–1225.
237 Y. Wang, B. Hou, J. Guo, Q. Ning, W. Pang, J. Wang, C. Lü and X. Wu, *Adv. Energy Mater.*, 2018, **8**, 1703252.
238 S. Ghosh, Z. Qi, H. Wang, S. K. Martha and V. G. Pol, *Chem. Commun.*, 2020, **56**, 9663–9666.
239 J.-K. Meng, W.-W. Wang, Q.-C. Wang, M.-H. Cao, Z.-W. Fu, X.-J. Wu and Y.-N. Zhou, *Electrochim. Acta*, 2019, **303**, 32–39.
240 B. Chen, H. Qin, K. Li, B. Zhang, E. Liu, N. Zhao, C. Shi and C. He, *Nano Energy*, 2019, **66**, 104133.
241 H. Wu, J. Hao, Y. Jiang, Y. Jiao, J. Liu, X. Xu, K. Davey, C. Wang and S.-Z. Qiao, *Nat. Commun.*, 2024, **15**, 575.
242 Z. Yang, A. Huang, C.-W. Lin, B. C. Kroes, X. Chang, M. F. El-Kady, Y. Li and R. B. Kaner, *ACS Appl. Mater. Interfaces*, 2025, **17**, 7595–7606.
243 L. Elbinger, E. Schröter, P. Zimmer, C. Friebe, M. Osenberg, I. Manke and U. S. Schubert, *J. Phys. Chem. C*, 2024, **128**, 11465–11476.
244 H. Yamauchi, J. Ikejiri, K. Tsunoda, A. Tanaka, F. Sato, T. Honma and T. Komatsu, *Sci. Rep.*, 2020, **10**, 9453.
245 Z. Li, Y. Hao, F. Cao, Y. Zhang, Y. Wang, S. Zhang and B. Tang, *ACS Appl. Mater. Interfaces*, 2025, **17**, 16072–16084.
246 C. Liu, D. Xu, J. Weng, S. Zhou, W. Li, Y. Wan, S. Jiang, D. Zhou, J. Wang and Q. Huang, *Materials*, 2020, **13**, 4622.
247 Y. Wang, X. Zhang and Z. Chen, *Appl. Energy*, 2022, **313**, 118832.
248 T. Qin, H. Yang, L. Wang, W. Xue, N. Yao, Q. Li, X. Chen, X. Yang, X. Yu, Q. Zhang and H. Li, *Angew. Chem., Int. Ed.*, 2024, **63**, e202408902.
249 A. D. Sendek and V. Viswanathan, *Electrochem. Soc. Interface*, 2025, **34**, 39–42.
250 Q. Hu, J. Lu, J. Hui, Z. Rao, Y. Ren and H. Wang, *Adv. Funct. Mater.*, 2025, e08438.
251 A. Bhowmik, M. Berecibar, M. Casas-Cabanas, G. Csanyi, R. Dominko, K. Hermansson, M. R. Palacin, H. S. Stein and T. Vegge, *Adv. Energy Mater.*, 2022, **12**, 2102698.
252 M. R. Nair and T. Roy, *Chem. Phys. Rev.*, 2025, **6**, 011311.
253 A. Bordes, G. Marlair, A. Zantman, A. Chesnaye, P.-A. L. Lore and A. Lecocq, *ACS Energy Lett.*, 2022, **7**, 3386–3391.
254 A. Yang, S. Xin, L. Mai and Y. You, *Adv. Energy Mater.*, 2021, **11**, 2000974.
255 M. Palanisamy, V. R. R. Boddu, P. M. Shirage and V. G. Pol, *ACS Appl. Mater. Interfaces*, 2021, **13**, 31594–31604.
256 Y. Yue, Z. Jia, Y. Li, Y. Wen, Q. Lei, Q. Duan, J. Sun and Q. Wang, *Process Saf. Environ. Prot.*, 2024, **189**, 61–70.
257 W. Mei, Z. Cheng, L. Wang, A. Teng, Z. Li, K. Jin, J. Sun and Q. Wang, *J. Energy Chem.*, 2025, **102**, 18–26.
258 A. Yang, C. Yang, K. Xie, S. Xin, Z. Xiong, K. Li, Y.-G. Guo and Y. You, *ACS Energy Lett.*, 2023, **8**, 836–843.
259 Y. Li, J. Wang, Y. Wang, S. Wang, L. Wu, B. Zhou, D. Yang, L. Jiang, L. Kan, Q. Zhu, M. Kurbanov and H. Wang, *Adv. Mater.*, 2025, **37**, 2419764.
260 X. Gao, X. Zhang, X. Liu, Y. Tian, Q. Cai, M. Jia and X. Yan, *Small Methods*, 2023, **7**, 2300152.
261 P. Dong, F. Peng, Q. Zhang, H. Wang, Y. Chu, C. Chen and C. Yang, *Angew. Chem., Int. Ed.*, 2025, **64**, e202502693.
262 Z. Yang, J. He, W. Lai, J. Peng, X. Liu, X. He, X. Guo, L. Li, Y. Qiao, J. Ma, M. Wu and S. Chou, *Angew. Chem.*, 2021, **133**, 27292–27300.
263 X. Zheng, Z. Gu, J. Fu, H. Wang, X. Ye, L. Huang, X. Liu, X. Wu, W. Luo and Y. Huang, *Energy Environ. Sci.*, 2021, **14**, 4936–4947.
264 J. Zheng, W. Li, X. Liu, J. Zhang, X. Feng and W. Chen, *Energy Environ. Mater.*, 2023, **6**, e12422.
265 P. Hu, Y. Zhang, X. Chi, K. Kumar Rao, F. Hao, H. Dong, F. Guo, Y. Ren, L. C. Grabow and Y. Yao, *ACS Appl. Mater. Interfaces*, 2019, **11**, 9672–9678.
266 T. Lan, C.-L. Tsai, F. Tietz, X.-K. Wei, M. Heggen, R. E. Dunin-Borkowski, R. Wang, Y. Xiao, Q. Ma and O. Guillon, *Nano Energy*, 2019, **65**, 104040.
267 B. Rui, S. Sun, X. Tan, C. (Michael) Chak, L. Ma and J. Xu, *J. Mater. Chem. A*, 2025, **13**, 12203–12215.
268 C. Vaalma, D. Buchholz, M. Weil and S. Passerini, *Nat. Rev. Mater.*, 2018, **3**, 18013.
269 T. Yang, D. Luo, Y. Liu, A. Yu and Z. Chen, *iScience*, 2023, **26**, 105982.
270 Z. Hu, L. Liu, X. Wang, Q. Zheng, C. Han and W. Li, *Adv. Funct. Mater.*, 2024, **34**, 2313823.
271 T. Liu, Y. Zhang, C. Chen, Z. Lin, S. Zhang and J. Lu, *Nat. Commun.*, 2019, **10**, 1965.
272 J. Xu, H. R. Thomas, R. W. Francis, K. R. Lum, J. Wang and B. Liang, *J. Power Sources*, 2008, **177**, 512–527.
273 M. L. Machala, X. Chen, S. P. Bunke, G. Forbes, A. Yegizbay, J. A. De Chalendar, I. L. Azevedo, S. Benson and W. A. Tarpeh, *Nat. Commun.*, 2025, **16**, 988.
274 J. F. Peters, M. Baumann, J. R. Binder and M. Weil, *Sustainable Energy Fuels*, 2021, **5**, 6414–6429.
275 Y. Zhao, Y. Kang, J. Wozny, J. Lu, H. Du, C. Li, T. Li, F. Kang, N. Tavajohi and B. Li, *Nat. Rev. Mater.*, 2023, **8**, 623–634.
276 S. Wickerts, R. Arvidsson, A. Nordelöf, M. Svanström and P. Johansson, *J Ind. Ecol.*, 2024, **28**, 116–129.
277 N. R, *Life Cycle Assessment on Sodium-Ion Cells for Energy Storage Systems: A Cradle-to-Gate Study Including* 16 *Environmental Perspectives, Focusing on Climate Change Impact*, https://www.diva-portal.org/smash/get/diva2:1790721/FULLTEXT01.pdf.
278 W. Guo, T. Feng, W. Li, L. Hua, Z. Meng and K. Li, *J. Energy Storage*, 2023, **72**, 108589.
279 S. Zhang, B. Steubing, H. K. Potter, P.-A. Hansson and Å. Nordberg, *Resour., Conserv. Recycl.*, 2024, **202**, 107362.
280 C. R, *Understanding the EU's Digital Battery Passport. Battery Technology*, https://www.batterytechonline.com/industry-outlook/understanding-the-eu-s-digital-battery-passport.

© 2025 The Author(s). Published by the Royal Society of Chemistry